NOTE TO USERS

Page(s) not included in the original manuscript and are unavailable from the author or university. The manuscript was scanned as received.

64,75,76,94,100,106,122,123.

This reproduction is the best copy available.

UMI®

STUDY OF TWO DIFFERENT TUNABLE VIBRATION ABSORBERS: VARIABLE STIFFNESS ABSORBER AND VARIABLE DAMPING ABSORBER

Liang Liao

March 12, 2003

A THESIS SUBMITTED IN PARTIAL FULFILLMENT OF
THE REQUIREMENT OF THE MScENG DEGREE
IN
CONTROL ENGINEERING
FACULTY OF ENGINEERING
LAKEHEAD UNIVERSITY
THUNDER BAY, ONTARIO

Your file Votre référence
ISBN: 0-612-92250-2
Our file Notre référence
ISBN: 0-612-92250-2

Abstract

A structure or machine will vibrate at the frequency of excitation when excited by a harmonic force. Vibration of the structure can be suppressed using a vibration absorber by setting the absorber's natural frequency equal to the exciting frequency. However, when the exciting frequency varies, vibration of the structure attached with the vibration absorber may increase significantly. A tunable vibration absorber is an adaptive-passive device that can overcome the shortcoming of a traditional vibration absorber. Such a device is capable of adjusting its parameter on-line based on a feedback loop. In this thesis, two different tunable vibration absorbers are studied. The first one is a variable stiffness vibration absorber that provides a means to vary the absorber stiffness to ensure that the absorber frequency follows the exciting frequency. The second one is a variable damping vibration absorber that provides a means to vary the absorber damping to ensure the best performance of the absorber. Both the vibration absorbers are used to suppress vibration of a beam structure.

The developed variable stiffness absorber is a cantilever-beam attached by a mass at its free end. The absorber stiffness is varied by changing the beam length through a DC motor drive system. Various models of the beam-absorber system are derived. The proposed tuning algorithm is based on the frequency information extracted from spectrum of the response. Using a simplified 2-degree-of-freedom (DOF) model, the computer simulation tests the tuning algorithm's ability to track a step change and a linear change in the exciting frequency. Factors affecting the performance of the absorber are investigated. The developed variable damping absorber is an electromagnetic damper that is based on the eddy current principle. Analytical study shows that there exist two crossing frequencies which determine whether damping should or should not be added to the absorber system. An on/off tuning control strategy is developed. Using a 2-DOF system, the computer simulation tests the tuning strategy when the exciting frequency experiences a multi-step change. For both the absorber systems, the experiment study focuses on validation of the tuning algorithms and addresses some practical issues encountered in implementation.

Acknowledgements

I gratefully acknowledge my supervisor Dr. K. Liu for his support and responsible supervision. The thesis would not have be possible without his knowledge and guidance. I would like to thank my co-supervisor Dr. A. Tayebi for his valuable suggestions. I would like to thank Dr. K. Natarajan for his technical guidance in the theory of electromagnetism on the electromagnet, Dr. X. Liu for his help in development of the PWM circuitry, Mr. M. Klein for his assistance in building the circuitry, Mr. K. Bhatia for his assistance in building the apparatus and Mr. G. Mezo of **Kilred Winding Industries Ltd.** for his assistance in making the electromagnet.

This work owes a lot to the efforts of many former researchers. Thanks are also extended to my colleagues Ms. M. Yektaii , Mr. Y. Zhao and Mr. S. Abdul.

Contents

List of Figures

List of Tables

List of Acronyms and Notations

DOF	Degree of Freedom
FFT	Fast Fourier Transform
tol	Frequency tolerance
rms	Root Mean Square
DAQ	Data Acquisition
PWM	Pulse-Width Modulation
DSP	Digital Signal Processor
emf	electromotive force

Chapter 1

Introduction

The notion that machines and structures are rigid bodies must be dispelled in favor of a system consisting of elastic components that respond to external forces with finite deformations. This capacity for relative motion allows vibration to take place. Vibration can often lead to a number of undesirable circumstances. For example, vibration of an automobile or truck can lead to driver discomfort and eventually, fatigue. Structural or mechanical failure can often result from sustained vibration (e.g., cracks in airplane wings). One of the ways to protect a device from a constant frequency harmonic excitation is a vibration absorber. Vibration of the mass having a vibration absorber without damping vanishes perfectly when the frequency of a sinusoidal force acting on the mass is equal to the natural frequency of the absorber. Since the phenomenon is just opposite to the resonance. the phenomenon is called "anti-resonance", and the frequency in which the vibration amplitude becomes minimum is called "anti-resonance frequency" in the present thesis. When the exciting frequency is different from the anti-resonance frequency, the vibration of the mass increases significantly. If the stiffness of the absorber is tunable, the vibration of the mass can be suppressed perfectly even if the exciting frequency varies.

Another approach to protecting a device from a constant frequency harmonic disturbance is to add a damper in the device. Damping is sometimes added to a vibration absorber to prevent resonance or to improve the effective bandwidth of operation. Also, a damper by itself is often used as a vibration absorber by dissipating the energy supplied by an applied force. Such devices are called vibration dampers rather than absorbers.

The rest of this chapter is organized as follows: Section 1 presents an overview of the previous studies on vibration absorbers and dampers, Section 2 lists the objectives of the thesis research, and Section 3 gives the outline of the thesis.

1.1 Overview of the Previous Studies on Vibration Absorbers

As pointed out in [1], the methods of vibration control can be classified into four types: (1) passive; (2) active; (3) hybrid; and (4) adaptive-passive. Passive control involves the use of reactive or resistive devices that either load the transmission path of the disturbing vibration or absorb vibrational energy. Vibration absorber is a typical example of the passive control.

A cruciform vibration absorber was introduced in [2]. In [3] vibration of beams is suppressed by an absorber consisting of a viscoelastic solids and beam. Phenomena of non-linear vibration absorbers have been discussed in [4]. Vibration absorbers have been used for suppressing vibrations of various structures [5, 6], and machines such as offshore platform [7]. Damped vibration absorber, which includes viscous damping in addition to the spring, can reduce vibration at resonance [8]. It cannot, however, reduce the vibration of a system to essentially zero. Thus there are limits to the performance of absorbers consisting of only passive components. Active control also loads the transmission path but achieves this loading through the use of force actuators requiring external energy. A control system of an active dynamic vibration absorbers with an electromagnetic servomechanism has been designed [9] and a control method is obtained to reduce the vibration to a low level over a wide range of frequencies, and eliminate it completely at several specified frequencies. Hybrid control integrates a passive approach with an active control structure. The hybrid approach is intended to reduce the amount of external power necessary to achieve control. Delayed resonator [10] is a typical hybrid vibration control device. By adding an actuator in parallel to the absorber spring, the delayed resonator can achieve the perfect vibration suppression even if there exists some damping and allow an on-line tuning in the event of a varying exciting frequency. The hybrid vibration absorbers has been discussed in [11] in which rigidity and

damping are varied by using a semiactive hydraulic controller, which possesses significant control authority and is adjustable but requires no power when compared with a fully active design. Adaptive-passive vibration control makes a passive device tunable such that optimal performance is guaranteed. Some of these designs for tunable vibration absorbers include an adjustable dual-leaf spring design [12], variable positioning of a fulcrum [13] and stiffening through appropriate use of a magnetic field [14]. Design variations of other tunable stiffness vibration absorber are application dependent. A particular system will have space and weight constraints that the mechanical design of the absorber must satisfy.

The type of adaptive-passive vibration control discussed in this thesis is an alternative to conventional approaches to dealing with time-varying excitations. While active control schemes are very effective at controlling harmonic disturbances comprising of a single frequency, the cost and energy requirements of the active control system prohibit its application to a wide class of systems. The alternative is passive control. If the disturbance frequency varies with time, then a passive approach will not provide satisfactory performance over the frequency variations of the disturbance. Adaptive-passive control addresses this limitation by effectively integrating a tuning control scheme with a tunable passive device such as tunable vibration absorber for harmonic vibration applications.

1.2 Objectives of the Thesis Research

The main objective of the thesis study is to compare two different tunable vibration absorbers: a variable stiffness absorber and a variable damping absorber. The study of a variable stiffness vibration absorber includes the following tasks:

1. design and build a variable stiffness vibration absorber;
2. develop a dynamic model for a beam structure attached with the variable stiffness vibration absorber;
3. develop an auto-tuning method for the absorber;
4. implement the auto-tuning method in an experimental system.

The study of a variable damping vibration absorber includes the following tasks:

1. design and build a variable damping vibration absorber;
2. develop a dynamic model for a beam structure attached with the variable damping vibration absorber;
3. develop an auto-tuning method for the absorber;
4. implement the auto-tuning method in an experimental system.

1.3 Outline of the Thesis

The following chapters of this thesis are organized as follows. Chapter 2 presents an analytical study of a variable stiffness vibration absorber system. This chapter includes the system modelling, development of an auto-tuning algorithm, testing of the auto-tuning algorithm using numerical simulation. Chapter 3 presents an experimental study of the variable stiffness vibration absorber system. This chapter includes description of the experimental setup and various experimental results. Chapter 4 presents an analytical study of a variable damping vibration absorber. This chapter includes system modelling, development of an auto-tuning algorithm, testing of the auto-tuning algorithm using a numerical simulation. Chapter 5 presents an experimental study and results of the variable damping vibration absorber. This chapter includes description of the experimental setup and various experimental results. Chapter 6 concludes this thesis with a summary of the research and recommendations for future work.

Chapter 2

Analytical Study of a Variable Stiffness Vibration Absorber

2.1 Introduction of a Simple Absorber System

The principle of vibration absorbers is explained in detail in [8]. In order to study the experimental system, the theory will be briefly introduced below. Figure 2.1 (a) shows a primary system subject to a sinusoidal force $F_0 sin\omega t$. When the forcing frequency equals the natural frequency of the primary mass the response is infinite. This is called resonance. Figure 2.1 (b) shows a mass-spring system is attached to the primary mass. The major effect

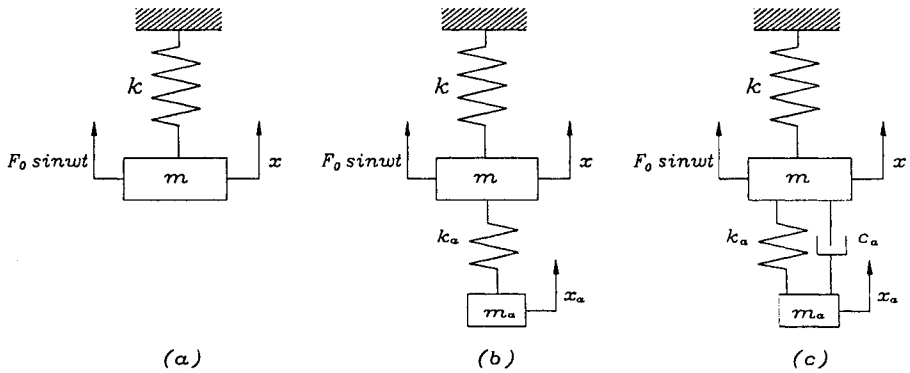

Figure 2.1: Absorber system model

of adding this secondary mass-spring system is to change from a 1-DOF system into a 2-DOF system. The new system has two natural frequencies. The added mass-spring system is called the vibration absorber. When the natural frequency of the absorber system coincides the exciting frequency of the sinusoidal force, the motion of the primary mass becomes zero. The equations of motion of the entire system (refer to [8]) are:

$$\begin{bmatrix} m & 0 \\ 0 & m_a \end{bmatrix} \begin{bmatrix} \ddot{x} \\ \ddot{x}_a \end{bmatrix} + \begin{bmatrix} k + k_a & -k_a \\ -k_a & k_a \end{bmatrix} \begin{bmatrix} x \\ x_a \end{bmatrix} = \begin{bmatrix} F_0 \sin \omega t \\ 0 \end{bmatrix} \tag{2.1}$$

where x is the displacement of the primary mass m, x_a is the displacement of the absorber mass m_a, k is the stiffness of the primary system, and k_a is the stiffness of the absorber system. Let the steady-state solutions $x(t)$ and $x_a(t)$ be the form of

$$x(t) = X \sin \omega t \tag{2.2}$$

$$x_a(t) = X_a \sin \omega t \tag{2.3}$$

where X and X_a are the magnitude of the steady-state vibration of the primary mass and absorber mass, respectively. Substituting equations (2.2) and (2.3) into equation (2.1) results in

$$X = \frac{(k_a - m_a\omega^2)F_0}{(k + k_a - m\omega^2)(k_a - m_a\omega^2) - k_a^2} \tag{2.4}$$

and

$$X_a = \frac{k_a F_0}{(k + k_a - m\omega^2)(k_a - m_a\omega^2) - k_a^2}. \tag{2.5}$$

The absorber parameters k_a and m_a can be chosen such that the magnitude of the steady-state vibration, X, is exactly zero. This is accomplished by equating the coefficient of F_0 in equation (2.4) to zero:

$$\omega = \omega_a = \sqrt{\frac{k_a}{m_a}} \tag{2.6}$$

where ω_a is referred to as the frequency of the absorber system or anti-resonance frequency of the entire system. In this event the steady-state motion of the absorber mass is calculated from equations (2.3) and (2.5) with $k_a = m_a\omega^2$ to be

$$x_a(t) = -\frac{F_0}{k_a} \sin \omega t. \tag{2.7}$$

Thus the absorber mass oscillates at the driving frequency with amplitude $X_a = -F_0/k_a$. When the frequency of the absorber system is tuned to be the driving frequency and the response has reached a steady state, the force provided by the absorber spring is equal in magnitude and opposite in direction to the exciting force. With zero net force acting on the primary mass, it does not move and the motion is "absorbed" by motion of the absorber mass.

The success of the vibration absorber depends on several factors. First the harmonic exciting frequency must be well known and not deviate much from its constant value. If the driving frequency drifts, the tuning condition will not be satisfied, and the primary mass will experience some oscillation. There is also some danger that the driving frequency could shift to one of the combined system's resonant frequencies, in which case the system would be driven to resonance and potentially fail. Another key factor in absorber design is that the absorber spring stiffness k_a must be capable of withstanding the full force of the excitation and hence must be capable of the corresponding deflections. The issue of spring size and deflection as well as the value of the absorber mass places a geometric limitation on the design of a vibration absorber system.

The issue of avoiding resonance in absorber design in case the driving frequency shifts can be quantified by examining the mass ratio μ, defined as the ratio of the absorber mass to the primary mass:

$$\mu = \frac{m_a}{m}. \tag{2.8}$$

In addition, it is convenient to define

$$\omega_p = \sqrt{\frac{k}{m}}$$

which is the natural frequency of the primary system without the absorber attached. Also note that

$$\frac{k_a}{k} = \mu\frac{\omega_a^2}{\omega_p^2} = \mu\beta^2$$

where $\beta = \frac{\omega_a}{\omega_p}$ is the frequency ratio. Substitution of the values for μ, ω_p, and ω_a into equation (2.4) yields (after some manipulation)

$$\left|\frac{X}{F_0/k}\right| = \left|\frac{Xk}{F_0}\right| = \left|\frac{1-\frac{\omega^2}{\omega_a^2}}{\left[1+\mu(\frac{\omega_a}{\omega_p})^2-(\frac{\omega}{\omega_p})^2\right]\left[1-(\frac{\omega}{\omega_a})^2\right]-\mu(\frac{\omega_a}{\omega_p})^2}\right| \tag{2.9}$$

where $|\frac{Xk}{F_0}|$ is the normalized magnitude. The absolute value of this expression is plotted in Figure 2.2. Such plot can be used to illustrate how much drift in the driving frequency can

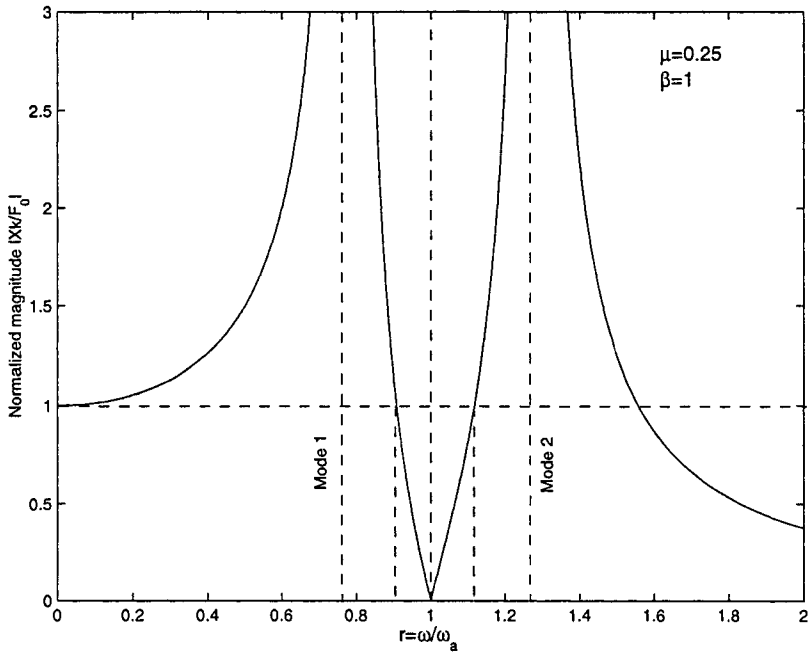

Figure 2.2: Normalized magnitude of the primary mass for the case $\mu = 0.25$ and $\beta = 1$.

be tolerated by the absorber design. If the driving frequency shifts such that $|\frac{Xk}{F_0}| > 1$, The dynamic displacement X is greater than the static deflection F_0/k. The static deflection is the deflection of the spring when a constant force F_0 is applied to the primary system. In such a case the absorber system is not an improvement over the original design of the primary system. However if the driving frequency drifts such that $|\frac{Xk}{F_0}| < 1$, the absorber design offers some protection to the primary system by reducing its steady-state vibration amplitude. Especially when $\omega = \omega_a$, the vibration of the primary system will be reduced to zero. However, this performance is realized at one frequency only and is extremely sensitive to proper tuning due to the narrow frequency band between the two resonant peaks. Consequently, the performance of a vibration absorber is sensitive to variations in the excitation

frequency.

To make the absorber system more robust to variations in the exciting frequency, the mass ratio μ can be increased which correspondingly increases the bandwidth between the resonant peaks. The normalized magnitude plots for two different mass ratios, namely $\mu = 0.01$ and 0.5, are shown in Figure 2.3. In most applications, the absorber mass should be as small as

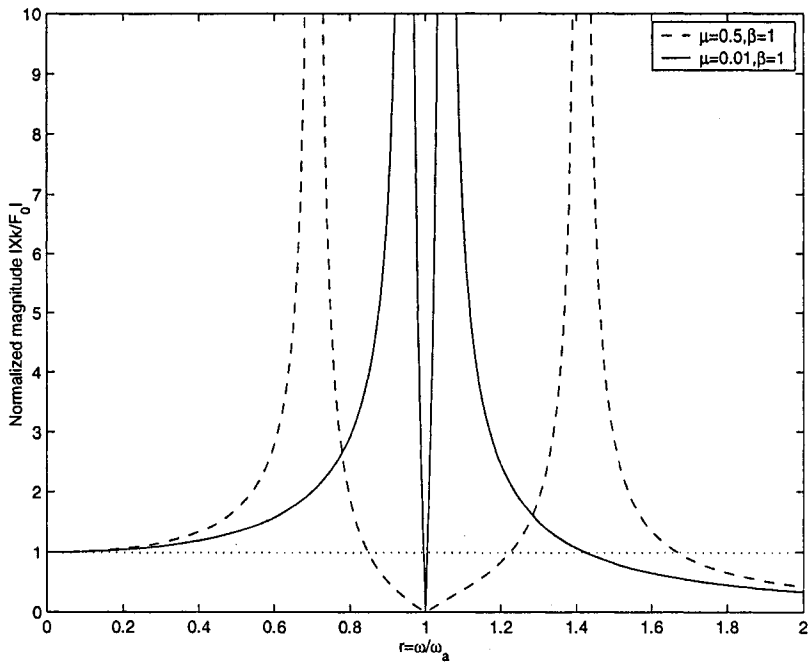

Figure 2.3: Effects of mass ratio

possible. However as shown in Figure 2.3, an absorber system with smaller mass ratio has a narrower operating bandwidth.

Alternatively, the robustness of an absorber system can be increased by adding viscous damping to the absorber as shown in Figure 2.1 (c). The normalized magnitude plot is shown in Figure 2.4 where the system values are the same as those for Figure 2.2 except that the damping ratio of the absorber is $\zeta_a = 0.1$ where $\zeta_a = \frac{c_a}{2m_a\omega_p}$. Although the amplitudes of the resonant peaks are low, the performance at the absorber natural frequency is substantially decreased. Selection of a proper trade-off between reducing performance sensitivity and maximizing vibration attenuation via the absorber damping has motivated investigations into optimization of the absorber mass and stiffness in the presence of the absorber damping

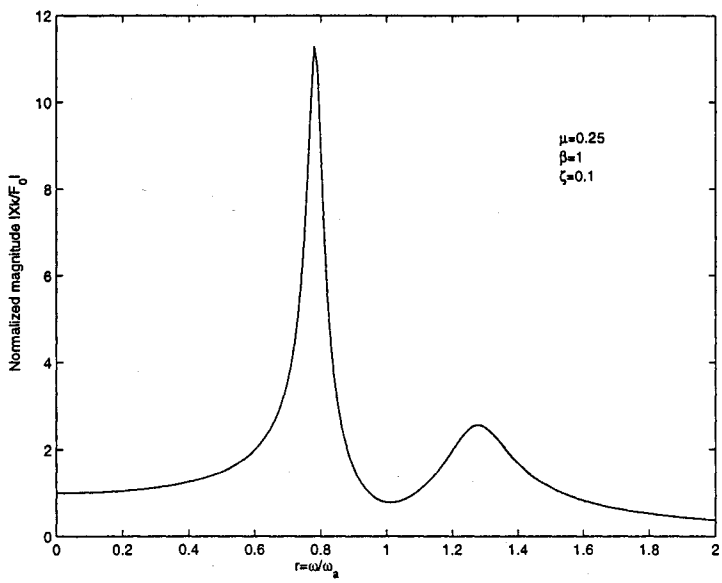

Figure 2.4: Frequency response plot of damped absorber $\zeta_a = 0.1$

[8].

In contrast to passively reducing performance sensitivity, a robust tuning algorithm with a tunable vibration absorber is studied in this thesis. The robust tuning scheme presented guarantees absorber tuning despite variations in the excitation frequency. The goal is to maximize the attenuation performance of an undamped vibration absorber while keeping the absorber mass small. Regardless of the physical mechanism that realizes absorber tuning, the purpose of an adaptive tuning strategy is to match the

absorber natural frequency to the exciting frequency. A feedback-based tuning scheme is developed to increase absorber robustness. The tunable vibration absorber used to verify this tuning strategy is a variable stiffness device. Therefor k_a is chosen to be the tuning parameter.

2.2 Beam-Absorber System

A beam-absorber system was developed to study the tunable absorber system which is shown in Figure 2.5.

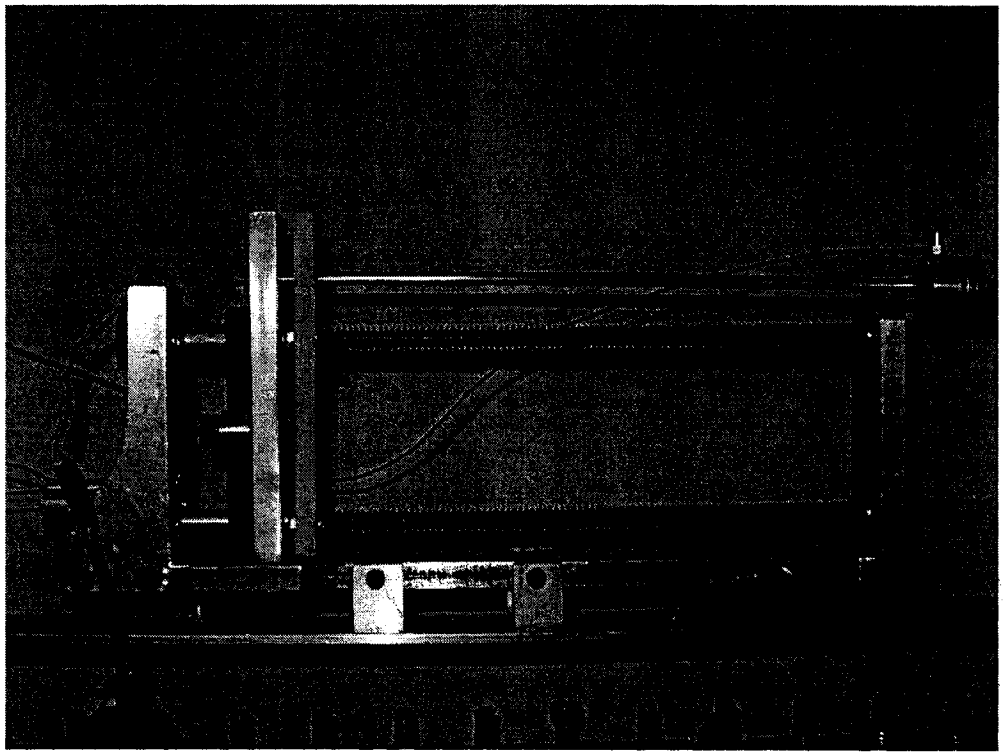

Figure 2.5: The tunable vibration absorber

The entire system consists of 2 subsystem: a clamped-clamped beam and a tunable absorber system as shown in Figure 2.6. The beam (11), made of aluminum, serves as a primary system. The tunable absorber apparatus was placed in the middle of the primary beam and consists of a 12V DC motor (4), a belt and pulley set (3), an encoder (5), two lead screws (7), absorber frame (10), absorber mass (6), absorber beam (9) and the movable support (8). The absorber beam is an aluminum rod with a diameter of 6.35 mm and a length of 306 mm. The movable support is driven by the lead screws. The screw pitch is 2.978 mm. The motor is a 12V DC permanent magnet reversible motor, the no load speed is 180.11 RPM and full load speed is 135.6 RPM at a torque of 19.28 oz-in. The angle of rotation of the motor is detected by the rotary encoder (5) attached to the upper lead

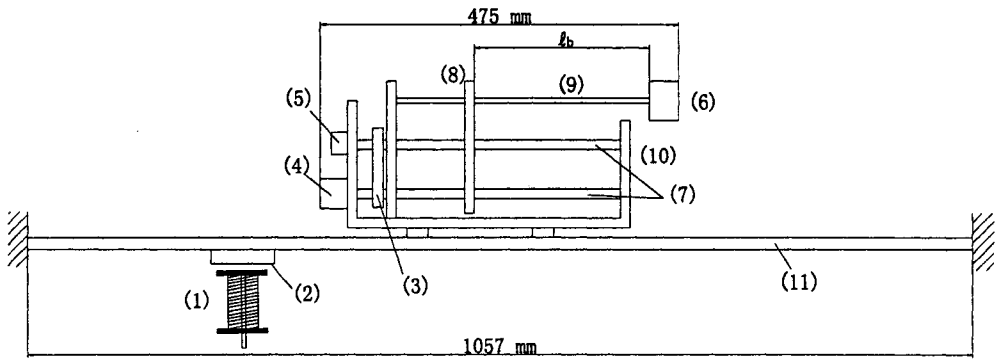

Figure 2.6: Schematic of the beam-absorber system

(1) Electromagnetic shaker	(2) Permanent magnet	(3) Belt and pulley set
(4) DC motor	(5) Encoder	(6) Absorber mass
(7) Lead screw	(8) Movable support	(9) Absorber beam
(10) Absorber frame	(11) Primary beam	

screw. The encoder is HEDS-7500 SWERIES Panel Mount Digital Potentiometer, the unit outputs two digital waveforms which are 90 degrees out of phase to provide resolution and direction information, the standard resolution is 256 pulses per revolution. The shaker (1) is an electromagnet and used to generate an exciting force. A small permanent magnetic plate (2) is glued on the beam to interact with the electromagnetic force. The distance ℓ_b between the movable support and the absorber mass is varied by moving the movable support. This way the spring constant of the absorber system can be changed.

To move the movable support of the absorber beam to a desired position requires the relation between the absorber beam length and the absorber natural frequency. If the absorber beam is modelled as a cantilever beam, in theory [8] the relation between the absorber beam length ℓ_b and the beam stiffness k_a is $k_a = \frac{3EI}{\ell_b^3}$ where E is Young's modulus and I is moment inertia of cross-sectional area of the absorber beam. Therefore the relation between the absorber beam length ℓ_b and the absorber natural frequency can be determined by equation (2.6) as $\sqrt{\frac{3EI}{m_a\ell_b^3}}$. However in the real system, the absorber beam is not an ideal clamped-free beam, because at the "clamped" end, there is a clearance between the hole of the movable plate and the beam, while at the "free" end there is the absorber mass at-

tached. The theoretical result of the relation is not accurate. Therefore an experiment was carried out to determine the relation between the absorber length and the absorber natural frequency. With the absorber system firmly fixed to the ground and the absorber beam adjusted to a known length, impact was applied to the absorber mass and the response of the absorber mass was measured using an accelerometer that was placed on the absorber mass. The frequency of the response was found by conducting the Fast Fourier Transform (FFT). The experiment was repeated for a new beam length.

Figure 2.7 shows the found relation. Dots are the measured absorber natural (anti-

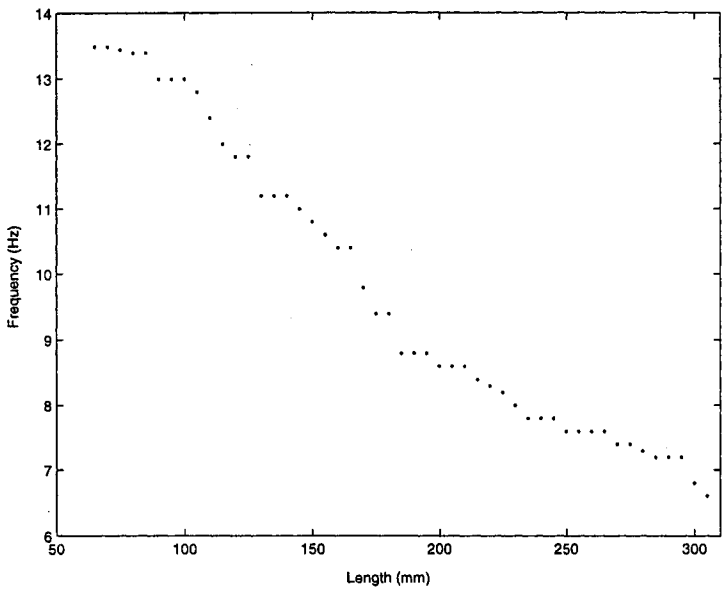

Figure 2.7: Relation between the absorber beam length ℓ_b and the absorber natural frequency f_a

resonance) frequencies at different absorber beam lengths, the frequency range is from 6.6 Hz to 13.5 Hz.

2.3 Model of the Experimental System

A model of the experimental system is shown in Figure 2.8. Table 2.1 lists the parameters of the entire system. The vertical motion of the primary beam at any point on the beam is

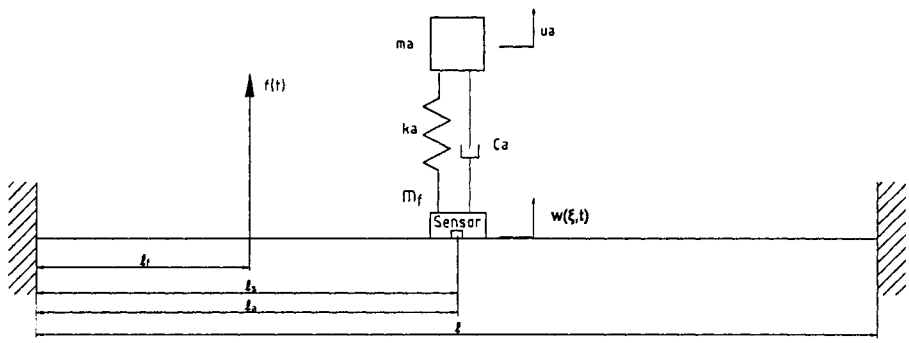

Figure 2.8: Model of the experimental system

a function of both the time t and the position along the beam, ξ. The displacement of the primary beam is thus denoted by $w(\xi, t)$. It is assumed that the displacement $w(\xi, t)$ can be written as the product of two functions, one depending only on ξ and the other depending only on t (hence separation of variables). Thus

$$w(\xi, t) = \sum_{i=1}^{\infty} \phi_i(\xi) q_i(t) \tag{2.10}$$

where $q_i(t)$ is referred to as the ith generalized coordinate and $\phi_i(\xi)$ is referred to as the ith mode shape. For a clamped-clamped beam, it is of the form:

$$\phi_i(\xi) = \cosh \beta_i \xi - \cos \beta_i \xi - \sigma_i(\sinh \beta_i \xi - \sin \beta_i \xi)$$

with

$$\sigma_i = \frac{\cosh \beta_i \ell - \cos \beta_i \ell}{\sinh \beta_i \ell - \sin \beta_i \ell}.$$

The values of $\beta_i \ell$ and σ_i for the first three modes are given in Table 2.2 [8].

From a preliminary test, it was found that the modes higher than the third mode are very weak, thus

$$w(\xi, t) = \sum_{i=1}^{3} \phi_i(\xi) q_i(t) = \Phi(\xi) q(t) \tag{2.11}$$

where

$$\Phi(\xi) = [\ \phi_1(\xi) \quad \phi_2(\xi) \quad \phi_3(\xi)\ ]$$

Absorber frame mass m_f	0.8887 kg
Absorber mass m_a	0.1770 kg
Mass of the primary beam m_b	0.7649 Kg
Density of the primary beam ρ	2800 kg/m^3
Length of the primary beam ℓ	1.057 m
Width of the primary beam b	50.8 mm
Height of the primary beam h	5.0876 mm
Cross-sectional area of the primary beam A	2.5845×10^{-4} m^2
Moment inertia of cross-sectional area I	5.5747×10^{-10} m^4
Young's modulus E	70.9×10^9 N/m^2
Location of the absorber ℓ_a	528.5 mm
Location of the excitation ℓ_f	247 mm
Location of the sensor ℓ_s	528.5 mm

Table 2.1: Parameters of the system

$modeNo$	1	2	3
$\beta_i \ell$	4.7300	7.8532	10.9956
σ_i	0.9825	1.0008	0.9999

Table 2.2: $\beta_i \ell$ and σ_i of the first three modes of a clamped-clamped beam

and

$$q(t) = \begin{bmatrix} q_1(t) \\ q_2(t) \\ q_3(t) \end{bmatrix}.$$

In what follows, first a model for the primary beam with the absorber frame is developed and then a model for the entire system is developed.

2.3.1 Primary Beam with the Absorber Frame

First the primary beam with the absorber frame is considered. The primary system of the experimental system is considered to be the clamped-clamped beam plus the absorber frame mass as shown in Figure 2.9.

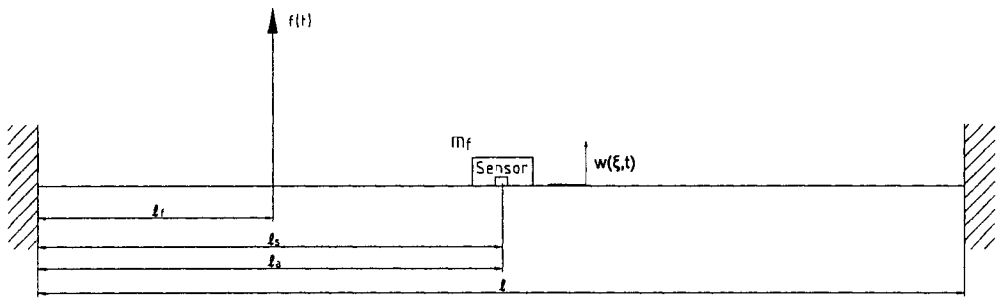

Figure 2.9: Primary beam with the absorber frame mass

Applying Newton's second law of motion to a differential element of the beam [8] results in

$$\rho A\frac{\partial^2 w(\xi,t)}{\partial t^2}+\gamma\frac{\partial w(\xi,t)}{\partial t}+EI\frac{\partial^4 w(\xi,t)}{\partial \xi^4}=F_0\sin\omega t\delta(\xi-\ell_f)-m_f\frac{\partial^2 w(\ell_a,t)}{\partial t^2}\delta(\xi-\ell_a) \quad (2.12)$$

where γ is damping value per unit beam length and $\delta(\xi-\ell_f)$ is a Dirac delta function indicating that a concentrated force is applied at $\xi=\ell_f$. Substituting equation (2.11) into equation (2.12) yields

$$\rho A\Phi(\xi)\ddot{q}(t)+\gamma\Phi(\xi)\dot{q}(t)+EI\Phi''''(\xi)q(t)=F_0\sin\omega t\delta(\xi-\ell_f)-m_f\Phi(\ell_a)\ddot{q}(t)\delta(\xi-\ell_a).$$

Premultiplying $\Phi^T(\xi)$ to the above equation on both sides and integrating over the length of the beam with respect to ξ yields

$$\rho A\int_0^l\Phi^T(\xi)\Phi(\xi)d\xi\ddot{q}(t)+\gamma\int_0^l\Phi^T(\xi)\Phi(\xi)d\xi\dot{q}(t)+EI\int_0^l\Phi^T(\xi)\Phi''''(\xi)d\xi q(t)$$
$$=F_0\sin\omega t\Phi^T(\ell_f)-m_f\Phi^T(\ell_a)\Phi(\ell_a)\ddot{q}(t) \quad (2.13)$$

where

$$\int_0^l \Phi^T(\xi)\Phi(\xi)d\xi = \ell I_{3\times 3} \tag{2.14}$$

because of the orthogonality of the mode shape functions where $I_{n\times n}$ denotes an $n \times n$ identity matrix and

$$\int_0^l \Phi^T(\xi)\Phi''''(\xi)dx = \ell \begin{bmatrix} \beta_1^4 & 0 & 0 \\ 0 & \beta_2^4 & 0 \\ 0 & 0 & \beta_3^4 \end{bmatrix} = \ell\Lambda \tag{2.15}$$

where

$$\Lambda = \begin{bmatrix} \beta_1^4 & 0 & 0 \\ 0 & \beta_2^4 & 0 \\ 0 & 0 & \beta_3^4 \end{bmatrix}.$$

Simplifying the above equations by substituting equation (2.14) and equation (2.15) into equation(2.13) yields

$$[m_f\Phi^T(\ell_a)\Phi(\ell_a) + \rho A\ell I_{3\times 3}]\ddot{q}(t) + \gamma\ell I_{3\times 3}\dot{q}(t) + EI\ell\Lambda q(t) = F_0 \sin\omega t\Phi^T(\ell_f).$$

The above equation can be written in a matrix form as follows

$$M\ddot{q}(t) + C\dot{q}(t) + Kq(t) = Bf(t) \tag{2.16}$$

where M is mass matrix

$$M = m_f\Phi^T(\ell_a)\Phi(\ell_a) + \rho A\ell I_{3\times 3}$$

C is damping matrix

$$C = \gamma\ell I_{3\times 3}$$

K is stiffness matrix

$$K = EI\ell\Lambda$$

B is input matrix

$$B = \Phi^T(\ell_f)$$

$f(t)$ is the exciting force

$$f(t) = F_0 \sin\omega t.$$

In order to solve the second order differential equation numerically, equation (2.16) can be transformed to the first order differential equation by the state space method

$$\dot{x}(t) = A_c x(t) + B_c f(t) \tag{2.17}$$

$$y(\ell_s, t) = C_c x(t) \tag{2.18}$$

where

$$A_c = \begin{bmatrix} 0_{3\times3} & I_{3\times3} \\ -M^{-1}K & -M^{-1}C \end{bmatrix}$$

is system matrix with $0_{n\times n}$ denoting an $n \times n$ zero matrix,

$$B_c = \begin{bmatrix} 0_{3\times1} \\ M^{-1}B \end{bmatrix}$$

is input influence matrix,

$$y(\ell_s, t) = w(\ell_s, t)$$

is the displacement of the primary beam at $\xi = \ell_s$,

$$C_c = \begin{bmatrix} \phi_1(\ell_s) & \phi_2(\ell_s) & \phi_3(\ell_s) & 0 & 0 & 0 \end{bmatrix}$$

is output influence matrix,

$$x(t) = \begin{bmatrix} q(t) \\ \dot{q}(t) \end{bmatrix}$$

is the state vector.

Taking the Laplace transform of both sides of equation (2.17) yields

$$sX(s) = A_c X(s) + B_c f(s).$$

Solving for $X(s)$ yields

$$X(s) = (sI_{6\times6} - A_c)^{-1} B_c f(s).$$

Taking the Laplace transform of both sides of equation (2.18) yields

$$Y(s) = C_c(sI_{6\times6} - A_c)^{-1} B_c f(s).$$

Transfer function of the system is obtained as follows

$$H(s) = \frac{Y(s)}{f(s)} = C_c(sI_{6\times 6} - A_c)^{-1}B_c. \tag{2.19}$$

With $s = j\omega$ in equation (2.19), the frequency response $H(j\omega)$ is obtained. Using the data given in Table 2.1 and $\gamma = 0.2142$, the frequency response can be evaluated.

Figure 2.10 shows the magnitude of the frequency response of the primary beam with the absorber frame. Because only three modes are considered, the system is a 3-DOF system

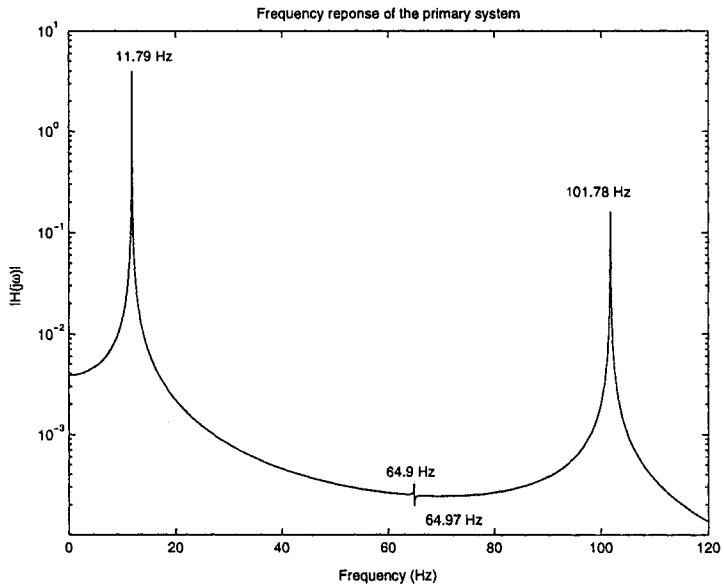

Figure 2.10: Frequency response of the primary beam with absorber frame

and has 3 peaks as shown in Figure 2.10. It also can be seen that the second peak is very weak and almost invisible, the reason is that the observation location is right in the middle of the primary beam which is the node of the second mode [8]. When the exciting frequency is equal to 11.79 Hz, 64.9 Hz or 101.8 Hz respectively, the system vibrates at resonance. On the contrary, when the exciting frequency is equal to 64.97 Hz, the vibration amplitude of the system is at a minimum value, such a frequency is defined as "*anti-resonance frequency*". Figure 2.11 shows the frequency response of the primary beam with the sensor at a different location $\ell_s = 422.8$ mm. In this case, the second peak at 64.9 Hz is clearly visible.

The natural frequencies and damping ratios of the system can be determined from the

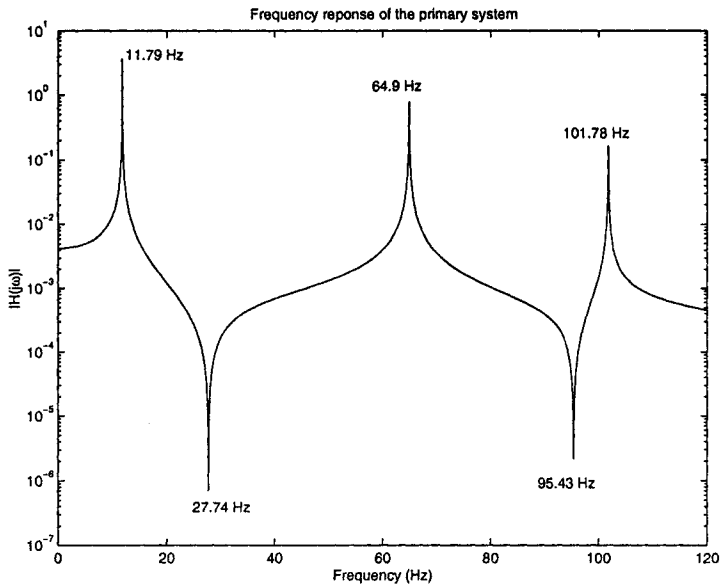

Figure 2.11: Frequency response of the primary beam with absorber frame

eigenvalues of the system matrix A_c. Let λ_i be the ith eigenvalue. The ith natural frequency ω_i and damping ratio ζ_i are given by [8]

$$\omega_i = \sqrt{Re(\lambda_i)^2 + Im(\lambda_i)^2}$$

and

$$\zeta_i = \frac{-Re(\lambda_i)}{\sqrt{Re(\lambda_i)^2 + Im(\lambda_i)^2}}$$

where $Re(\lambda_i)$ denotes the real part of λ_i and $Im(\lambda_i)$ denotes the imaginary part of λ_i.

2.3.2 Primary Beam with the Absorber System

Now, consider the primary beam with the absorber mass and spring as shown in Figure 2.8. Applying Newton's second law of motion to a differential element of the primary beam results in

$$\rho A \frac{\partial^2 w(\xi,t)}{\partial t^2} + \gamma \frac{\partial w(\xi,t)}{\partial t} + EI \frac{\partial^4 w(\xi,t)}{\partial \xi^4} =$$
$$F_0 \sin \omega t \delta(\xi - \ell_f) + k_a \left[u_a - w(\ell_a,t)\right] \delta(\xi - \ell_a) +$$

$$c_a\left[\dot{u}_a - \frac{\partial w(\ell_a,t)}{\partial t}\right]\delta(\xi-\ell_a) - m_f\frac{\partial^2 W(\ell_a,t)}{\partial t^2}\delta(\xi-\ell_a). \tag{2.20}$$

Applying Newton's second law of motion to the absorber mass results in

$$m_a\ddot{u}_a(t) = -c_a\left[\dot{u}_a(t) - \frac{\partial w(\ell_a,t)}{\partial t}\right] - k_a\left[u_a(t) - w(\ell_a,t)\right]. \tag{2.21}$$

Substituting equation (2.10) into equation (2.20) yields

$$\begin{aligned}\rho A\Phi(\xi)\ddot{q}(t) + \gamma\Phi(\xi)\dot{q}(t) + EI\Phi''''(\xi)q(t) = \\ F_0\sin\omega t\delta(\xi-\ell_f) + k_a\left[u_a(t) - \Phi(\ell_a)q(t)\right]\delta(\xi-\ell_a) + \\ c_a\left[\dot{u}_a(t) - \Phi(\ell_a)\dot{q}(t)\right]\delta(\xi-\ell_a) - m_f\Phi(\ell_a)\ddot{q}(t)\delta(\xi-\ell_a).\end{aligned} \tag{2.22}$$

Premultiplying $\Phi^T(\xi)$ to the above equation on both sides and integrating over the length of the beam with respect to ξ yields

$$\begin{aligned}\rho A\int_0^\ell \Phi^T(\xi)\Phi(\xi)d\xi\ddot{q}(t) + \gamma\int_0^\ell \Phi^T(\xi)\Phi(\xi)d\xi\dot{q}(t) + EI\int_0^\ell \Phi^T(\xi)\Phi''''(\xi)d\xi q(t) = \\ F_0\sin\omega t\Phi^T(\ell_f) + k_a\Phi^T(\ell_a)\left[u_a(t) - \Phi(\ell_a)q(t)\right] + \\ c_a\Phi^T(\ell_a)\left[\dot{u}_a(t) - \Phi(\ell_a)\dot{q}(t)\right] - m_f\Phi^T(\ell_a)\Phi(\ell_a)\ddot{q}(t).\end{aligned} \tag{2.23}$$

Substituting equations (2.14) and (2.15) into equation (2.23) yields

$$\begin{aligned}[m_f\Phi^T(\ell_a)\Phi(\ell_a) + \rho A\ell\ I_{3\times3}]\ddot{q}(t) + [\gamma\ \ell\ I_{3\times3} + c_a\Phi^T(\ell_a)\Phi(\ell_a)]\dot{q}(t) - c_a\Phi^T(\ell_a)\dot{u}(t) \\ +[EI\ell\Lambda + k_a\Phi^T(\ell_a)\Phi(\ell_a)]q(t) - k_a\Phi^T(\ell_a)u(t) = F_0\sin\omega t\Phi^T(\ell_f).\end{aligned} \tag{2.24}$$

Rearranging equation (2.21) yields

$$m_a\ddot{u}_a(t) + c_a\dot{u}_a(t) - c_a\Phi(\ell_a)\dot{q}(t) + k_au(t) - k_a\Phi(\ell_a)q(t) = 0. \tag{2.25}$$

Combining equations(2.24) and (2.25) results in a matrix equation

$$M\begin{bmatrix}\ddot{q}(t)\\ \ddot{u}_a(t)\end{bmatrix} + C\begin{bmatrix}\dot{q}(t)\\ \dot{u}_a(t)\end{bmatrix} + K\begin{bmatrix}q(t)\\ u_a(t)\end{bmatrix} = Bf(t) \tag{2.26}$$

where M is mass matrix

$$M = \begin{bmatrix}m_f\Phi^T(\ell_a)\Phi(\ell_a) + \rho A\ell I_{3\times3} & 0_{3\times1}\\ 0_{1\times3} & m_a\end{bmatrix}$$

C is damping matrix

$$C = \begin{bmatrix} \gamma \ell I_{3\times 3} + c_a \Phi^T(\ell_a)\Phi(\ell_a) & -c_a \Phi^T(\ell_a) \\ -c_a \Phi(\ell_a) & c_a \end{bmatrix}$$

K is stiffness matrix

$$K = \begin{bmatrix} EI\ell\Lambda + k_a \Phi^T(\ell_a)\Phi(\ell_a) & -k_a \Phi^T(\ell_a) \\ -k_a \Phi(\ell_a) & k_a \end{bmatrix}$$

B is input matrix

$$B = \begin{bmatrix} \Phi^T(\ell_f) \\ 0 \end{bmatrix}$$

$f(t)$ is the exciting force

$$f(t) = F_0 \sin \omega t.$$

In order to solve the second order differential equation numerically, equation (2.26) can be transformed to the first order differential equation by the state space method

$$\dot{x}(t) = A_c x(t) + B_c f(t) \tag{2.27}$$

$$y(\ell_s, t) = C_c x(t) \tag{2.28}$$

where

$$A_c = \begin{bmatrix} 0_{4\times 4} & I_{4\times 4} \\ -M^{-1}K & -M^{-1}C \end{bmatrix}$$

is system matrix,

$$B_c = \begin{bmatrix} 0_{4\times 1} \\ M^{-1}B \end{bmatrix}$$

is input influence matrix,

$$y(\ell_s, t) = w(\ell_s, t)$$

is the displacement of the primary beam at $\xi = \ell_s$,

$$C_c = \begin{bmatrix} \phi_1(\ell_s) & \phi_2(\ell_s) & \phi_3(\ell_s) & 0 & 0 & 0 & 0 & 0 \end{bmatrix}$$

is output influence matrix,

$$x(t) = \begin{bmatrix} q(t) \\ u_a(t) \\ \dot{q}(t) \\ \dot{u}_a(t) \end{bmatrix}$$

is the state vector.

Taking the Laplace transform of both sides of equation (2.27) yields

$$sX(s) = A_c X(s) + B_c f(s).$$

Solving for $X(s)$ yields

$$X(s) = (sI - A_c)^{-1} B_c f(s).$$

Taking the Laplace transform of both sides of equation (2.28) yields

$$Y(\ell_s, s) = C_c(sI - A_c)^{-1} B_c f(s).$$

Transfer function of the system is obtained as follows

$$H(s) = \frac{Y(s)}{f(s)} = C_c(sI - A_c)^{-1} B_c. \tag{2.29}$$

With $s = j\omega$ in equation (2.29), the frequency response $H(j\omega)$ is obtained. Using the data given in Table 2.1 and assuming $\gamma = 0.2142$, $c_a = 0$ kg/s, the frequency response can be evaluated.

Figure 2.12 shows the magnitude of the frequency response at $\xi = \ell_a$ when the absorber natural frequency is $f_a = 11.79$ Hz. When the exciting frequency is equal to 9.73 Hz, 14.29 Hz, 64.9Hz or 101.79 Hz, the entire system vibrates at resonance. On the contrary when the exciting frequency is equal to the *anti-resonance* frequency which is 11.79 Hz or 64.967 Hz, the vibration of the beam at $\xi = \ell_a$ is minimum. The bandwidth between the first two natural frequencies is 4.56 Hz which is very narrow, the exciting frequency is very sensitive to the narrow bandwidth, therefore a variable stiffness absorber is needed to change the anti-resonance frequency by tuning the stiffness of the absorber when the exciting frequency varies.

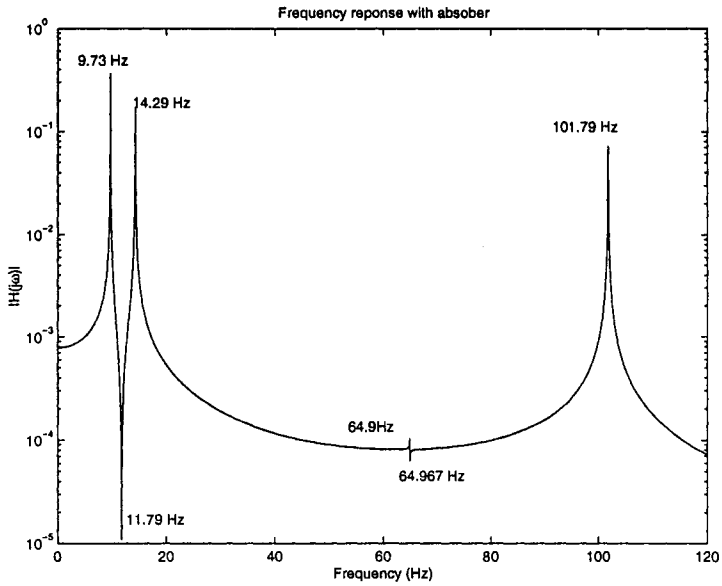

Figure 2.12: Frequency response of the primary beam at $\xi = \ell_a$ when $f_a = 11.79$ Hz

From Figure 2.12 it can be seen that after attaching the absorber mass to the primary beam, the whole system changes from a 3-DOF system to a 4-DOF system, The anti-resonance frequency 11.79 Hz is equal to the absorber frequency $f_a = 11.79$ Hz, which is tuned to be equal to the natural frequency of the primary system without the absorber mass. The third and fourth natural frequencies are far away from the first and second natural frequencies, as mentioned in the previous section that the adjustable absorber frequency range is from 6.6 Hz to 13.5 Hz, therefore the third and fourth natural frequencies can be ignored in the experiment.

Figure 2.13 shows the magnitude of the frequency response of the primary beam at $\xi = \ell_a$ when the absorber natural frequency changes from the smallest adjustable value $f_a = 6.6$ Hz to the largest adjustable value $f_a = 13.5$ Hz. The anti-resonance frequency varies when the absorber frequency changes and follow the absorber frequency. It can be seen when the absorber natural frequency is $f_a = 6.6$ Hz, the anti-resonance frequency is very close to the resonance frequency, the exciting frequency is very sensitive, but with a variable stiffness absorber, the anti-resonance frequency can be changed when the exciting frequency drifts.

The Runge-Kutta method of 4th order with fixed step size 0.001 second is used to solve

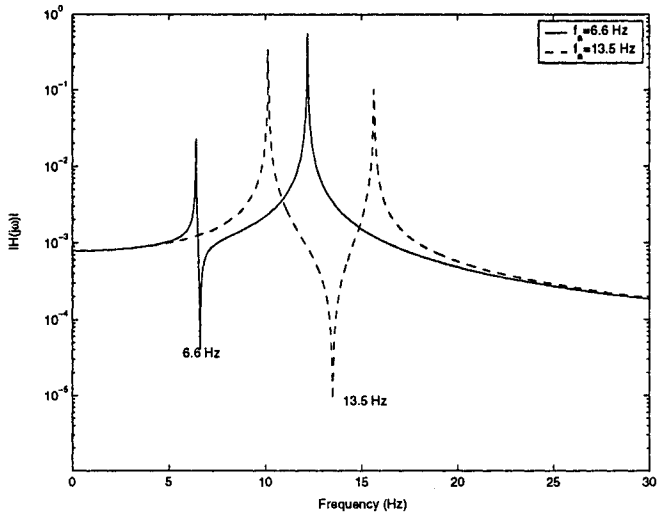

Figure 2.13: Frequency response of the primary beam at $\xi = \ell_a$ for various values of f_a

equation (2.27), assuming the initial condition $x(0) = 0$. Figure 2.14 shows the time responses of the primary beam at $\xi = \ell_a$ and the absorber mass when the absorber frequency is tuned to be equal to the natural frequency of the primary system 11.79 Hz. It can be seen that the vibration of the primary beam at $\xi = \ell_a$ is very small while the vibration of the absorber mass is significantly large.

Figure 2.15 shows the time response of the system when it is excited at the first natural frequency 9.73 Hz and the absorber frequency is $f_a = 11.79$ Hz. The vibrations of both the primary beam at $\xi = \ell_a$ and the absorber mass are significantly large. The absorber system does not provide any protection to the primary beam.

Figure 2.16 shows the time response of the system at the second resonance, i.e., the exciting frequency $f = 14.29$ Hz and the absorber frequency $f_a = 11.79$ Hz.

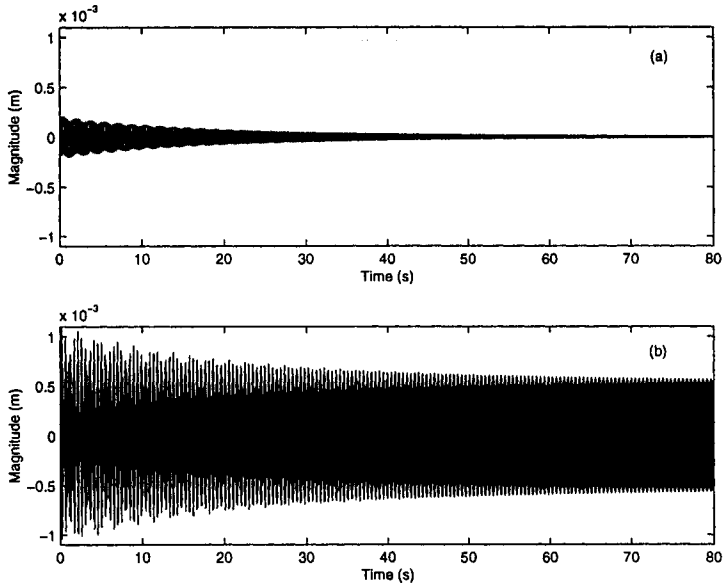

Figure 2.14: Time response when the absorber frequency equals the exciting frequency $f = 11.79$ Hz: (a) $w(\ell_s, t)$; (b) $u_a(t)$

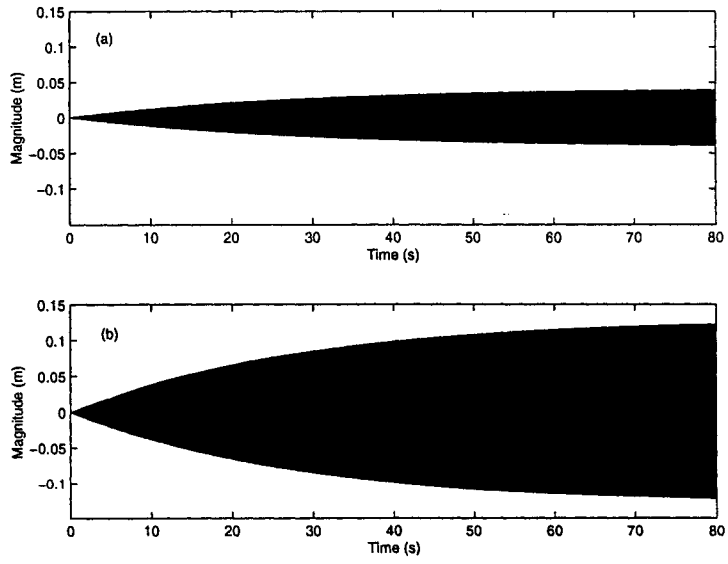

Figure 2.15: Time response at the first resonance: (a) $w(\ell_s, t)$; (b) $u_a(t)$

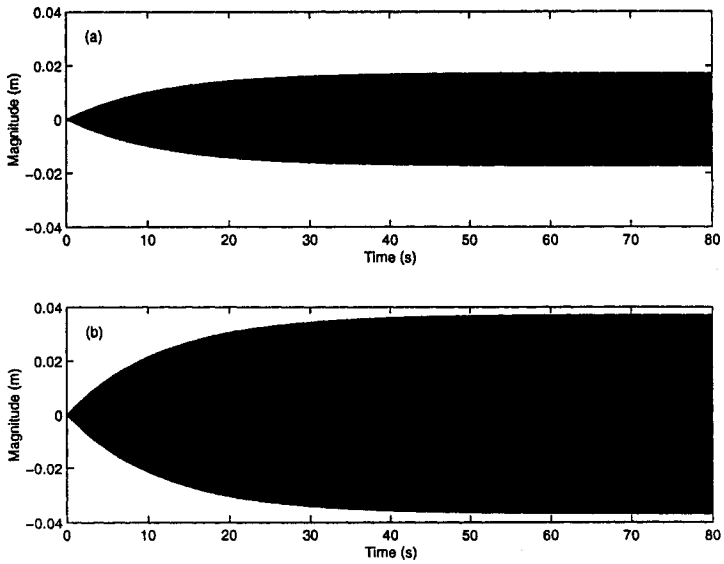

Figure 2.16: Time response at the second resonance: (a) $w(\ell_s, t)$; (b) $u_a(t)$

2.4 Design of Auto-Tuning and Simulation

In this section, an auto-tuning algorithm is developed. To this end, a simplified 2-DOF model is used. As shown previously, within the range of the absorber frequency variation, the system behaves strongly like a 2-DOF system. The 2-DOF system used in the following study is shown in Figure 2.17. The primary beam and the absorber mass is replaced by a lumped-parameter 1-DOF system. The mass m is given by

$$m = m_b + m_f = 1.6354\ kg.$$

The stiffness k is obtained by finding the equivalent stiffness of a clamped-clamped beam [15]

$$k = \frac{192EI}{\ell^3} = 6426\ N/m.$$

The damping value is chosen to be

$$c = 2\zeta\sqrt{km} = 1.025\ kg/s$$

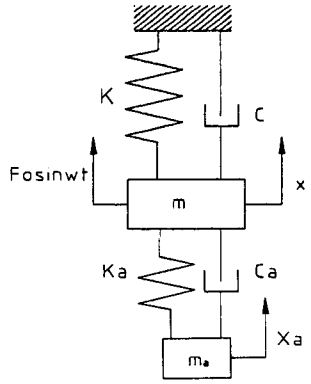

Figure 2.17: Simplified 2-DOF model

where $\zeta = 0.005$. The natural frequency of the primary system is

$$\omega_p = \sqrt{\frac{k}{m}} = 62.2842\ rad/s \quad or \quad f_p = 9.976\ Hz$$

The damping value of the absorber system is calculated by

$$c_a = 2\zeta_a m_a \omega_p = 0.111\ kg/s$$

where ζ_a is assumed to be 0.005.

2.4.1 Auto-Tuning Algorithm

The objective of auto-tuning is to automatically adjust the stiffness of the absorber such that $f_a = f$. The exciting frequency f will be determined by using the response of the primary mass. The proposed tuning method contains the following steps:

1. Sample the response x of the primary system over a specified time period at a sampling interval Δt. The time period of each group of the data is chosen to be $T = 2^n \Delta t$ where n is an integer such as 10 or 11.

2. Obtain the spectrum of the response by applying the FFT to the sampled responses and find the frequency corresponding to the maximum magnitude of the spectrum. Let this frequency be the new measured exciting frequency f^{new}.

3. Compare f^{new} with the absorber frequency f_a determined in the last iteration, if $|f^{new} - f_a| > tol$, where tol is a prescribed frequency tolerance, let the absorber frequency $f_a = f^{new}$, go to step 4. Otherwise keep f_a unchanged, go to step 1.

4. Calculate a new absorber stiffness $k_a^{new} = (2\pi f_a)^2 m_a$, update k_a with k_a^{new} and go to step 1.

2.4.2 Computer Simulation

In this section Simulink is used to implement the dynamic simulation. For building up the Simulink model, the equations of motion of the 2-DOF system as shown in Figure 2.17 should be known first and are given in a matrix form as

$$\begin{bmatrix} m & 0 \\ 0 & m_a \end{bmatrix} \begin{bmatrix} \ddot{x} \\ \ddot{x}_a \end{bmatrix} + \begin{bmatrix} c + c_a & -c_a \\ -c_a & c_a \end{bmatrix} \begin{bmatrix} \dot{x} \\ \dot{x}_a \end{bmatrix} + \begin{bmatrix} k + k_a & -k_a \\ -k_a & k_a \end{bmatrix} \begin{bmatrix} x \\ x_a \end{bmatrix} = \begin{bmatrix} F_0 \sin \omega t \\ 0 \end{bmatrix}. \tag{2.30}$$

Rearranging equations (2.30), the expression of $\ddot{x}$ and $\ddot{x_a}$ are obtained as below

$$\ddot{x} = \frac{1}{m}[-(c + c_a)\dot{x} + c_a\dot{x}_a - (k + k_a)x + k_a x_a + F_0 sin\omega t]$$

and

$$\ddot{x}_a = \frac{1}{m_a}(c_a\dot{x} - c_a\dot{x}_a + k_a x - k_a x_a).$$

Figure 2.18 is the Simulink model of the 2-DOF absorber system. The main block is a 2-D system that is based on equation (2.30).

In Figure 2.18, the generator produces sinusoidal exciting force which is used as the disturbance to the system. The absorber stiffness k_a is variable based upon the change of the measured exciting frequency from the FFT subsystem. The FFT subsystem is a S function block which is used to measure the exciting frequency here. The entire system consists of two timer tasks [3], one operates with a fast sampling time and the other one operates with a slow sampling time. The base sampling time of the FFT subsystem is 0.001 second. Figure 2.19 illustrates the FFT Subsystem. A S-Function block "buffer2048" is used to collect a group of data in a specified period. The sampling time of "buffer2048" block

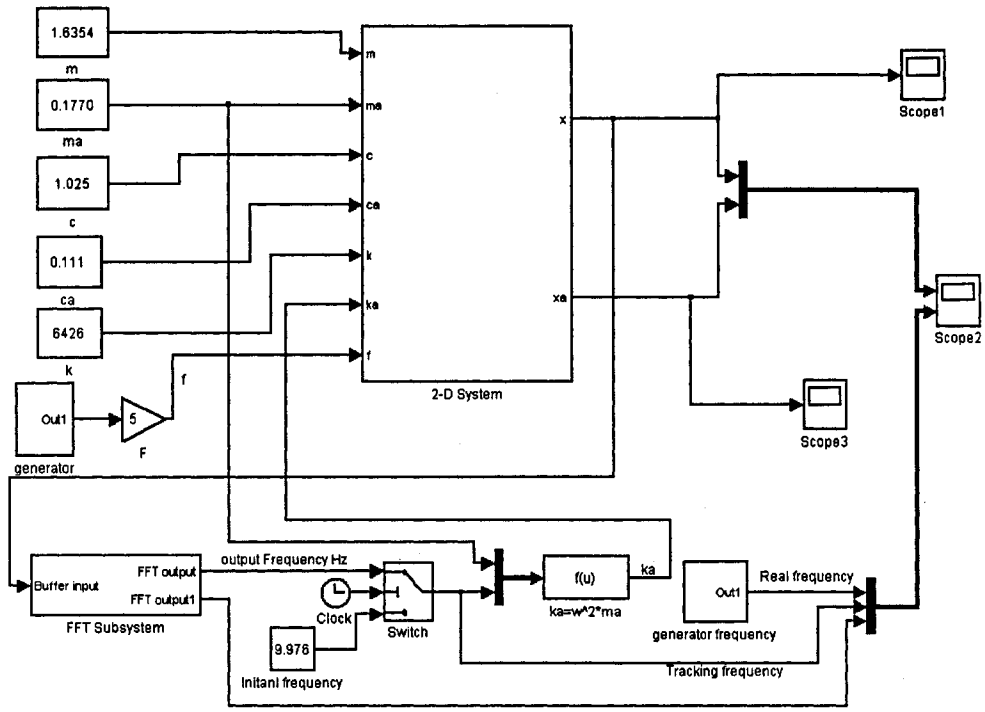

Figure 2.18: Simulink Model of the absorber system

is 0.001 second. A *Zero-Order Hold* block with a sampling time $\Delta t = 0.001$ second is used in front of "buffer2048" to discretize the response. A S-function block "fft2048tol" is used to execute the FFT computation. A *Zero-Order Hold* block with a sampling time of 2.048 seconds is inserted between "buffer2048" and "fft2048tol". Therefore, block "fft2048tol" is executed every 2.048 seconds. Overall, the execution time for the FFT subsystem is 2.048 seconds. The "FFT output" of "fft2048tol" block is the absorber frequency. The value is fed back to the input of the block "fft2048tol" via a *Unit Delay* with a sampling time of 2.048 seconds, the "FFT output1" is the measured exciting frequency. The FFT subsystem function is implemented by Multiple Timer Task Mode [?]. In the multiple timer task mode, each sample time forms a separate timer task and these timer tasks can interrupt each other. If data vectors are transferred directly between blocks with different sample times (called sample-rate transition), data inconsistency could result. Because of this data inconsistency the blocks that are executed with different sample times cannot be directly

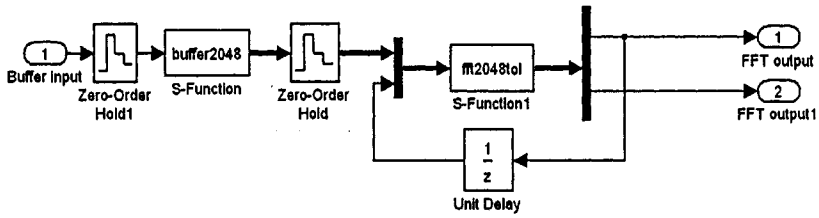

Figure 2.19: FFT Subsystem

connected. Instead, a special block needs to be inserted into such a connection: the *Zero-Order Hold* block for a fast-to-slow sample-rate transition and the *Unit Delay* block for a slow-to-fast sample-rate transition. As shown in Figure 2.19, the *Zero-Order Hold* between "buffer2048" and "fft2048tol" is used for a fast-to-slow sample-rate transition.

2.4.3 Tracking a Step Change in the Exciting Frequency

The motivation of this test is to verify the tuning capability of the absorber based on the measured exciting frequency. The absorber natural frequency is initially set to be 9.976 Hz which equals to the exciting frequency. Note that this frequency is the natural frequency of the primary system without the absorber mass. At the time of 10 second, the exciting frequency is changed to $f = 8.47$ Hz which is the first natural frequency of the entire system.

Figure 2.20 shows the response of the primary mass when the absorber natural frequency remains unchanged at 9.976 Hz or the tuning is not activated. The amplitude of the response increases significantly after the exciting frequency varies because the system is excited at resonance.

Figure 2.21 shows the frequency tracking when the frequency tolerance is chosen to be tol=1.5 Hz. The first period of 2.048 seconds is the time needed to determine the exciting frequency. During this period, the transient response is dominant in the response. The measured exciting frequency provided by the FFT subsystem is not the real exciting frequency, but one of the natural frequencies of the entire system. During the second FFT execution period, as the system vibrates at a steady state, therefore after 4.096 seconds the measured

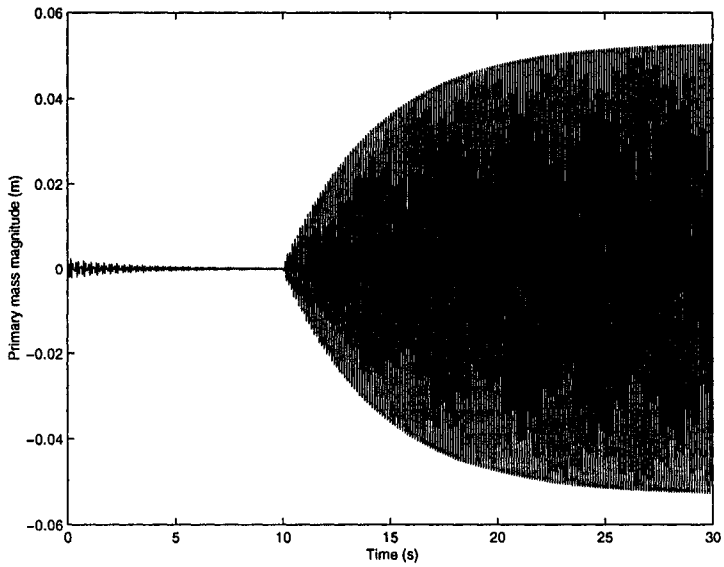

Figure 2.20: Time response of the primary mass with a constant absorber frequency when the exciting frequency experiences a step change

exciting frequency is about 10.25 Hz which is close to the real exciting frequency 9.976 Hz. Note that FFT computation only can give an approximate result. The accuracy of the measured exciting frequency depends on the number of FFT samples, the more the samples, the more accurate the measured exciting frequency. It can be seen that the absorber frequency does not change after the measured exciting frequency is determined, because the change of the measured exciting frequency is less than the frequency tolerance 1.5 Hz.

Figure 2.22 shows the FFT spectrum during the periods from 2.048 to 4.096 second (1) and from 4.096 to 6.144 second (2).

Figure 2.23 shows the frequency tracking when the frequency tolerance is chosen to be tol=1.46 Hz. The first two FFT execution periods are the same as when the frequency tolerance is chosen to be 1.5 Hz. After the real exciting frequency is determined, because the frequency tolerance 1.46 Hz is less than the change of the measured exciting frequency, the absorber frequency follows the measured exciting frequency. However, after the absorber frequency is adjusted to the measured exciting frequency, a transient response is induced. The measured exciting frequency provided by the FFT subsystem from 6.144 second to

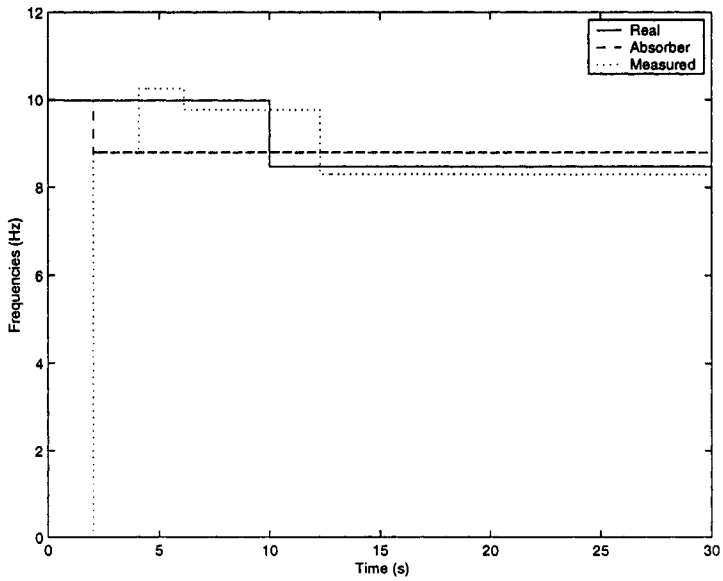

Figure 2.21: Frequency tracking when the exciting frequency experiences a step change: tol=1.5 Hz

8.192 second is first natural frequency of the entire system because the transient response is dominant in the response. Because the frequency tolerance tol=1.46 Hz is less than the change of the measured exciting frequency during this period, the absorber frequency is adjusted to the measured exciting frequency. This phenomenon repeats in the simulation, therefore the system is not stable because the frequency tolerance is too small.

Figure 2.24 shows the FFT spectrum during the periods from 2.048 to 4.096 second (1), from 4.096 to 6.144 second (2), from 6.144 to 8.192 second (3) and from 8.192 to 10.24 second (4).

Figure 2.25 shows the frequency tracking when the frequency tolerance is chosen to be tol=1.47 Hz. With this frequency tolerance, during the period from 6.144 second to 8.192 second, the frequency tolerance is greater than the change of the measured exciting frequency, the absorber frequency keeps unchanged. The measured exciting frequency provided by the FFT subsystem is one of the natural frequencies of the entire system as the transient response is dominant in the system. At the time of 10 second the real exciting frequency is changed into 8.47 Hz. In about 2 seconds, the measured frequency is about 8.3 Hz which is close

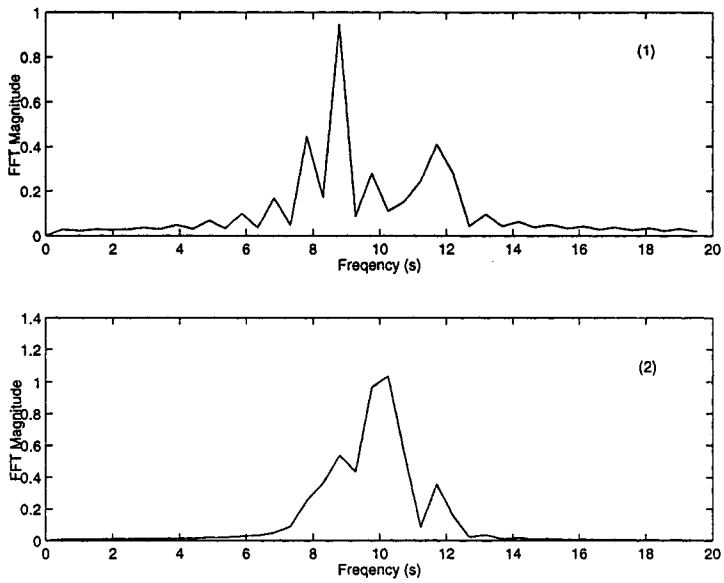

Figure 2.22: FFT of responses of the primary beam: tol=1.5 Hz

to the real exciting frequency. After the absorber frequency is adjusted to be equal to the measured exciting frequency, the transient response appears and is dominant in the system. This can be seen from the measured exciting frequency. However as the frequency tolerance is greater than the change of the measured exciting frequency, the absorber frequency keeps unchanged. Therefore the frequency tolerance tol=1.47 Hz is chosen to be the proper value for the frequency tolerance because 1.46 Hz does not work and 1.5 Hz is too large.

Figure 2.26 shows the FFT spectrum during the periods from 2.048 to 4.096 second (1), from 4.096 to 6.144 second (2), from 6.144 to 8.192 second (3) and from 14.336 to 16.384 second (4).

In Figure 2.27 and Figure 2.28 the time responses of the primary mass the absorber mass are shown. During the period of the first 10 seconds, the vibration of the primary mass is significantly small and the vibration of the absorber mass is large, because the absorber frequency is set to match the exciting frequency already. At the time of 10 second, the exciting frequency is changed to 8.47 Hz which is one of the natural frequencies of the entire system. The vibration of the primary mass keeps increasing significantly for around 2 seconds, which is the FFT execution time. After FFT subsystem determines the exciting

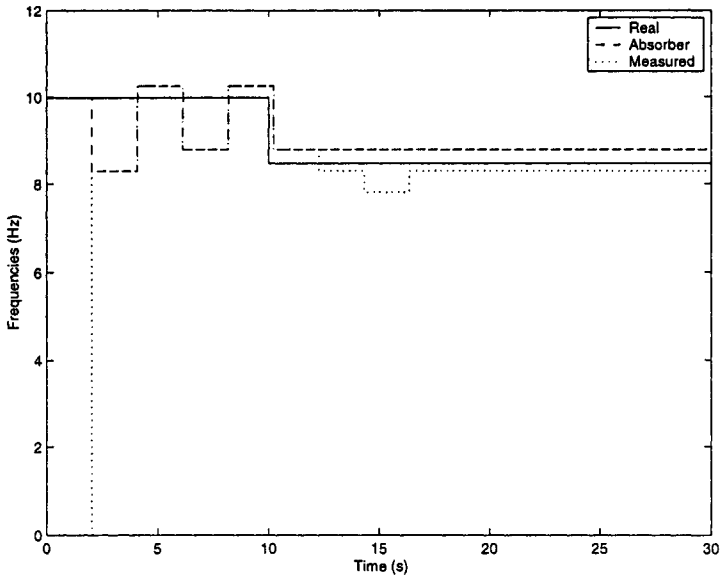

Figure 2.23: Frequency tracking when the exciting frequency experiences a step change: tol=1.46 Hz

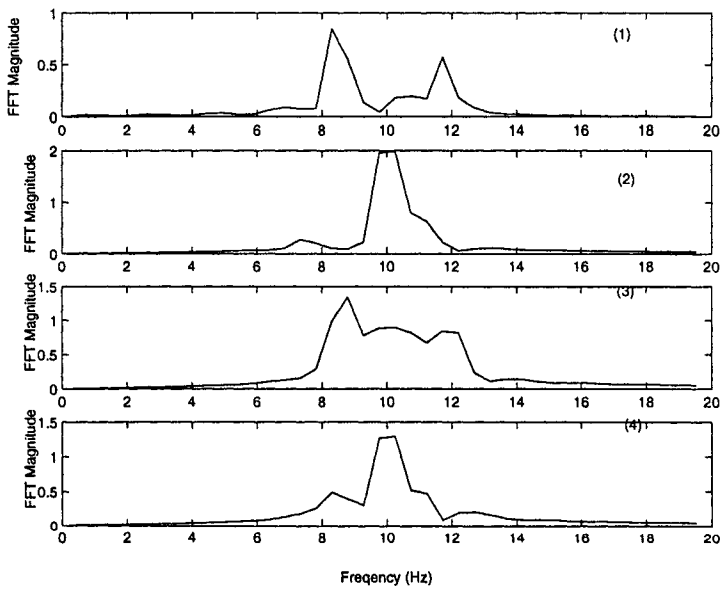

Figure 2.24: FFT of responses of the primary beam: tol=1.46 Hz

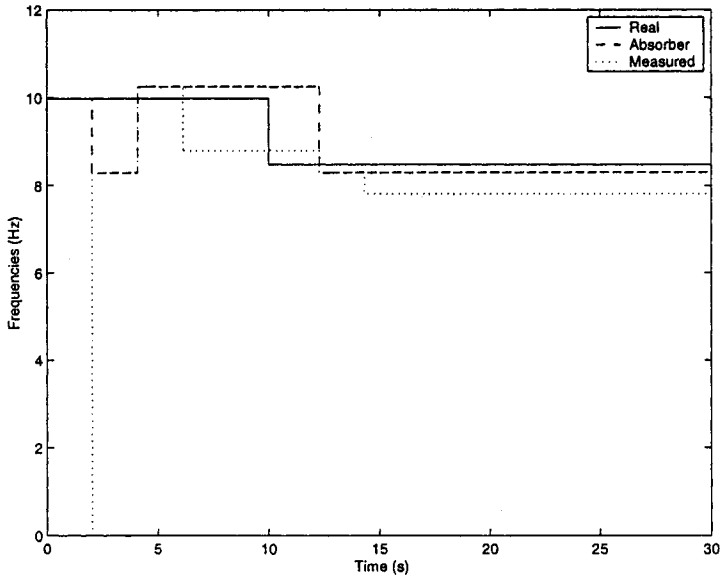

Figure 2.25: Frequency tracking when the exciting frequency experiences a step change: tol=1.47 Hz

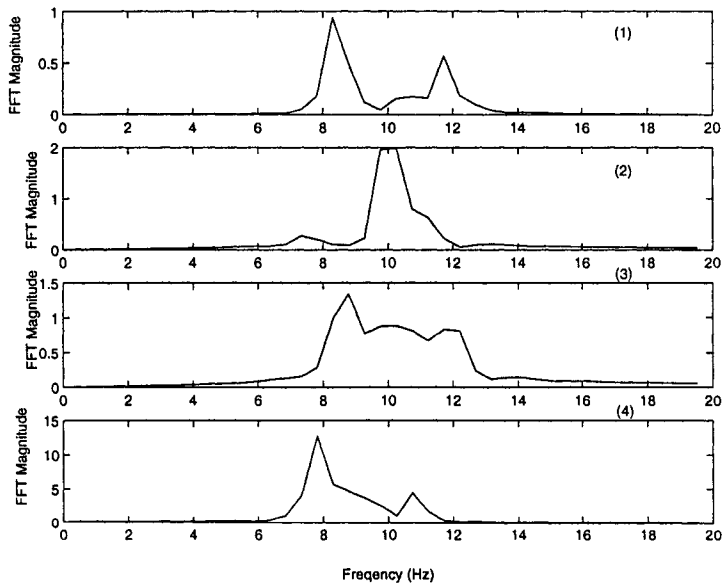

Figure 2.26: FFT of responses of the primary beam: tol=1.47 Hz

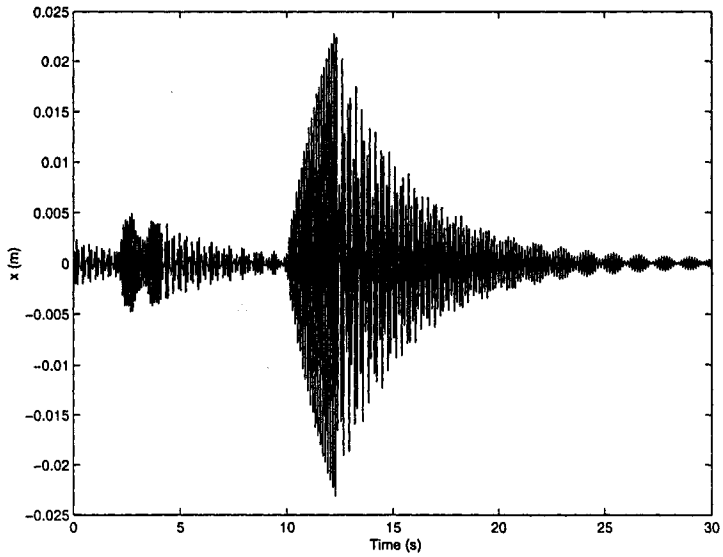

Figure 2.27: Time response of the primary mass when the exciting frequency experiences a step change

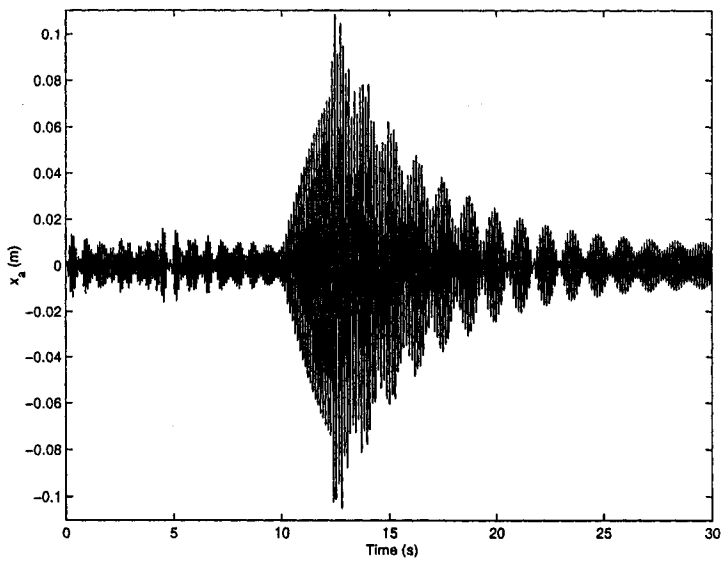

Figure 2.28: Time response of the absorber mass when the exciting frequency experiences a step change

frequency, the absorber frequency is tuned to match the measured exciting frequency. The vibration of the primary mass is decreased. It is noted that the vibration of the primary mass is not minimized because the absorber frequency is not exactly equal to the exciting frequency. But it can be seen that the vibration is reduced significantly after the absorber frequency is tuned.

Comparing Figure 2.20 and 2.27, with the control of the tunable absorber, the vibration of the primary mass is suppressed significantly when the exciting frequency varies here. For the purpose of comparison to the uncontrolled cases, a root mean squared value of the response is defined as

$$rms = \sqrt{\frac{\Sigma_{i=1}^{N} x^2(i)}{N}}$$

where N is the number of sampled or discretized responses during the period of interest. An attenuation index is defined as

$$Attenuation = 20 \log_{10} \frac{rms_{no\ control}}{rms_{control}}\ dB$$

The vibration attenuation of the primary mass is 15.5 dB.

Next, some simulation tests have also been carried out when 1024 samples are used for FFT computation or the execution time of the FFT subsystem is 1.024 seconds. Figure 2.29 shows the frequency tracking when the frequency tolerance is tol=1.47 Hz. The first period of 1.024 seconds is the time needed to determine the exciting frequency. During this period, the transient response is dominant in the response. The measured exciting frequency provided by the FFT subsystem is not the real exciting frequency, but one of the natural frequencies of the entire system. At the time of 1.024 second, the absorber frequency is adjusted to be the measured exciting frequency. Such an adjustment alters the natural frequencies of the entire system and induces some new transient responses. Therefore at the time $t = 2.048$ second, the FFT subsystem outputs a peak frequency which is not the exciting frequency, but one of the new natural frequencies of the entire system. After 3.072 seconds, as the response approaches a steady state, the measured exciting frequency is about 9.77 Hz which is close to the real exciting frequency 9.976 Hz. It can be seen that the absorber frequency does not change after the measured exciting frequency is determined, because the change of the measured exciting frequency 0.97 Hz is less than the frequency tolerance 1.47 Hz.

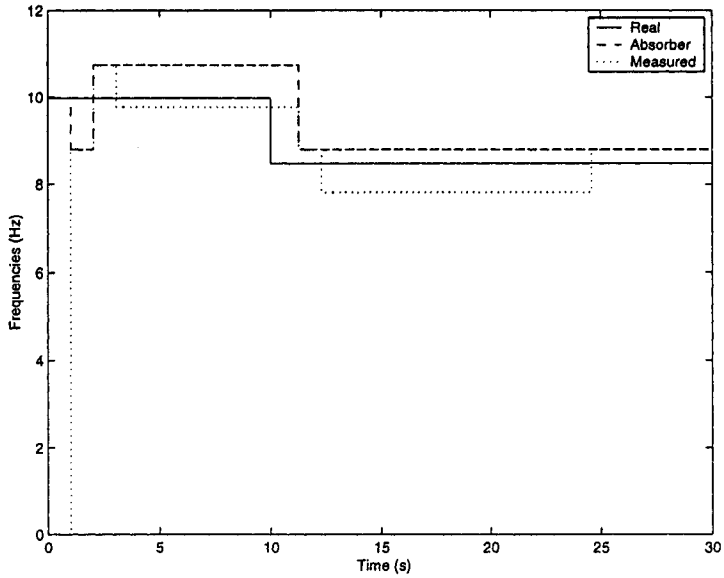

Figure 2.29: Frequency tracking when the exciting frequency experiences a step change: tol=1.47 Hz

Therefore, the frequency tolerance is chosen to be tol=0.9 Hz for another frequency tracking test.

Figure 2.30 shows the FFT spectrum during the periods from 2.048 to 4.096 second (1), from 4.096 to 6.144 second (2), from 6.144 to 8.192 second (3) and from 24.576 to 26.624 second (4).

Figure 2.31 shows the frequency tracking when the frequency tolerance is tol=0.9 Hz. After 3.072 seconds, the absorber frequency is adjusted to be equal to the measured exciting frequency. However, the transient response is induced and is dominant in the response during this period, the measured exciting frequency provided by the FFT subsystem is not the real exciting frequency, but one of the natural frequencies of the new entire system. It can be seen that every time when the absorber frequency is adjusted, the transient response appears and is dominant. Therefore the system is not stable when the frequency tolerance is chosen to be tol=0.9 Hz.

Figure 2.32 shows the FFT spectrum during the periods from 2.048 to 4.096 second (1), from 4.096 to 6.144 second (2), from 6.144 to 8.192 second (3) and from 8.192 to 10.24 second

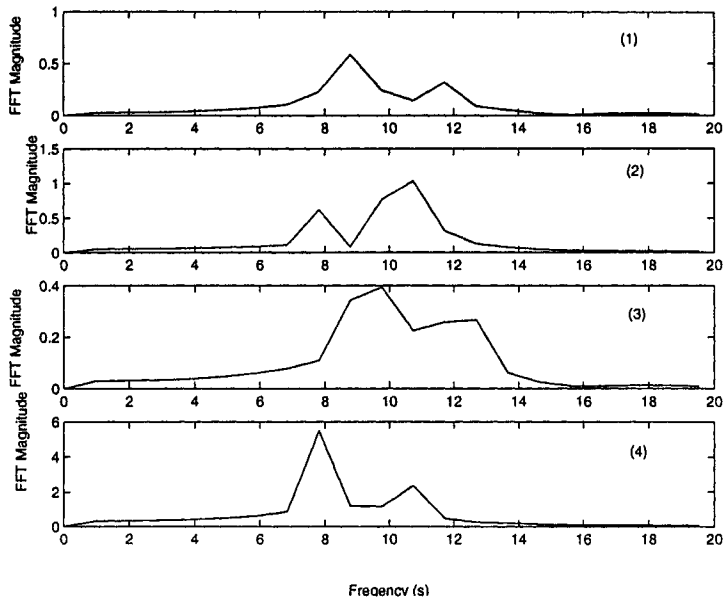

Figure 2.30: FFT of responses of the primary beam: tol=1.47 Hz

(4).

Figures 2.33 and 2.34 show the simulation results when the frequency tolerance is chosen to be tol=1.47 Hz and the number of samples for FFT is 1024. Figure 2.33 shows that the vibration amplitude reduction of the primary system more effective than the one when the FFT execution time is 2.048 seconds. This can be explained in Figure 2.29, which shows the FFT computation time is shorter, so that suppression of the primary system can be carried out faster. However, the difference between the measured exciting frequency and the real exciting frequency is relatively large comparing with the one when the FFT execution time is 2.048 seconds. When the FFT execution time is 1.024 second, the accuracy of FFT computation result is worse than the result when the FFT execution time is 2.048 seconds. Therefore the shorter FFT execution time will reduce the accuracy of the FFT computation result, but increase the tuning speed.

Comparing Figure 2.20 and 2.33, with the control of the tunable absorber, the vibration of the primary mass is suppressed when the exciting frequency varies. The vibration attenuation achieved is 19.2 dB.

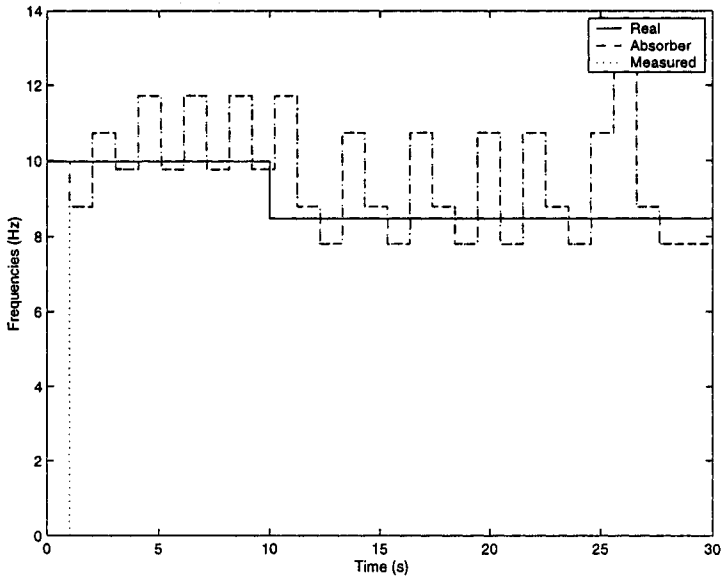

Figure 2.31: Frequency tracking when the exciting frequency experiences a step change: tol=0.9 Hz

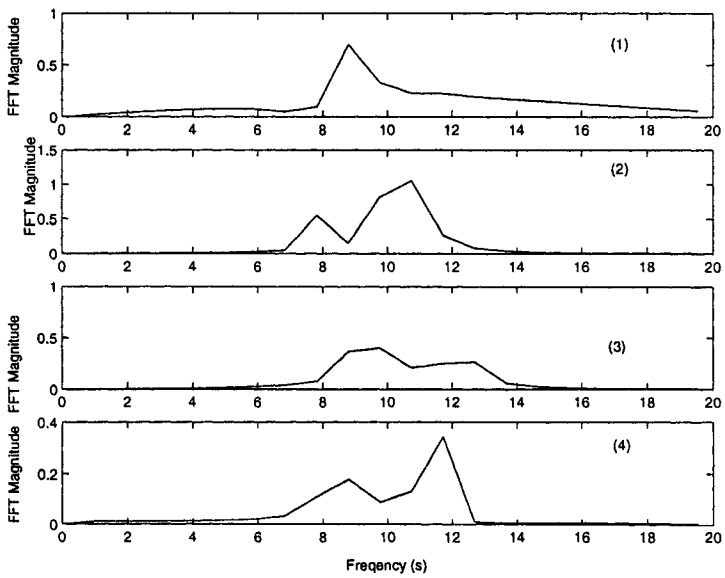

Figure 2.32: FFT of responses of the primary beam: tol=0.9 Hz

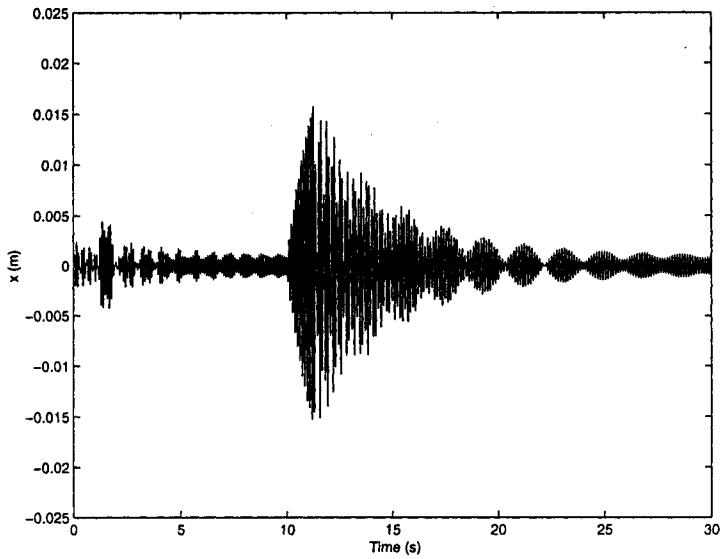

Figure 2.33: Time response of the primary mass when the exciting frequency experiences a step change

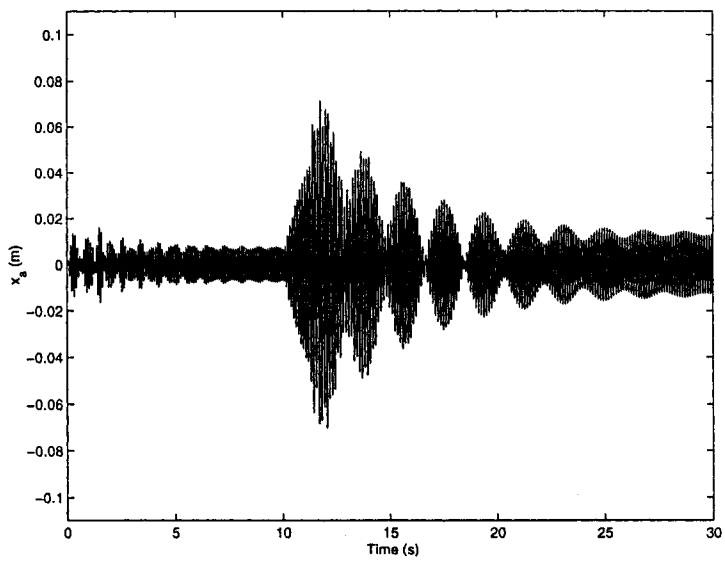

Figure 2.34: Time response of the absorber mass when the exciting frequency experiences a step change

2.4.4 Tracking a Linear Change in the Exciting Frequency

For this test, the absorber natural frequency is initially set to be 9.976 Hz which equals to the exciting frequency. Note that this frequency is the natural frequency of the primary system without the absorber mass. At the time of 10 second, the exciting frequency is changed linearly from 9.976 Hz to 8.47 Hz in a time interval of 10 seconds. Therefore at the time of 20 second, the exciting frequency becomes 8.47 Hz.

Figure 2.35 shows the response of the primary mass with the absorber natural frequency fixed at 9.976 Hz when the exciting frequency experiences the linear change. Figure 2.36

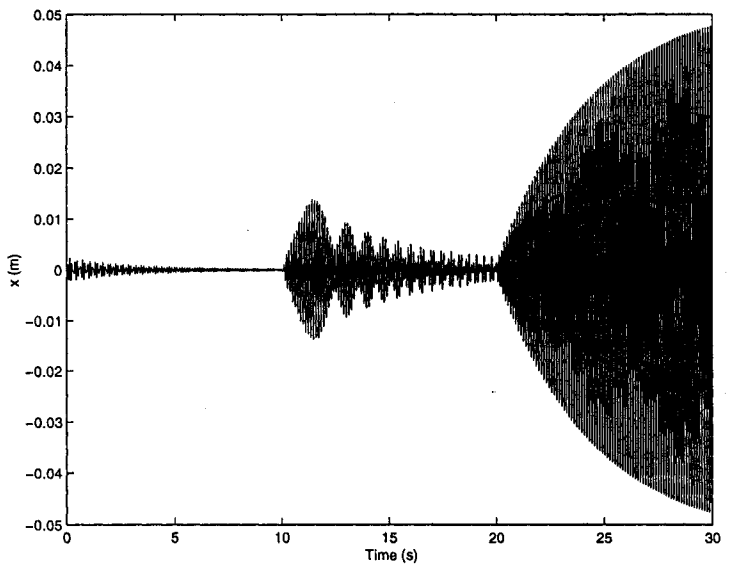

Figure 2.35: Time response of the primary mass with a fixed absorber when the exciting frequency experiences a linear change

shows the frequency tracking when the frequency tolerance is chosen to be tol=1.47 Hz. The first period of 2.048 seconds is the time needed to determine the exciting frequency. During this period, the transient response is dominant in the response. The measured exciting frequency provided by the FFT subsystem is not the real exciting frequency, but one of the natural frequencies of the entire system. During the second FFT execution period, as the response is close to a steady state, therefore after 4.096 seconds the measured exciting frequency is about 10.25 Hz which is close to the real exciting frequency 9.976

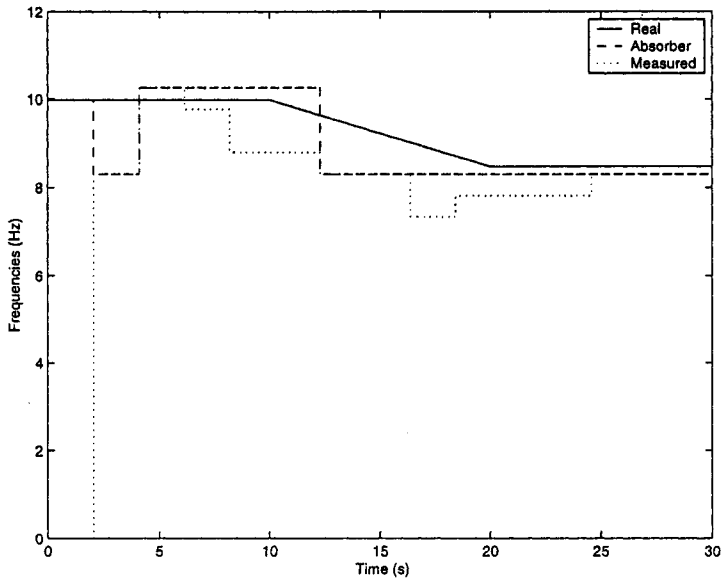

Figure 2.36: Frequency tracking when the exciting frequency experiences a linear change: tol=1.47 Hz

Hz. After 6.144 seconds, the measured exciting frequency changes slightly, but within the frequency tolerance, the absorber frequency keeps unchanged. During the period of the linear change from 10 second to 20 second, the absorber frequency does not follow the real exciting frequency. But after 20 seconds, the absorber frequency follows the exciting frequency again.

Figure 2.37 shows the response of the primary mass. It can be seen that, from 10 to 20 second the response is close to the uncontrolled case (Figure 2.35) and after $t = 20$ second, the response is suppressed. Comparing Figure 2.35 and 2.37, with the control of the tunable absorber, the vibration attenuation of the primary mass achieved during the entire period is 14.3 dB. The vibration attenuation achieved during the linear change period which is from 10 second to 20 seconds is -0.6 dB. Figure 2.38 shows the corresponding response of the absorber mass when the exciting frequency experiences the linear change.

In the above test, as the frequency tolerance used was big, the absorber frequency did not follow the measured exciting frequency. In the following test, a smaller frequency tolerance is used. Figure 2.39 shows the frequency tracking when the frequency tolerance is chosen to be tol=0.4 Hz. It can been seen that the measured exciting frequency is not stable. The

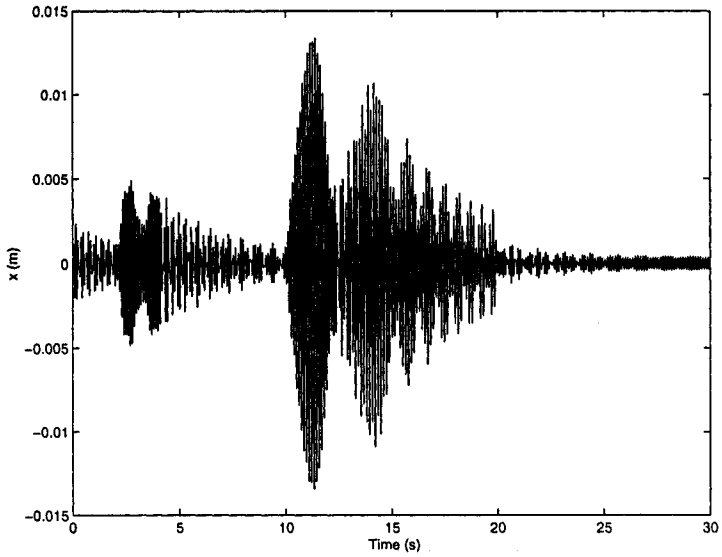

Figure 2.37: Time response of the primary mass when the exciting frequency experiences a linear change

frequency tolerance is small so that the absorber frequency is equal to the measured exciting frequency. Every time when the absorber frequency is adjusted, the transient response is induced. The measured exciting frequency provided by the FFT subsystem is one of the natural frequencies of the new entire system.

Figure 2.40 shows the response of the primary mass when the exciting frequency experiences the linear change with the frequency tolerance tol=0.4 Hz. It can be seen that the vibration attenuation is not acceptable for the period after $t = 20$ second. Comparing Figure 2.35 and 2.40, with the control of the tunable absorber, the vibration attenuation of the primary mass achieved during the entire period is 17.5 dB. The vibration attenuation achieved during the linear change period which is from 10 second to 20 seconds is 4.3 dB. Figure 2.41 shows the corresponding response of the absorber mass.

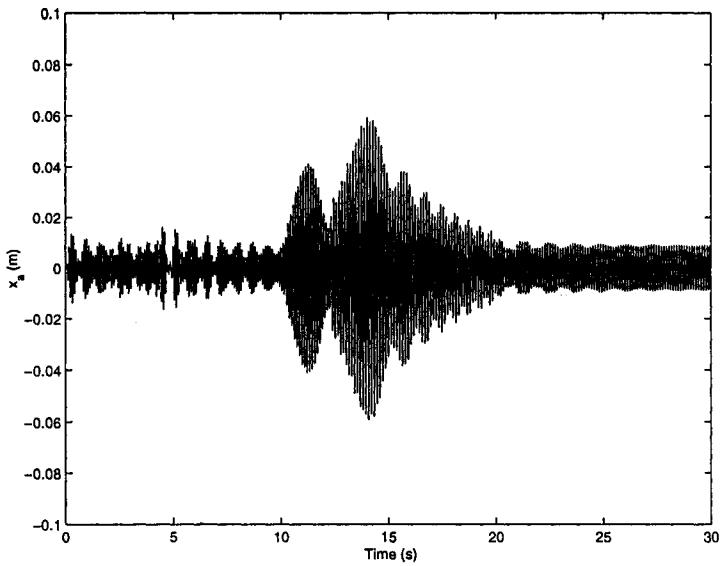

Figure 2.38: Time response of the absorber mass when the exciting frequency experiences a linear change

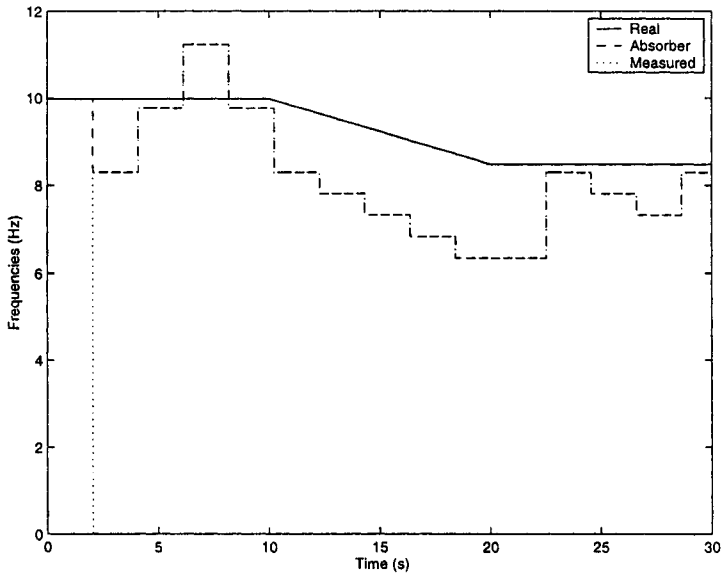

Figure 2.39: Frequency tracking when the exciting frequency experiences a linear change: tol=0.4 Hz

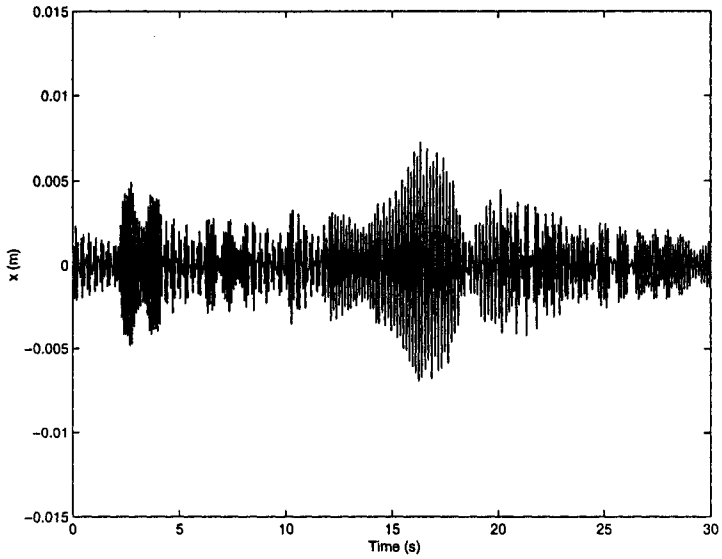

Figure 2.40: Time response of the primary mass when the exciting frequency experiences a linear change

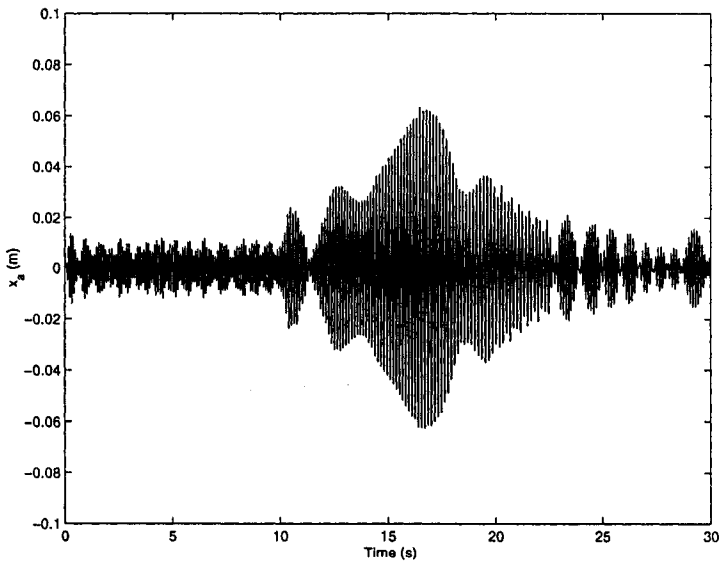

Figure 2.41: Time response of the absorber mass when the exciting frequency experiences a linear change

Next, some simulation tests have also been carried out when 1024 samples are used for FFT computation or the execution time of the FFT subsystem is 1.024 seconds. Figure 2.42 shows the frequency tracking when the frequency tolerance is tol=1.47 Hz. The first period of

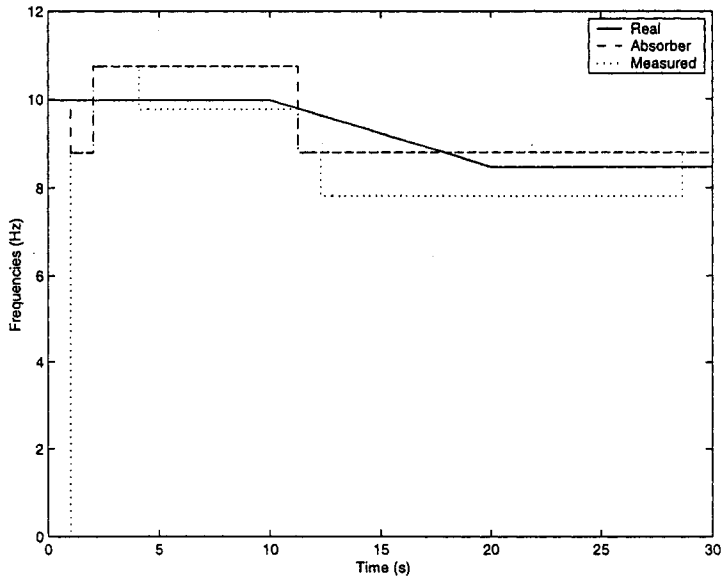

Figure 2.42: Frequency tracking when the exciting frequency experiences a linear change: tol=1.47 Hz

1.024 seconds is the time needed to determine the exciting frequency. During this period, the transient response is dominant in the response. The measured exciting frequency provided by the FFT subsystem is one of the natural frequencies of the entire system. During the second FFT execution period, as the response is at a steady state, therefore after 2.048 seconds the measured exciting frequency is about 10.75 Hz. After 4.096 seconds, the measured exciting frequency becomes closer to the real exciting frequency. Because the change is within the frequency tolerance, the absorber frequency is not updated. During the period from 10 second to 20 second, the absorber frequency does not follow the real exciting frequency. After 20 seconds, the absorber frequency is close to the exciting frequency.

Figure 2.43 shows the corresponding time response of the primary mass. It can be seen that from 10 to 20 second, the vibration suppression is not significant. After $t = 20$ second, the response demonstrates a beat phenomenon indicating the response is mainly composed

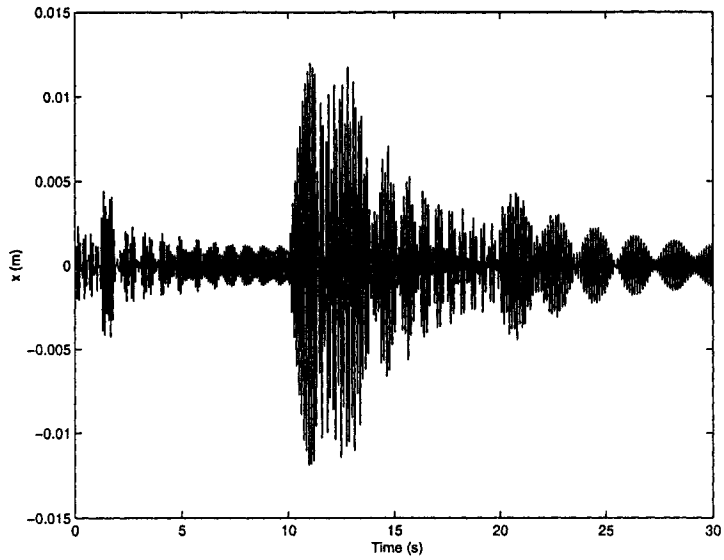

Figure 2.43: Time response of the primary mass when the exciting frequency experiences a linear change

of two frequencies: the exciting frequency and one of the natural frequencies. Comparing Figure 2.35 and 2.43, with the control of the tunable absorber, the vibration attenuation achieved is 14.8 dB. The vibration attenuation achieved during the linear change period which is from 10 second to 20 seconds is 0.2 dB. Figure 2.44 shows the corresponding time response of the absorber mass.

The following simulation examines the case when a smaller frequency tolerance is used. From Figure 2.42, after 4.096 seconds, the change of the measured exciting frequency is about 0.98 Hz. Therefore the frequency tolerance is chosen to be tol=0.97 Hz. Figure 2.45 shows the frequency tracking when the frequency tolerance is chosen to be tol=0.97 Hz. It can been seen that the measured exciting frequency is not stable. The frequency tolerance is small so that the absorber frequency is updated. Every time the absorber frequency is adjusted, the transient response is excited. When the transient response is stronger than the steady state response, the FFT subsystem fails to identify the exciting frequency.

Figure 2.46 shows the response of the primary mass when the frequency tolerance tol=0.97 Hz is used. Figure 2.47 shows the corresponding response of the absorber mass.

Comparing Figure 2.35 and 2.46, with the control of the tunable absorber, the vibration

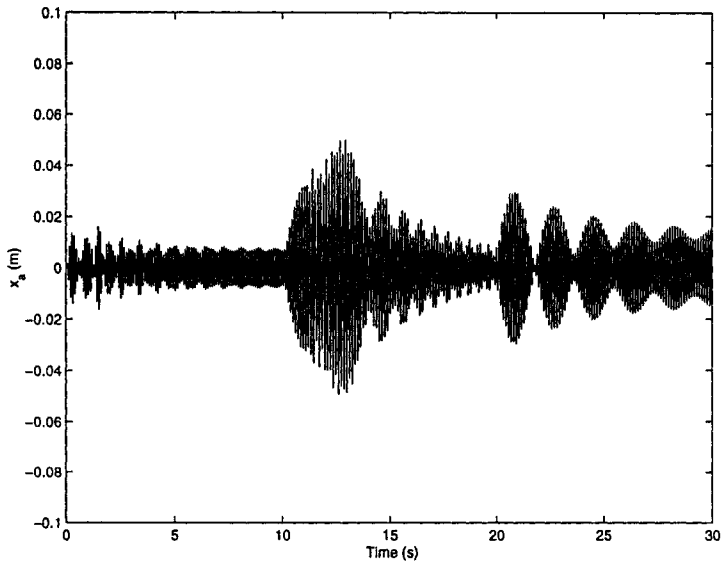

Figure 2.44: Time response of the absorber mass when the exciting frequency experiences a linear change

attenuation achieved during the entire period is 12.5 dB. The vibration attenuation achieved during the linear change period which is from 10 second to 20 seconds is -2.3 dB.

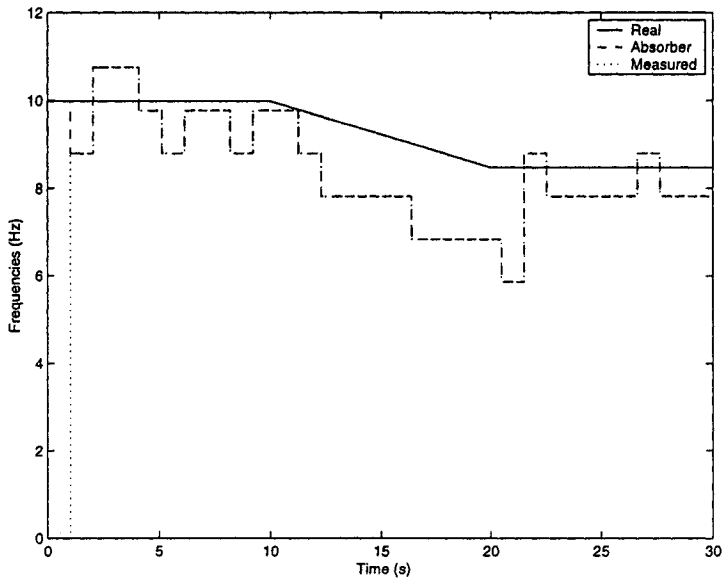

Figure 2.45: Frequency tracking when the exciting frequency experiences a linear change: tol=0.97 Hz

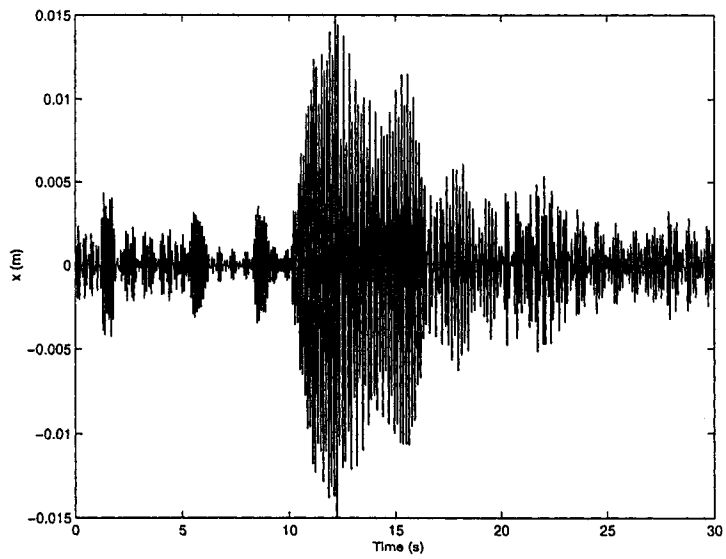

Figure 2.46: Time response of the primary mass when the exciting frequency experiences a linear change

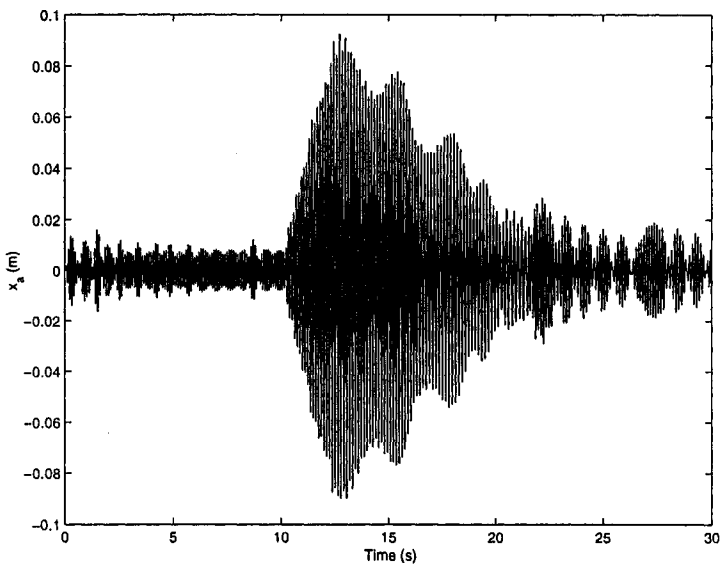

Figure 2.47: Time response of the absorber mass when the exciting frequency experiences a linear change

Chapter 3

Experimental Study of a Variable Stiffness Vibration Absorber

In order to validate the auto-tuning method developed in the previous chapter, an experimental study has been carried out. This chapter presents the experimental results.

3.1 Description of the Experimental System

An experimental system has been developed. The entire system consists of 3 subsystem: a clamped-clamped beam, a tunable absorber system, and a computer control system, as shown in Figure 3.1.

The computer which is used to control the system is a Pentium III with a speed of 550MHZ processor and 192 MB RAM. The Data Acquisition (DAQ) Board board is DS1102 Digital Signal Processor (DSP) controller board from dSPACE. The DS1102 is based on the Texas Instruments TMS320C31 third generation floating-point DSP, which builds the main processing unit, providing fast instruction cycle time for numeric intensive algorithms. It contains 128K words memory fast enough to allow zero wait state operation. Several peripheral subsystems are implemented to support a wide range of digital signal processing applications. ControlDesk (dSpace) is used to interface between Matlab, Simulink and DS1102.

The acceleration signals are measured by the accelerometers. After amplified by the

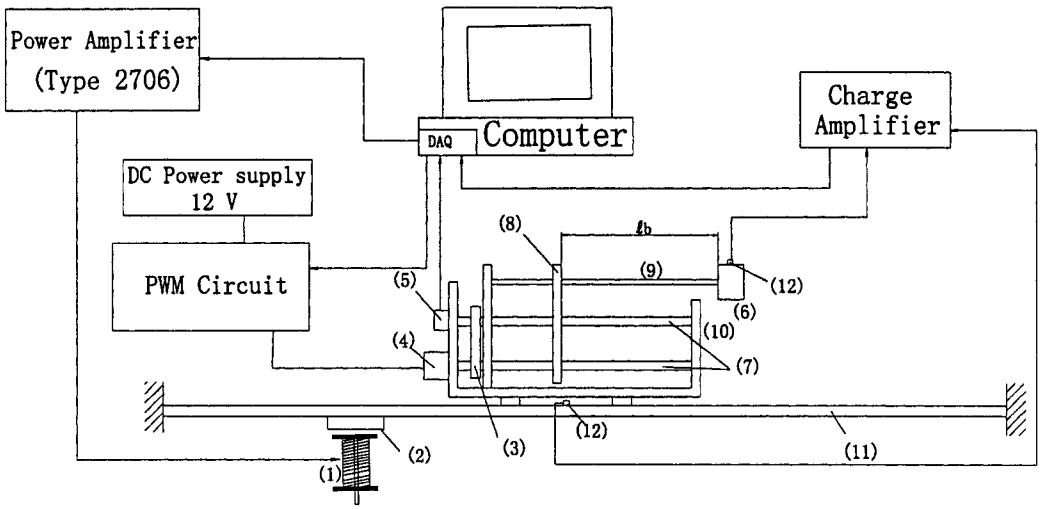

Figure 3.1: Schematic of the experimental system

(1) Electromagnetic shaker	(2) Permanent magnet	(3) Belt and pulley set
(4) DC motor	(5) Encoder	(6) Absorber mass
(7) Lead screw	(8) Movable support	(9) Absorber beam
(10) Absorber frame	(11) Primary beam	(12) Accelerometer

charge amplifier, the acceleration signals are input to channels ADC1 and ADC2 of the DAQ board. The acceleration signal of the primary beam is used to determine adjustment of the absorber beam length. The acceleration signal of the absorber mass is used for comparison. The motor is driven by a Pulse-Width Modulation (PWM) circuitry. A PWM signal is generated and output though channel CAP0 to the PWM circuit. Channel A and channel B of the encoder are connected to the non-inverted input channels Phi0, Phi90 of the DAQ board respectively. The inverted inputs Phi0/, Phi90/ and Index/ of the DAQ board are connected to 1.5V. Figure 3.2 shows how to generate the 1.5V voltage. The exciting signal is generated and output through channel DAC1 to the power amplifier to drive the non contact shaker. The non contact shaker is an electromagnet made of a Gauge 18 wire coil with a 1/2 inch low carbon steel bolt as the core. The electromagnet is driven by the power supply (B&K 2706). A permanent magnetic plate is glued to the bottom of the primary beam to interact with the magnetic force.

In order to produce a constant magnitude sinusoidal force, the dynamics of the electromagnetic circuit is studied. Figure 3.3 is the equivalent RL circuit of the electromagnetic

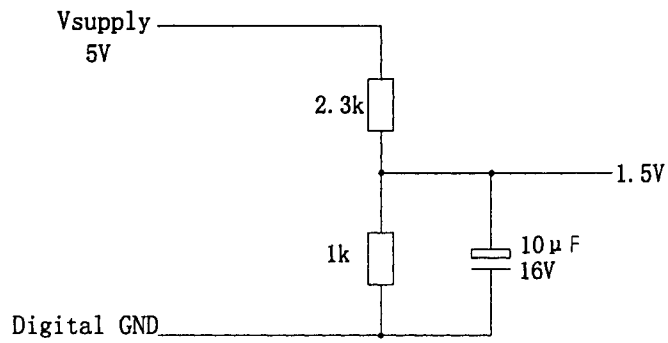

Figure 3.2: 1.5V generation for encoder

shaker system. The inductance of the coil is measured to be $L = 0.03$ H, the resistance

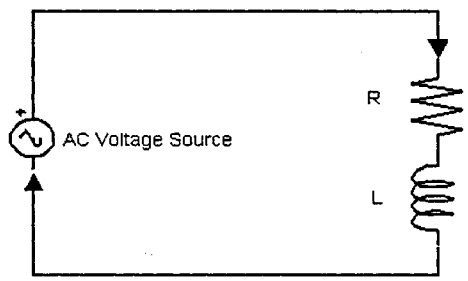

Figure 3.3: Electromagnetic shaker equivalent circuit

of the coil is $R = 2.9$ ohm and the AC voltage source is $u(t) = Asin\omega t$ V, where A is the voltage amplitude. Applying Kirchhoff's voltage law to the system yields

$$L\frac{di(t)}{dt} + Ri(t) = u(t)$$

where $i(t)$ is the current of the system. Taking Laplace transform of the above equation and assuming zero initial conditions yields

$$I(s) = \frac{U(s)}{sL(s) + R(s)}$$

where

$$u = Asin\omega t \Rightarrow U(s) = A\frac{\omega}{s^2 + \omega^2},$$

therefore

$$I(s) = \frac{A\omega}{(s^2+\omega^2)[sL(s)+R(s)]}.$$

Taking inverse Laplace transform of the above equation yields

$$i(t) = Icos(\omega t - \theta) + \frac{a}{L}e^{-\frac{R}{L}t}$$

where

$$I = \frac{A}{\sqrt{R^2+L^2\omega^2}} \tag{3.1}$$

is the steady-state amplitude of the current,

$$\theta = \tan^{-1}(\frac{R}{L\omega})$$

is the phase of the current and

$$a = \frac{L^2A\omega}{R^2+L^2\omega^2}.$$

From equation (3.1), it can be seen that when the frequency changes, the current amplitude will change if the voltage amplitude is constant. Roughly, the amplitude of the electromagnetic force is proportional to the amplitude of the current. Therefore in order to generate a constant amplitude force, the voltage amplitude must be adjusted when the frequency changes.

Figure 3.4 illustrates the signal generator subsystem. Based upon equation (3.1), the

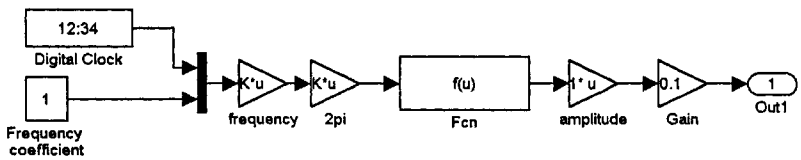

Figure 3.4: Signal generator subsystem in Simulink

function inside the *Fcn* block is $\sqrt{R^2+L^2u(2)^2}sin[u(1)]$ where $u(2)$ denotes the frequency ω and $u(1)$ denotes ωt. The *amplitude* block denotes the current amplitude I. Therefore through the signal generator system, a constant amplitude sinusoidal force can be provided.

3.2 Method of Auto-Tuning

The objective of an auto-tuning control is to position the movable plate such that the absorber frequency coincides with the exciting frequency, i.e., $\omega_a = \omega$. A two-step auto tuning strategy of the beam-absorber system is developed. It consists of a coarse tuning and a fine tuning.

The first step is coarse tuning which is developed based on the auto-tuning algorithm of computer simulation in Chapter 2. In the simulation the desired stiffness k_a is the variable parameter to be tuned and is obtained from the relation $k_a = (2\pi f_a)^2 m_a$. In the experiment, the desired stiffness k_a is implemented by changing the absorber beam length ℓ_b, therefore ℓ_b is the variable parameter to be tuned. As shown in Figure 3.5, the acceleration signal

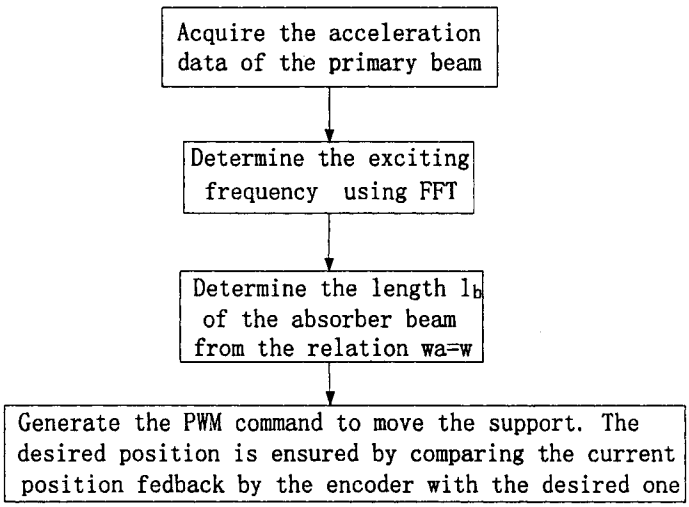

Figure 3.5: Flow chart of control (Coarse adjustment)

data are collected by the DAQ board, the auto-tuning algorithm from Chapter 2 is used here for the FFT computation to determine the exciting frequency. Using the measured exciting frequency and the relation between the exciting frequency and the absorber frequency $\omega_a = \omega$, the absorber beam length is determined from the relation between the absorber frequency and the absorber beam length. The absorber beam length is compared with the actual absorber beam length which is measured by the rotary encoder. The difference between the desired beam length and the actual one is used to generate a PWM command to the motor.

The motor is rotated until the length difference is equal to a prescribed tolerance.

The coarse adjustment may not be able to exactly bring the absorber frequency to be the exact exciting frequency. The reasons for this problem are: (1) the resolution of the FFT spectrum may not be small enough; (2) the frequency tolerance cannot be too small in order to avoid unsettling tuning; (3) the relation between the absorber frequency and beam length may not be very accurate. The fine tuning control is required.

The fine tuning process is shown in Figure 3.6. 2048 samples of acceleration signals of the

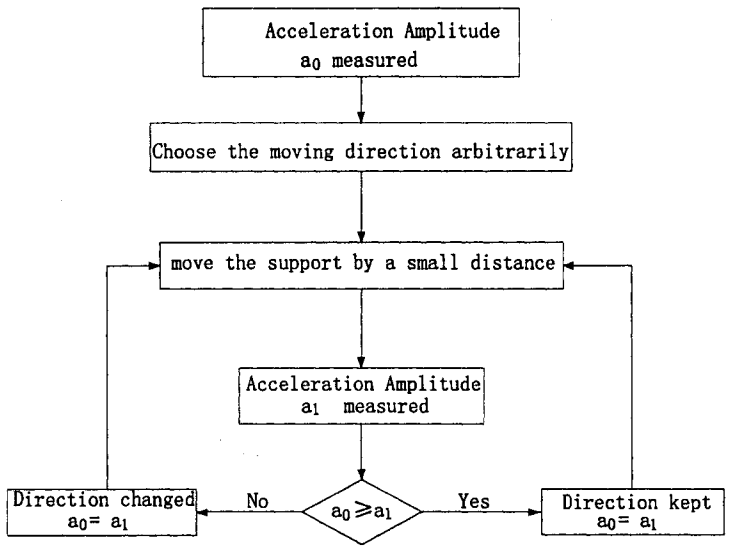

Figure 3.6: Flow chard control (Fine adjustment)

primary beam are collected, an average a_o of the absolute acceleration signals is computed. A moving direction is chosen arbitrarily. The movable support is moved by a small distance. Then a group of the acceleration signals is collected again. The average value a_1 of the absolute acceleration signals is computed. Compare a_0 with a_1, if $a_0 \geq a_1$, it means that the adjustment results in a reduction in vibration, let $a_0 = a_1$, the moving direction is kept and the support is moved again. The process repeats. If not, let $a_0 = a_1$, the moving direction is reversed and the support is moved again. The process repeats.

3.3 Simulink Model

Figure 3.7 is the Simulink Model of the control system which is built up based upon the simulation model used in Chapter 2. Acceleration signal data are input into the Simulink

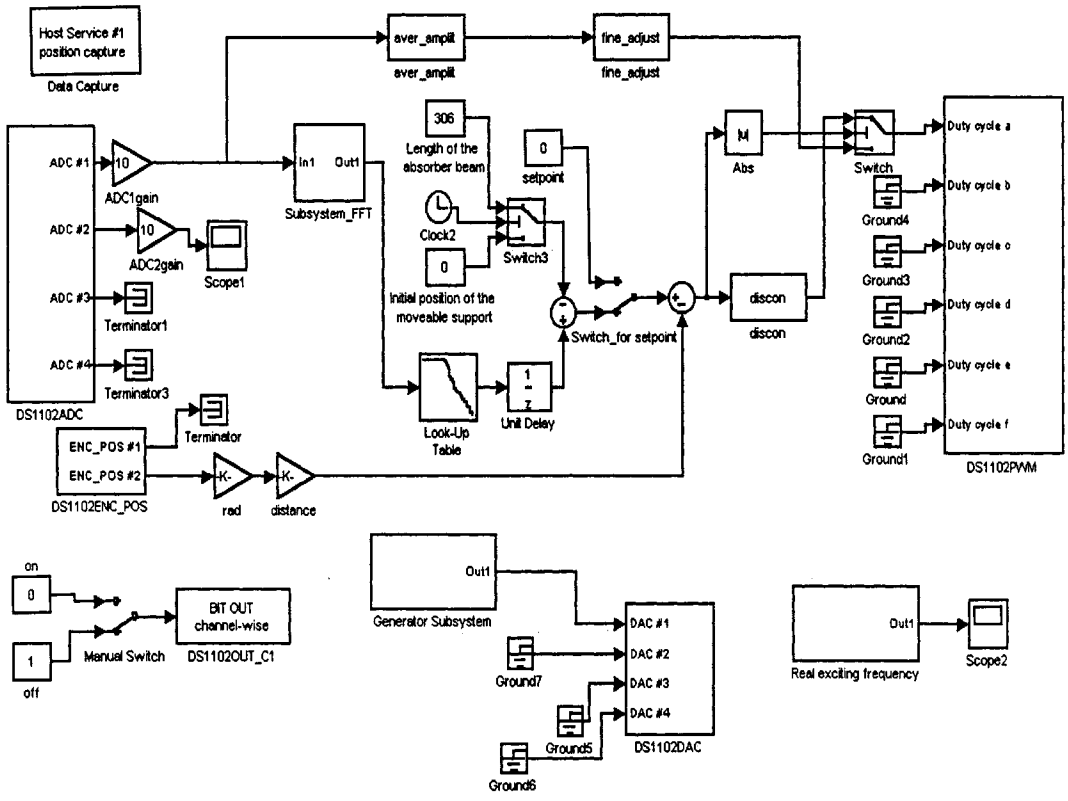

Figure 3.7: Simulink model of the control system

model from ADC #1 (signal from the primary beam) and ADC #2 (signal from the absorber mass). The sampled acceleration signals are fed into ADC1gain block to increase their amplitudes by 10 times before they are input into FFT subsystem block for the FFT computation. Figure 3.8 shows the subsystem of FFT. A S-Function block "buffer2048" is used to collect a group of data in a specified period. The sampling time of "buffer2048" block is 0.001 second. A S-function block "fft2048tol" is used to execute the FFT computation. A *Zero-Order Hold* block with a sampling time of 2.048 seconds is inserted between "buffer2048" and "fft2048tol". Therefore, block "fft2048tol" is executed every 2.048 sec-

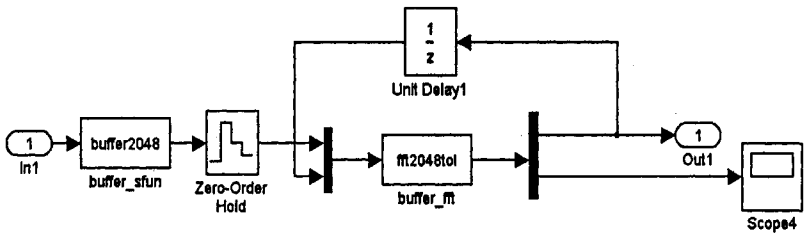

Figure 3.8: FFT subsystem

onds. Overall, the execution time for the FFT subsystem is 2.048 seconds. The "output1" of "fft2048tol" block is the absorber frequency. The value is fed back to the input of the block "fft2048tol" via a *Unit Delay* with a sampling time of 2.048 seconds, the other output of "fft2048tol" is the measured exciting frequency. The output of the FFT subsystem is the desired absorber frequency. The experimental calibration of the absorber length to the absorber natural frequency was programmed into Simulink block "Look-Up Table", which is used to linearize the frequency between every two points. This facilitates the calculation of the appropriate desired absorber beam length. A *Unit Delay* with a sampling time of 2.048 seconds is inserted after the "Look-up Table" for a slow-to-fast sample-rate transition. The difference between the output of *Unit Delay* and the length of the absorber beam is the desired position of the movable support from the left end of the entire absorber beam. A block "DS1102ENC_POS" is used here to collect data from the rotary encoder. After converted "rad" into "distance", the output of the "distance" block is the present position of the movable support. A S function block "discon" conducts the distance control of the movable support. The input of "discon" block is the error between the present position and the desired position of the movable support. When the error is greater than 3 mm, "discon" outputs PWM control command 1 (a 100% duty-cycle represents full drive to one direction) to drive the DC motor to a maximum speed so that the movable support is moving at the maximum speed to the right direction, if the error is less than -3 mm, "discon" outputs PWM control command 0 (a 0% duty-cycle represents full drive to the opposite direction) to drive the DC motor so that the movable support is moving at the maximum speed to the left direction, otherwise the PWM command is 0.5 (a 50% duty-cycle represents zero drive)

to stop the DC motor. This process is the coarse tuning. It takes 40 seconds to drive the movable plate from one end to the other end at full speed, therefore the maximum speed of the movable plate is about 6.8 mm/s. S function block "aver_amplit" and "fine_ adjust" conduct the fine tuning. If the absolute value of the error is greater than the threshold of "Switch" which is set to be 3 mm, the coarse tuning is conducted, otherwise the fine tuning is conducted, a PWM command 0.56 or 0.44 is generated from "fine_ adjust" to drive the motor so that the movable support moves at a very low speed. The base sampling time of the entire system is 0.001 second.

3.4 Experimental Results

Experimental results includes: impact response of the primary beam, impact response of the primary beam with the absorber frame and without the absorber mass, forced response of the primary beam with the absorber, forced response when the exciting frequency changes, and testing of frequency tracking ability of the auto-tuning control.

3.4.1 Experimental Results without and with the Absorber System

Figure 3.9 depicts the spectrum of an impact response of the primary beam only. The impact was done by hitting the primary beam. There are 3 visible peaks at 20.6 Hz, 56.2 Hz, and 110.4 Hz, very close to their corresponding theoretical frequencies 23.6 Hz, 64.9 Hz, and 114 Hz. Impact tests show that the modes higher than 3 modes are very weak and can be ignored.

Figure 3.10 is the spectrum of the primary beam with the absorber frame and without the absorber mass. The system has been changed significantly. As the absorber frame is relatively massive, adding it to the primary beam lowers the first natural frequency substantially to 7.8 Hz.

Figure 3.11 shows the spectrum of the primary beam with the absorber system. The absorber frequency f_a is adjusted to be equal to the first natural frequency of the beam plus

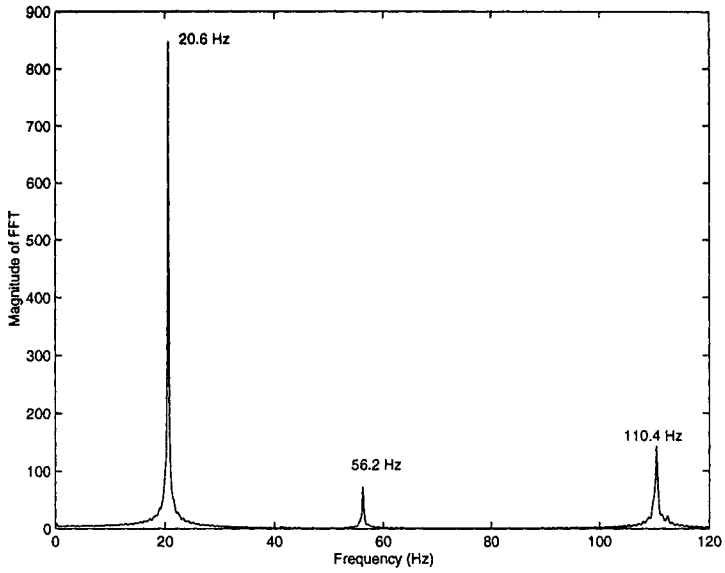

Figure 3.9: Spectrum of an impact response of the primary beam

the absorber frame (7.8 Hz). As shown in Figure 3.11, two new natural frequencies 7 Hz and 9.2 Hz appear. These two new frequencies are very close which makes the vibration suppression performance sensitive to the exciting frequency changes.

Figure 3.12 shows the time response of the primary beam of the system with the absorber frame and without the absorber mass when the exciting frequency equals 7.8 Hz. The figure shows that without the absorber mass, the vibration amplitude is unacceptably large.

Figure 3.13 shows the time response of the primary beam with the absorber system when $f = f_a = 7.8$ Hz. With the absorber system tuned, the vibration amplitude of the primary beam was greatly reduced (comparing to Figure 3.12). The reduction achieved with the absorber at this test was 34.67 dB.

Figure 3.14 shows a comparison of the responses of the primary beam and the absorber mass when $f = f_a = 7.8$ Hz.

Figure 3.15 shows that when the exciting force excited at the first resonance frequency, the primary beam and the absorber mass vibrated in phase. Figure 3.16 shows that when the exciting force excited at the second resonance frequency, the primary beam and absorber mass vibrated out of phase.

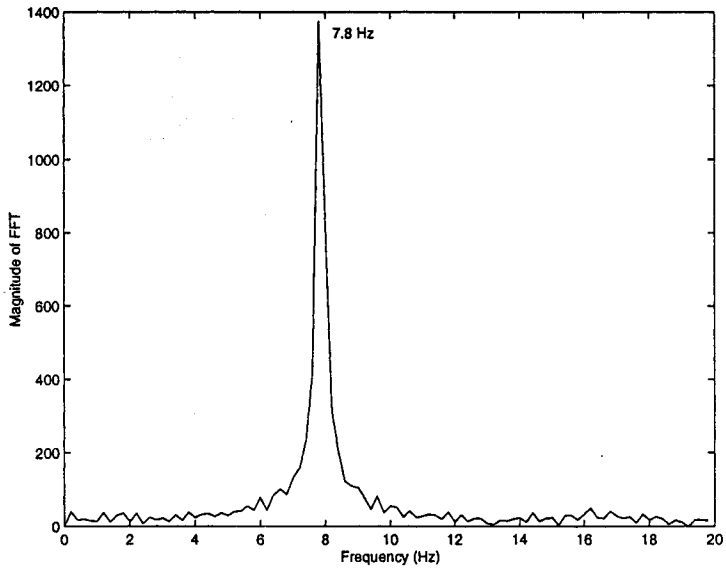

Figure 3.10: Spectrum of an impact response of the primary beam with the absorber frame

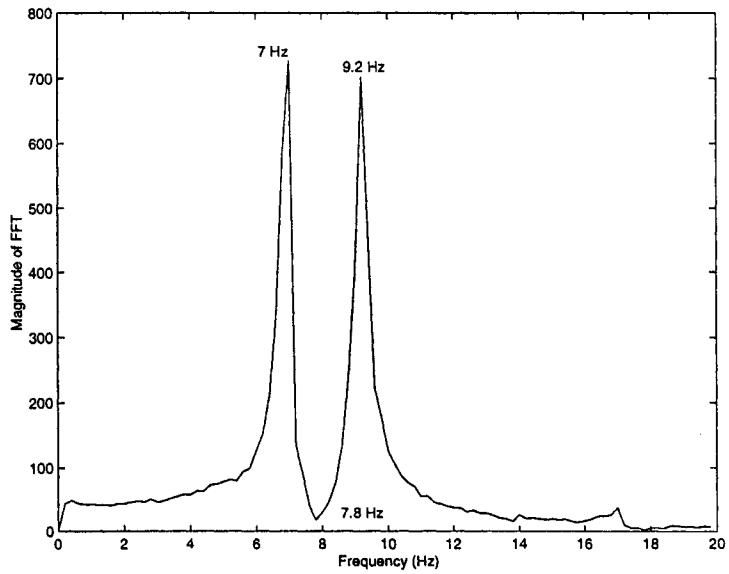

Figure 3.11: Spectrum of an impact response of the entire system

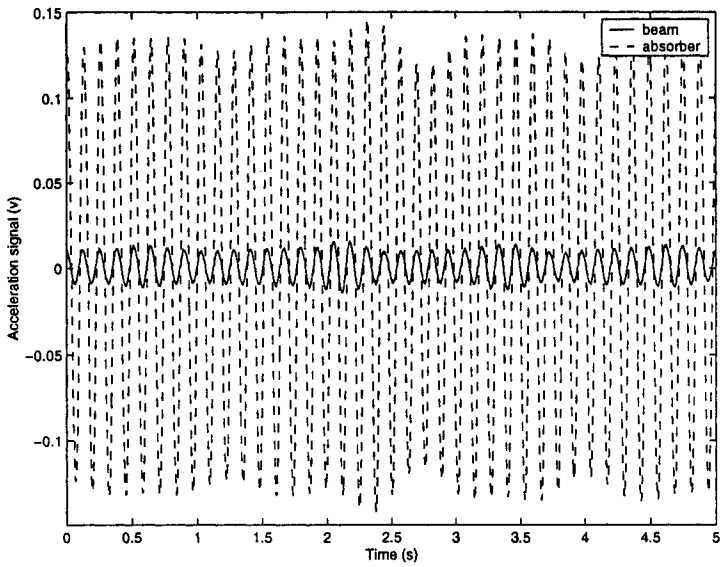

Figure 3.14: Comparison of the responses of the primary beam and the absorber mass when $f = f_a = 7.8$ Hz

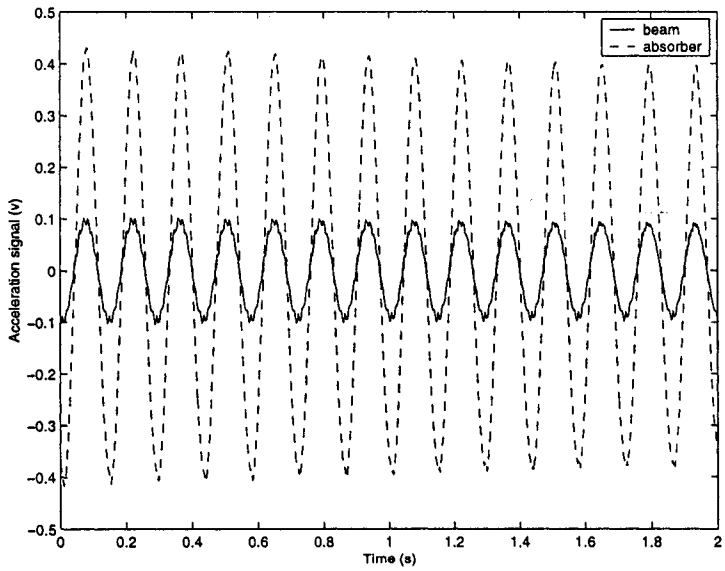

Figure 3.15: Comparison of the responses of the primary beam and the absorber mass when $f = 7$ Hz, i.e., the first resonance frequency

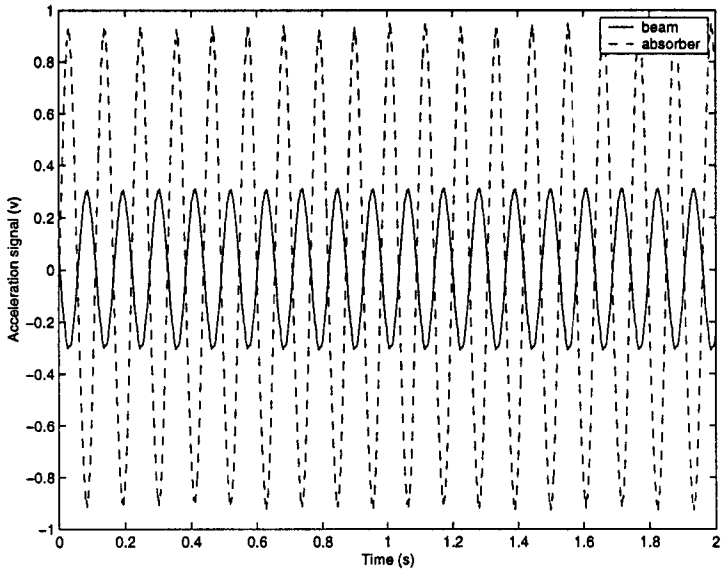

Figure 3.16: Comparison of the responses of the primary beam and the absorber mass when $f = 9.2$ Hz, i.e., the second resonance frequency

3.4.2 Tracking a Step Change in the Exciting Frequency

For this test, the absorber frequency of the system was initially set to be 6.6 Hz. The exciting frequency started from 7 Hz which was very close to the absorber frequency. At the time $t = 10$ second, the exciting frequency changed suddenly to 8.6 Hz.

Figure 3.17 shows the response of the primary beam when the absorber frequency remained unchanged, i.e., auto-tuning was not activated. The amplitude of the response increases significantly after the exciting frequency varied because the system was excited at resonance.

Figure 3.18 shows the frequency tracking when the frequency tolerance was chosen to be tol=0.4 Hz. The absorber frequency and the measured exciting frequency were exactly the same because the frequency tolerance tol was chosen to be relatively smaller. When the motor was moving to change the stiffness of the absorber, the transient response was induced. Therefore, when the transient response was dominant in the signal, the FFT computation would output a frequency associated with one of the natural frequencies. If the error between

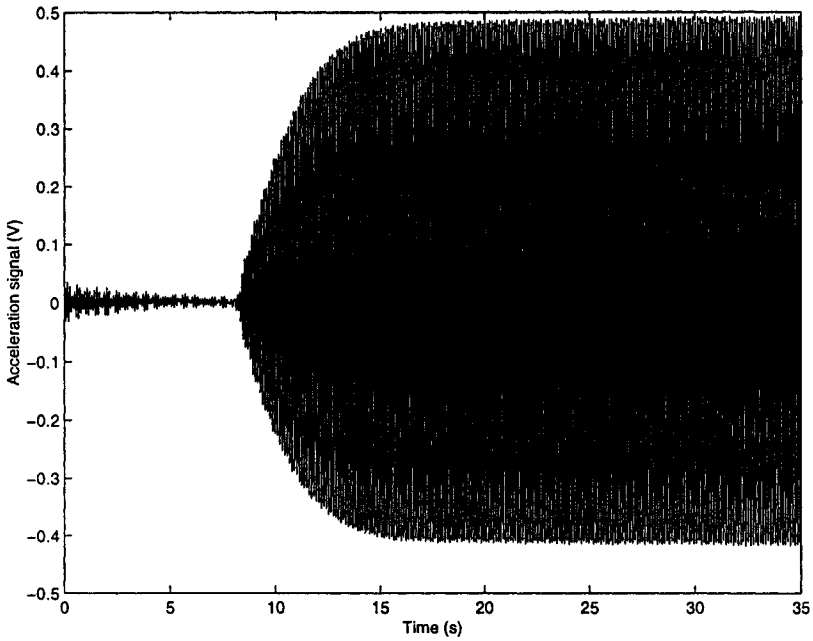

Figure 3.17: Response of the primary beam without the control of the absorber when the exciting frequency experiences a step change

this false exciting frequency and the absorber frequency exceeded the frequency tolerance, a new adjustment was made according to the false exciting frequency. The result was that the absorber frequency started oscillating.

Figure 3.19 shows the frequency tracking when the frequency tolerance was chosen to be tol=2 Hz. Obviously the frequency tolerance was too large, such that the absorber frequency kept unchanged when the exciting frequency varied.

Figure 3.20 shows the frequency tracking when the frequency tolerance was chosen to be tol=1 Hz. The first period of 2.048 seconds was the time to determine the exciting frequency, because the response just started and the transient response was present in the signal, therefore the measured exciting frequency after 2.048 seconds was one of the natural frequencies of the entire system. During the second FFT execution period, the system vibrated at a steady state, therefore after 4.096 seconds the measured exciting frequency was about 6.5 Hz which is close to the real exciting frequency 7 Hz. During the period when the exciting frequency was 7 Hz, the measured exciting frequency changed slightly sometimes but within

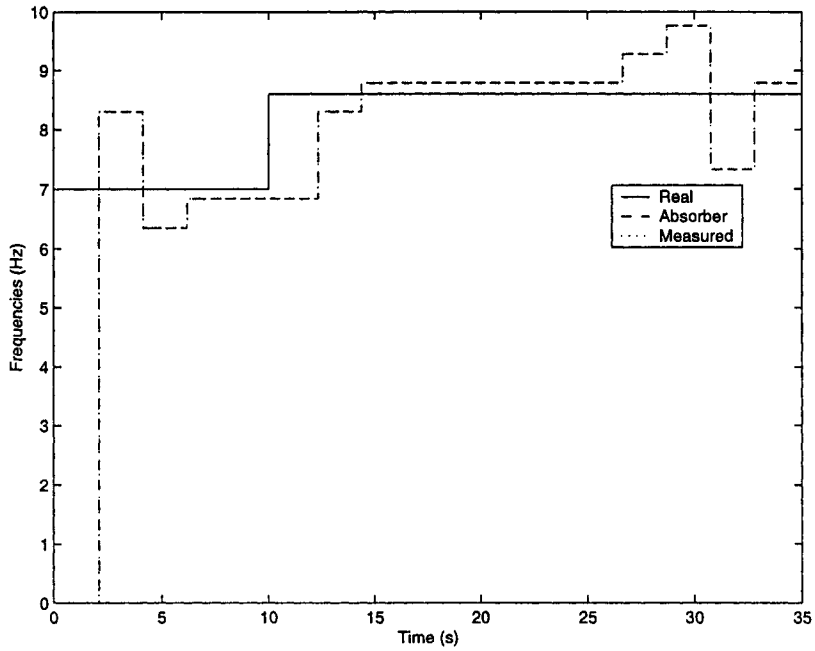

Figure 3.18: Frequency tracking when the exciting frequency experiences a step change: tol=0.4 Hz

the frequency tolerance. Therefore, the absorber frequency kept unchanged. At the time $t = 10$ second when the exciting frequency changed suddenly to 8.6 Hz, after approximately 2 seconds which was the FFT execution time, the measured exciting frequency followed the exiting frequency. During the rest of time, the absorber frequency kept unchanged as the variation of the measured exciting frequency was within the frequency tolerance. Therefore tol=1 Hz was considered to be a proper frequency tolerance.

Figure 3.21 shows the response of the primary beam when the auto-tuning control was enforced and the frequency tolerance was tol=1 Hz. Figure 3.22 shows the corresponding response of the absorber mass. The time history of the absorber frequency calculated from the encoder reading is shown in Figure 3.23. Figure 3.21 clearly illustrates the vibration reduction accomplished by the tunable absorber. The exciting frequency started from 7 Hz which is very close to the absorber frequency 6.6 Hz. The response of the primary beam remained small until $t = 10$ second. During the first period of 2.048 seconds the system was performing the fine tuning, the movable support of the absorber system was moving back

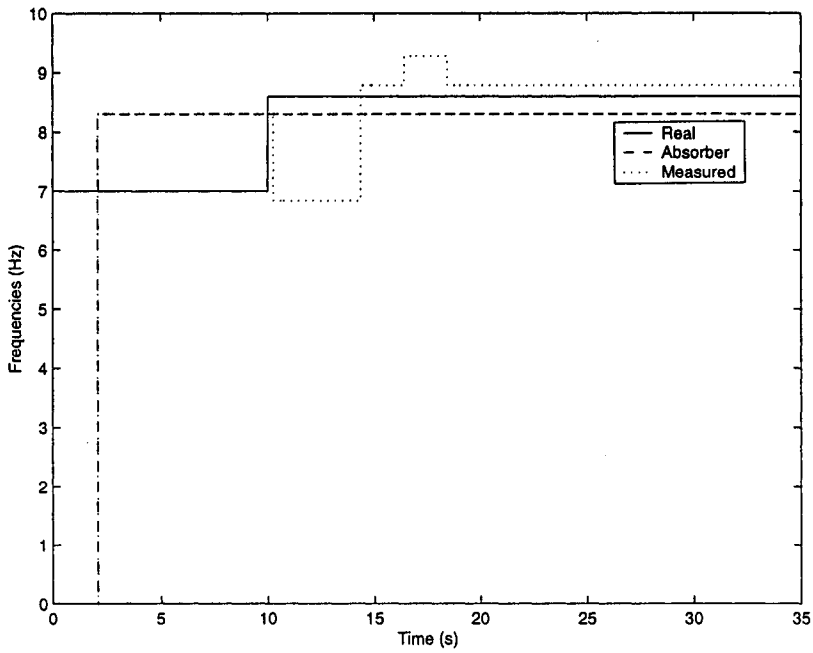

Figure 3.19: Frequency tracking when the exciting frequency experiences a step change: tol=2 Hz

and forth to change the stiffness of the absorber. After 10 seconds, the exciting frequency was changed to 8.6 Hz suddenly which is one of the natural frequencies of the entire system. The accelerometer signal of the primary beam was increased significantly at first, but with the control of the absorber, the new absorber frequency was adjusted to be close to the exciting frequency. Hence the accelerometer signal of the primary beam was decreased significantly. This process lasted approximately 15 seconds. The slow tuning speed was due to the Maximum travelling speed of the movable support. Restricted by the DC motor and lead-screw drive, the maximum travelling speed is about 6.8 mm/s. The residual vibration of the primary beam is attributed to several factors such as a slightly mismatching of the exciting frequency and absorber frequency and the inherent damping.

Comparing Figure 3.17 and 3.21, with the control of the tunable absorber, the vibration of the primary beam was suppressed significantly when the exciting frequency varied. The vibration attenuation achieved with the tunable vibration absorber at the 8.6 Hz frequency was 6.7 dB.

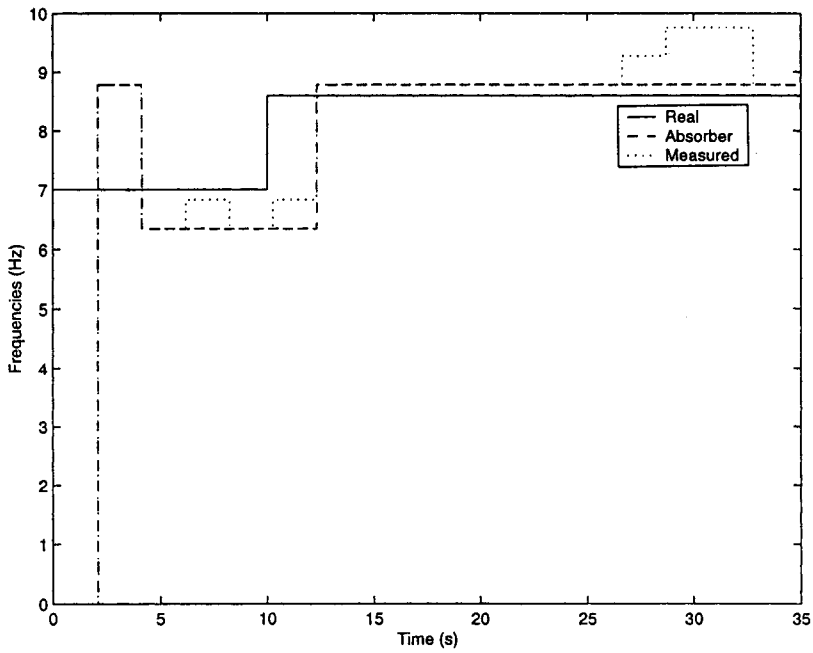

Figure 3.20: Frequency tracking when the exciting frequency experiences a step change: tol=1 Hz

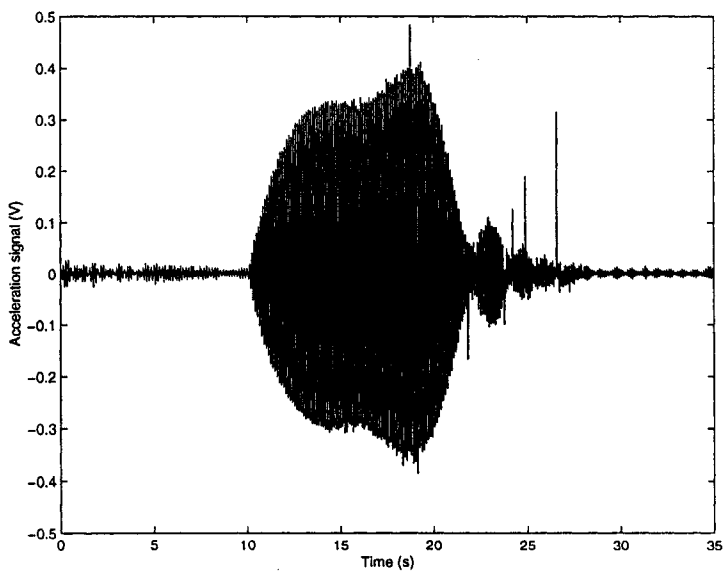

Figure 3.21: Response of the primary beam with the control of the absorber when the exciting frequency experiences a step change

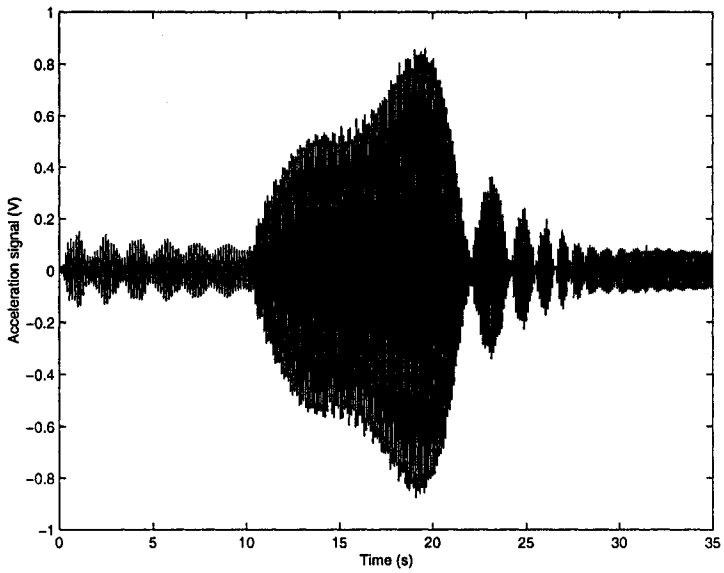

Figure 3.22: Response of the absorber mass when the exciting frequency experiences a step change

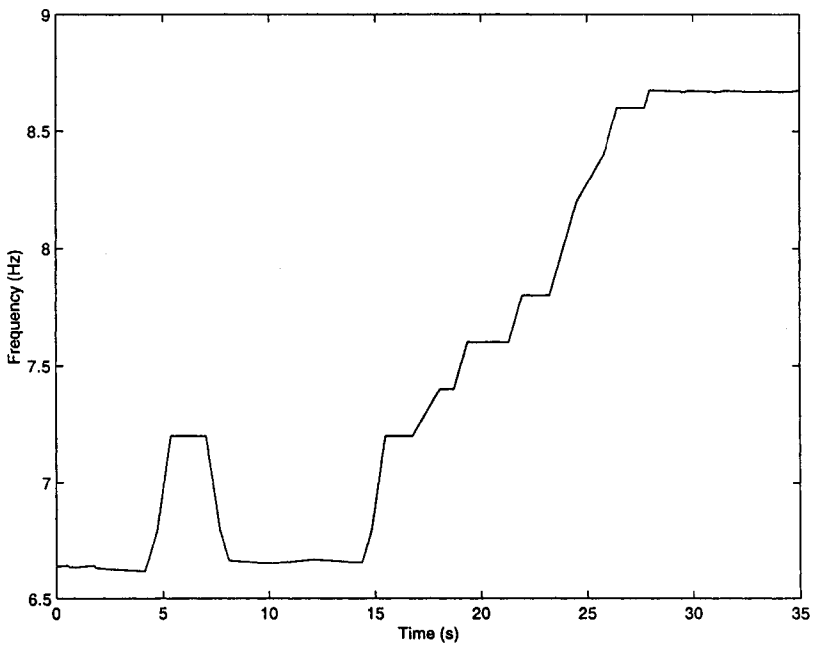

Figure 3.23: The absorber frequency calculated from the encoder reading

Next, some experimental tests have also been carried out when 1024 samples were used for FFT computation or the execution time of the FFT subsystem was 1.024 seconds. Figure 3.24 shows the frequency tracking when the frequency tolerance was tol=1 Hz. The first

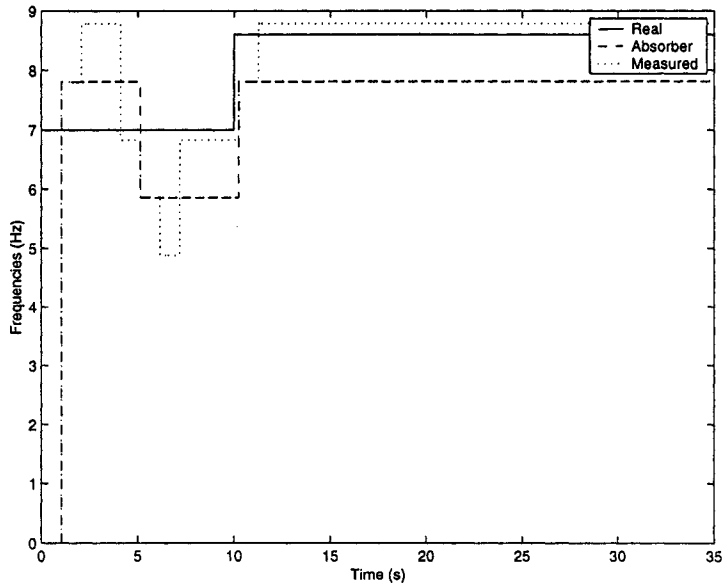

Figure 3.24: Frequency tracking when the exciting frequency experiences a step change: tol=1 Hz

period of 1.024 seconds was the time needed to determine the exciting frequency. During this period, the transient response was dominant in the response. The measured exciting frequency provided by the FFT subsystem was not the real exciting frequency, but one of the natural frequencies of the entire system. From 1.024 second to 2.048 seconds, after the absorber frequency was adjusted to be equal to the measured exciting frequency, the transient response was still dominant in the response. The measured exciting frequency was another new natural frequency of the entire system. This lasted until $t = 4.096$ second. After 4.096 seconds, as the system vibrated at a steady state, the measured exciting frequency was about 6.84 Hz which was close to the real exciting frequency 7 Hz. The absorber frequency kept unchanged from 4.096 seconds to 5.120 seconds because the change of the measured exciting frequency is within the frequency tolerance. After 5.120 seconds, the measured exciting frequency was one of the natural frequencies because of the transient response again. It can

be seen that the measured exciting frequency was not stable, and the absorber frequency did not follow the measured exciting frequency when the system vibrated at a steady state.

Figure 3.25 shows the frequency tracking when the frequency tolerance is tol=0.9 Hz. The

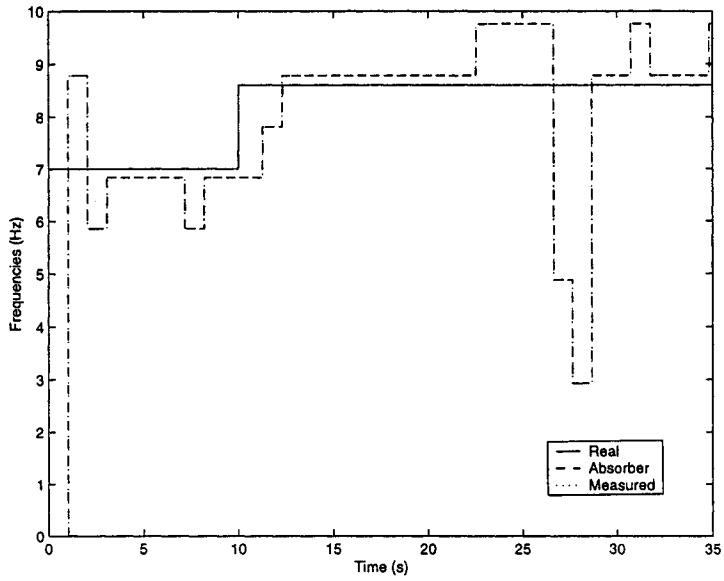

Figure 3.25: Frequency tracking when the exciting frequency experiences a step change: tol=0.9 Hz

absorber frequency was equal to the measured exciting frequency during the entire period with this smaller frequency tolerance. It can be seen that many times when the absorber frequency was adjusted, the transient response appeared and was dominant. Therefore the absorber frequency was not stable when the frequency tolerance was chosen to be tol=0.9 Hz.

Figure 3.26 shows the response of the primary beam when the frequency tolerance was chosen to be tol=1 Hz. Figure 3.27 shows the corresponding response of the absorber mass. The time history of the absorber frequency calculated from the encoder reading is shown in Figure 3.28.

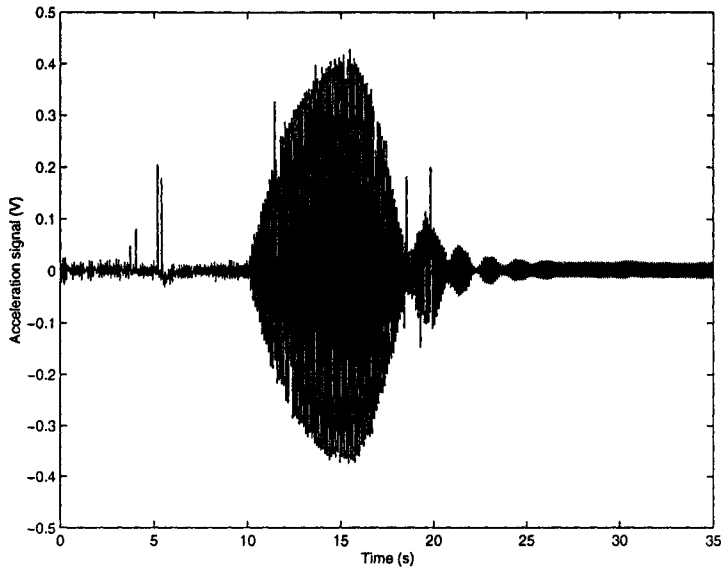

Figure 3.26: Time response of the primary mass when the exciting frequency experiences a step change

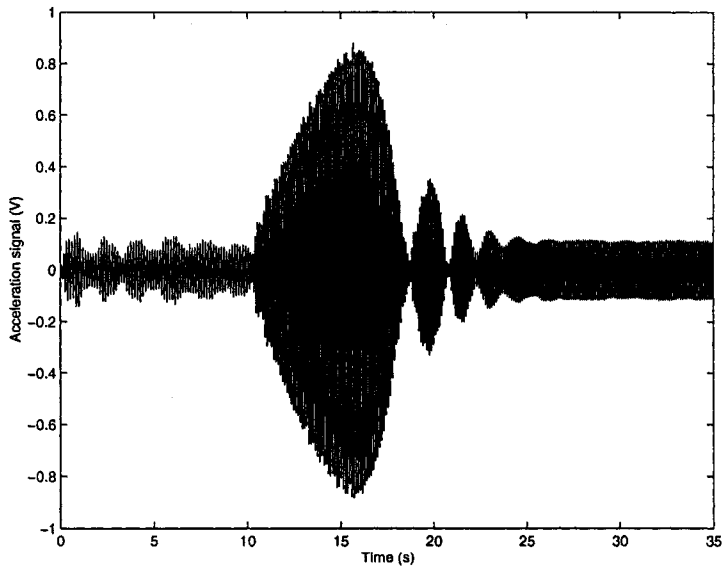

Figure 3.27: Time response of the absorber mass when the exciting frequency experiences a step change

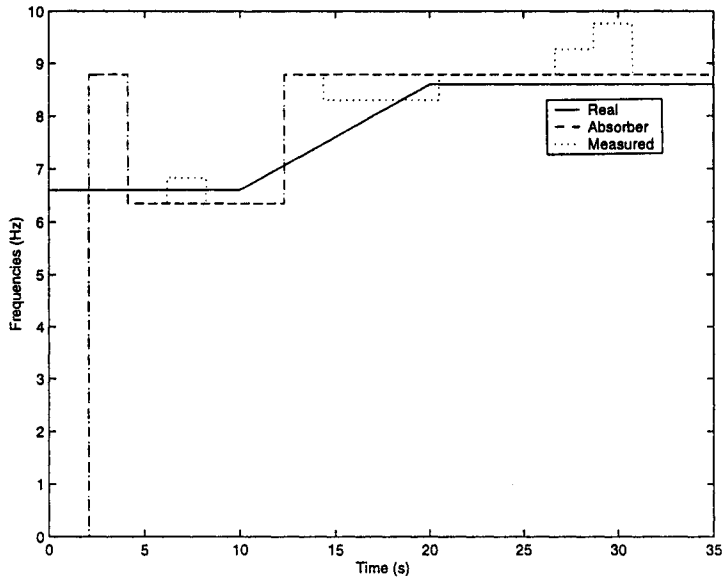

Figure 3.30: Frequency tracking when the exciting frequency experiences a linear change: tol=1 Hz

Figure 3.32 shows the response of the primary beam when the auto-tuning control was enforced and the frequency tolerance was tol=1 Hz. Figure 3.33 shows the corresponding response of the absorber mass. The time history of the absorber frequency calculated from the encoder reading is shown in Figure 3.34.

Comparing Figure 3.29 and 3.32, with the control of the tunable absorber, the vibration of the primary beam was suppressed significantly when the exciting frequency was changed into 8.6 Hz, but was almost unchanged when the exciting frequency experienced a linear change. The vibration attenuation achieved with the tunable absorber during the entire test time was 14 dB. However the vibration attenuation achieved during the linear change period which is from 10 seconds to 20 seconds was 0.67 dB. Because during the linear change of the exciting frequency, the absorber frequency did not follow and match the exciting frequency, the anti-resonance state could not be created.

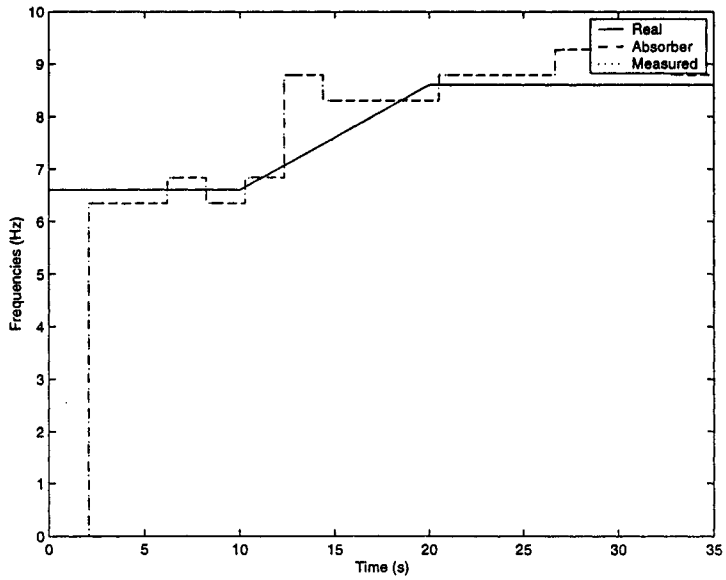

Figure 3.31: Frequency tracking when the exciting frequency experiences a linear change: tol=0.4 Hz

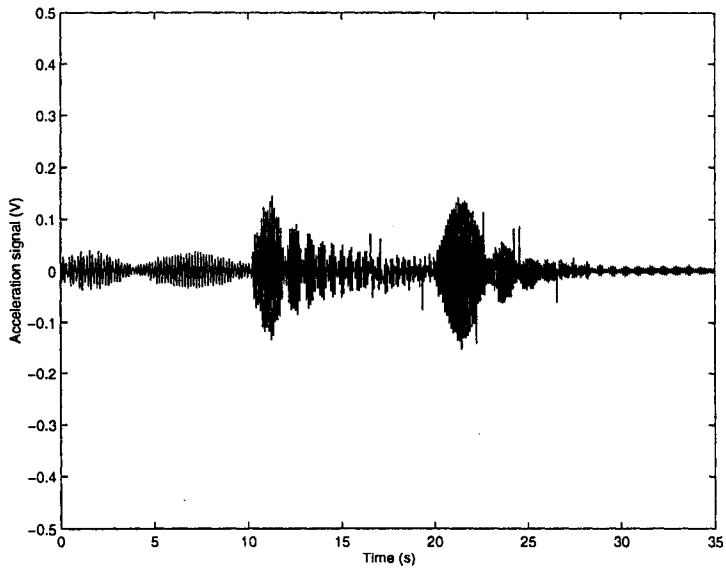

Figure 3.32: Experimental time response of the primary beam with the control of the absorber when the exciting frequency experiences a linear change

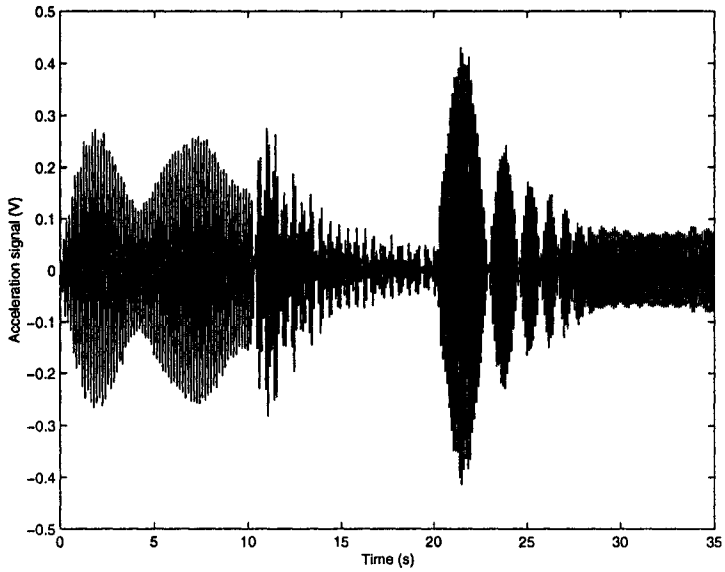

Figure 3.33: Experimental time response of the absorber mass with the control of the absorber when the exciting frequency experiences a linear change

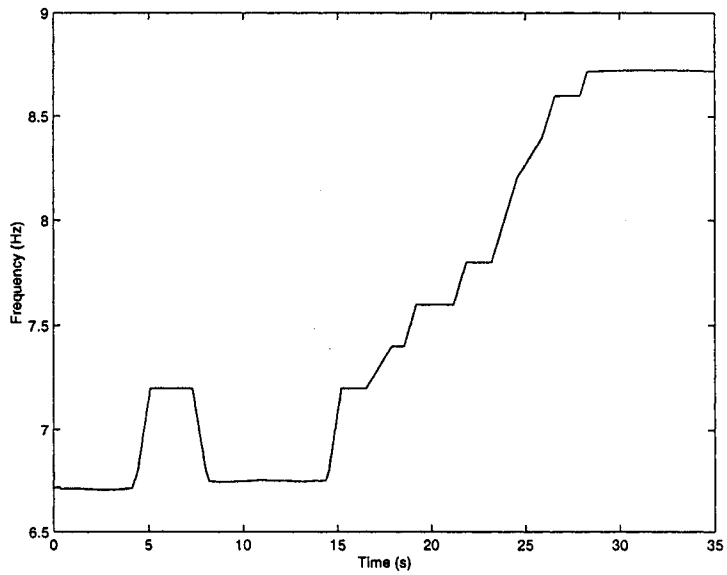

Figure 3.34: The absorber frequency calculated from the encoder reading

Next, some simulation tests have also been carried out when 1024 samples were used for FFT computation or the execution time of the FFT subsystem was 1.024 seconds. Figure 3.35 shows the frequency tracking when the frequency tolerance was tol=1 Hz. The first

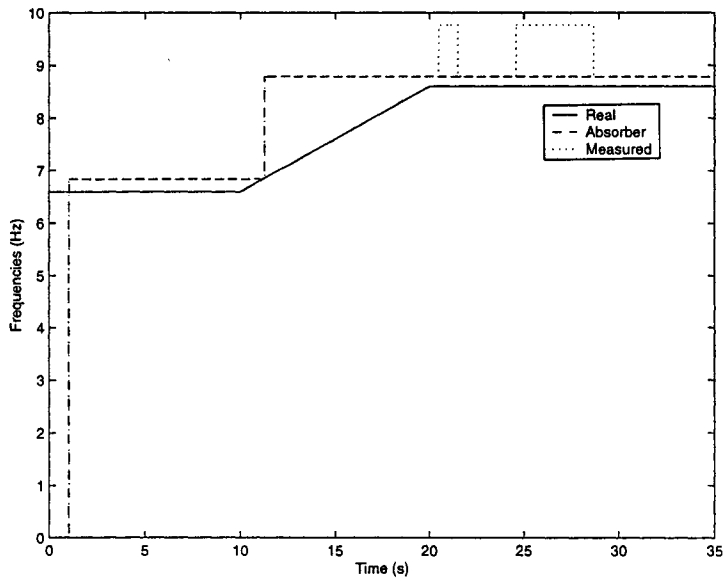

Figure 3.35: Frequency tracking when the exciting frequency experiences a linear change: tol=1 Hz

period of 1.024 seconds was the time needed to determine the exciting frequency. After 1.024 seconds the measured exciting frequency was about 6.85 Hz which is close to the real exciting frequency 6.6 Hz. During the period of linear change from 10 second to 20 second, the transient response was dominant in the signal, the absorber frequency did not follow the real exciting frequency, but followed one of the natural frequencies of the entire system. After 20 seconds, the absorber frequency followed the exciting frequency again. The measured exciting frequency changed slightly during this period, but within the frequency tolerance, the absorber frequency kept unchanged.

Figure 3.36 shows the frequency tracking when the frequency tolerance was tol=0.4 Hz. After 20 seconds, the measured exciting frequency changed slightly, and the absorber frequency followed the measured exciting frequency because the frequency tolerance was too small. Therefore the absorber frequency was not stable when the frequency tolerance was

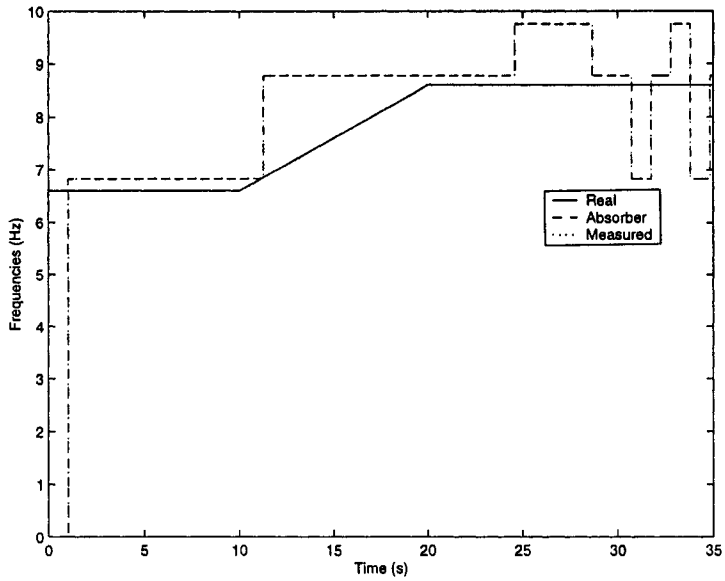

Figure 3.36: Frequency tracking when the exciting frequency experiences a linear change: tol=0.4 Hz

chosen to be tol=0.4 Hz.

Figure 3.37 shows the response of the primary beam when the auto-tuning control was enforced and the frequency tolerance was tol=1 Hz. It can be seen that from 10 to 20 second the vibration amplitude was not suppressed effectively because the absorber frequency did not match the real exciting frequency, but decreased again after 20 seconds when the absorber frequency followed the exciting frequency. Figure 3.38 shows the corresponding response of the absorber mass.

The time history of the absorber frequency calculated from the encoder reading is shown in Figure 3.39.

Comparing Figure 3.29 and 3.37, with the control of the tunable absorber, the vibration attenuation of the primary beam achieved during the entire period was 15.6 dB. However the vibration attenuation achieved during the linear change period which is from 10 second to 20 seconds was 0.5 dB, almost unchanged.

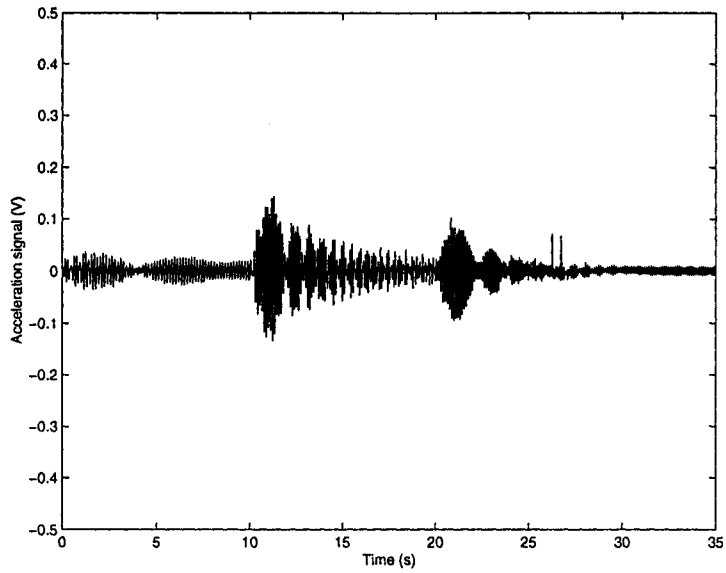

Figure 3.37: Time response of the primary mass when the exciting frequency experiences a linear change

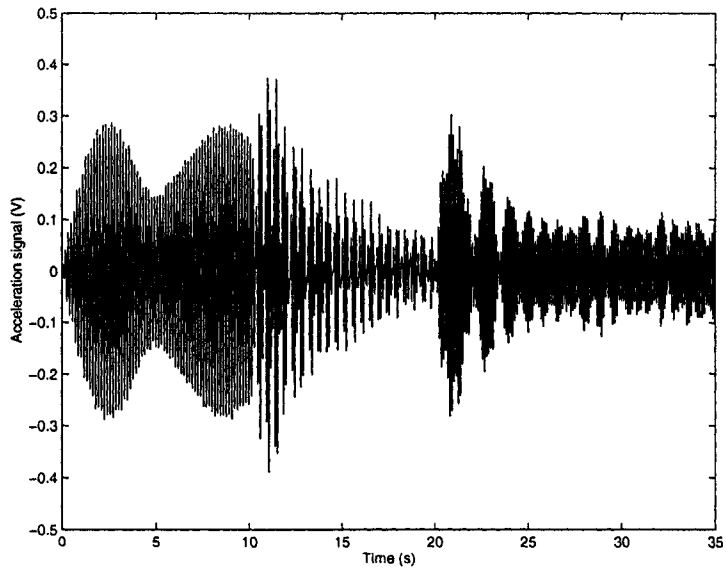

Figure 3.38: Time response of the absorber mass when the exciting frequency experiences a linear change

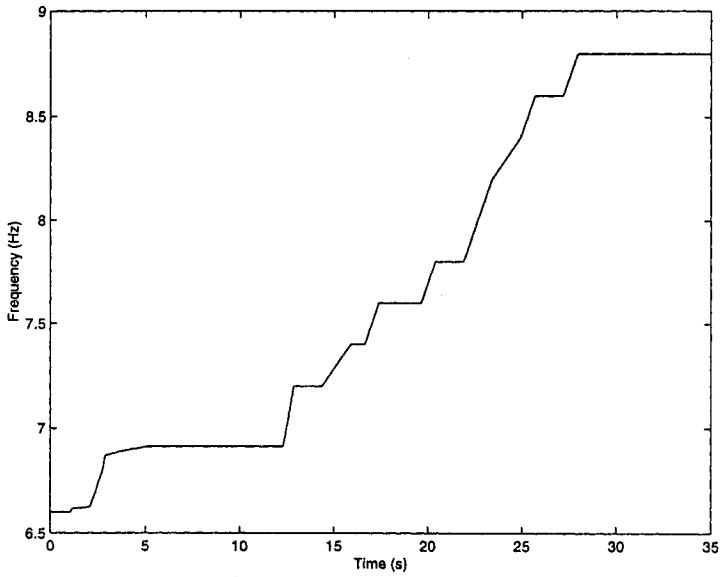

Figure 3.39: The absorber frequency calculated from the encoder reading

Chapter 4

Analytical Study of a Variable Damping Vibration Absorber

Damping is often present in devices and has the potential for destroying the ability of a vibration absorber to completely suppress the primary system vibration. However, damping is sometimes added to a vibration absorber to prevent resonance or to improve the effective operation bandwidth of the vibration absorber. Also, a damper by itself is often used as a vibration absorber by dissipating the energy supplied by an applied force. Such devices are called vibration dampers rather than absorbers. This chapter investigates a vibration absorber with variable damping. Figure 4.1 shows a vibration absorber with a magnetic damper developed for the purpose of this study. Figure 4.2 shows the a schematic of a primary beam attached by the absorber. It contains two subsystem: a clamped-clamped aluminum (6601-T6) beam and an absorber-damper system. The beam (1) serves as a primary system. The absorber-damper system consists of a C shape electromagnet (4), a clamp support (3), an absorber mass (6), an absorber beam (7), a copper plate (5) and an absorber beam clamp (2). The absorber beam is a thin steel plate, the stiffness can be adjusted by varying the beam length manually. The rectangular copper plate conductor is inserted between the two poles of the C shape electromagnet. When the copper plate conductor vibrates, the magnetic force is generated. The force is proportional to the velocity of the copper plate and opposite to the direction of the velocity. Therefore the force is a retarding force and such damping is so-called viscous damping (The principle of electromagnetic damping will be introduced in

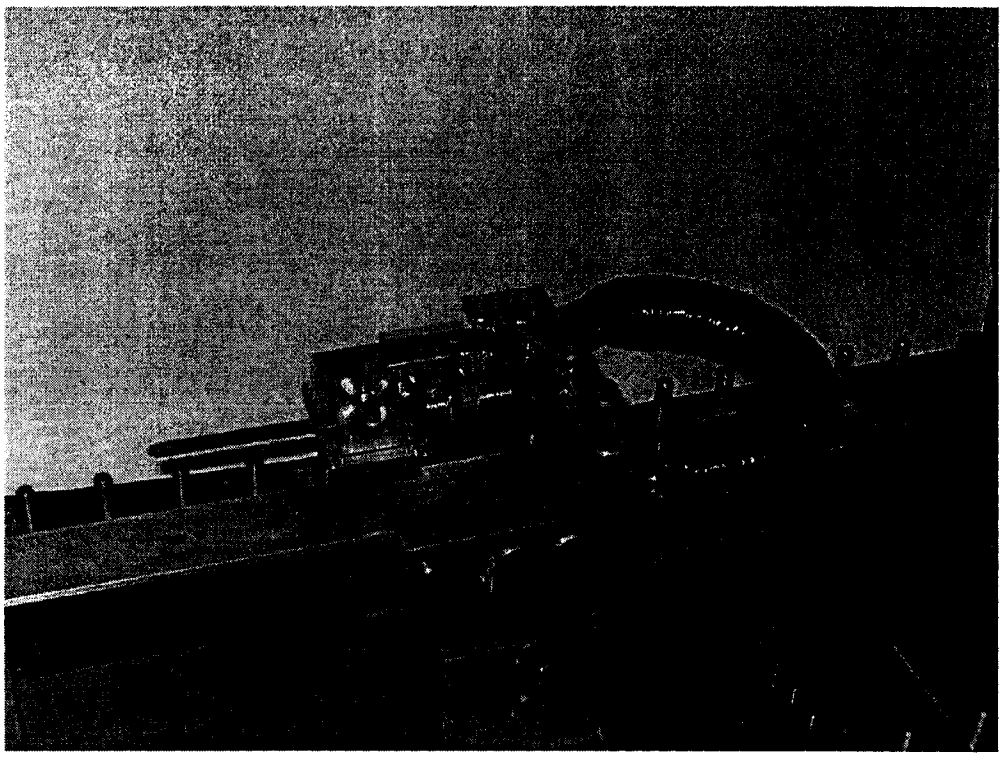

Figure 4.1: Vibration absorber with an electromagnetic damper

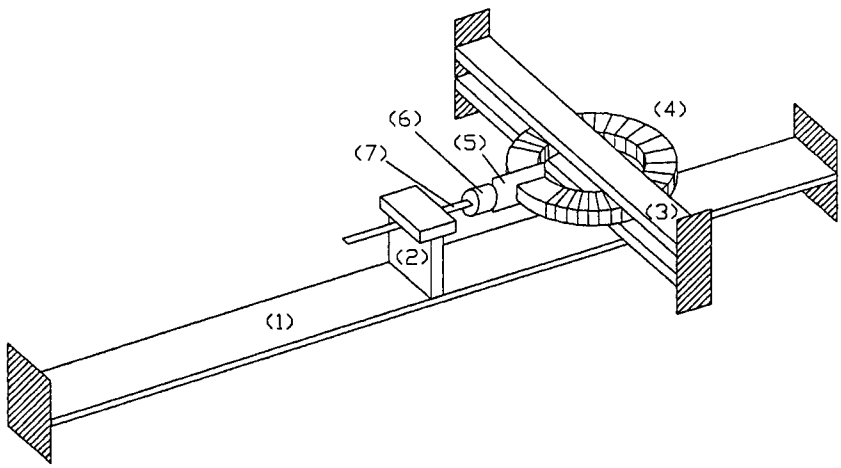

Figure 4.2: Schematic of a primary beam and a vibration absorber with damper

(1) Primary beam
(2) Absorber beam clamp
(3) Clamp support
(4) Electromagnet
(5) Copper plate
(6) Absorber mass
(7) Absorber beam

the next Chapter). The damping coefficient can be varied by adjusting the current of the coil of the electromagnet. In this chapter, an analytical model of the system is developed and an auto-tuning method is presented.

4.1 Analytical Model

A model of the beam-absorber system is shown in Figure 4.3 (a) where c_d is the variable damping value of the absorber system and $f(t) = F_0 sin\omega t$ is the exciting force. A simplified 2-DOF model is used to replace this beam-absorber model. When the primary system is composed of a clamp-clamp beam and the absorber beam clamp, it behaves like a 1-DOF system. Figure 4.3 (b) is the simplified equivalent model of the beam-absorber system where $m = m_b + m_f$. Table 4.1 lists the parameters of the entire system.

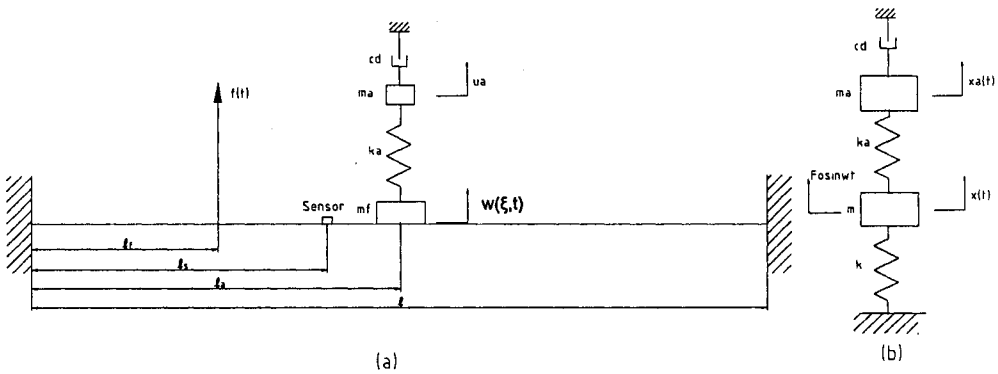

Figure 4.3: Schematics of the models: (a) Primary beam with the absorber; (b) Simplified 2-DOF model

Applying Newton's second law to the primary mass m yields

$$m\ddot{x}(t) + kx(t) + k_a\left[x(t) - x_a(t)\right] = F_0 sin\omega t. \tag{4.1}$$

Applying Newton's second law to the damper mass yields

$$m_a\ddot{x}_a(t) + k_a\left[x_a(t) - x(t)\right] + c_d\dot{x}_a(t) = 0. \tag{4.2}$$

Absorber beam clamp mass m_f	0.2038 kg
Absorber mass m_a	0.0326 kg
Mass of the primary beam m_b	0.7649 Kg
Frequency of the primary system f_p	14.4 Hz
Stiffness of the primary system k	7930 N/m
Stiffness of the absorber system k_a	266.8711 N/m
Density of the primary beam ρ	2800 kg/m^3
Length of the primary beam ℓ	1.057 m
Width of the primary beam b	50.8 mm
Height of the primary beam h	5.0876 mm
Cross-sectional area of the primary beam A	2.5845×10^{-4} m^2
Moment of inertia of cross-sectional area I	5.5747×10^{-10} m^4
Young's modulus E	70.9×10^9 N/m^2
Location of the absorber ℓ_a	528.5 mm
Location of the excitation ℓ_f	247 mm
Location of the sensor ℓ_s	422.8 mm

Table 4.1: Parameters of the Beam-Damper system

Combining equations (4.1) and (4.2) results in a matrix equation

$$M \begin{bmatrix} \ddot{x}(t) \\ \ddot{x}_a(t) \end{bmatrix} + C \begin{bmatrix} \dot{x}(t) \\ \dot{x}_a(t) \end{bmatrix} + K \begin{bmatrix} x(t) \\ x_a(t) \end{bmatrix} = Bf(t) \tag{4.3}$$

where M is mass matrix

$$M = \begin{bmatrix} m & 0 \\ 0 & m_a \end{bmatrix}$$

C is damping matrix

$$C = \begin{bmatrix} 0 & 0 \\ 0 & c_d \end{bmatrix}$$

K is stiffness matrix

$$K = \begin{bmatrix} k + k_a & -k_a \\ -k_a & k_a \end{bmatrix}$$

B is input matrix

$$B = \begin{bmatrix} 1 \\ 0 \end{bmatrix}$$

f is the exciting force

$$f(t) = F_0 sin\omega t.$$

To find the steady-state solutions of equation (4.3), let $F_0 sin\omega t$ be represented in exponential form by $F_0 e^{j\omega t}$ in equation (4.3) and assume that the steady-state solution is of the form

$$\begin{bmatrix} x(t) \\ x_a(t) \end{bmatrix} = \begin{bmatrix} X \\ X_a \end{bmatrix} e^{j\omega t} \tag{4.4}$$

where X is the amplitude of vibration of the primary mass and X_a is the amplitude of vibration of the absorber mass. Substituting $x(t)$ into equation (4.3) yields

$$\begin{bmatrix} k + k_a - m\omega^2 & -k_a \\ -k_a & j\omega c_d + k_a - m_a\omega^2 \end{bmatrix} \begin{bmatrix} X \\ X_a \end{bmatrix} e^{j\omega t} = \begin{bmatrix} F_0 \\ 0 \end{bmatrix} e^{j\omega t}. \tag{4.5}$$

Note that the coefficient matrix X has complex elements. Dividing equation (4.5) by the nonzero scalar $e^{j\omega t}$ yields a complex matrix equation in the amplitudes X and X_a. Solving for X and X_a yields

$$\begin{bmatrix} X \\ X_a \end{bmatrix} = \frac{\begin{bmatrix} k_a - m_a\omega^2 + j\omega c_d & k_a \\ k_a & k + k_a - m\omega^2 \end{bmatrix} \begin{bmatrix} F_0 \\ 0 \end{bmatrix}}{det(K - \omega^2 M + \omega j C)}. \tag{4.6}$$

Here the determinant in the denominator is given

$$det(K - \omega^2 M + \omega j C) = [(k - m\omega^2)(k_a - m_a\omega^2) - m_a k_a \omega^2] + j\omega c_d(k + k_a - m\omega^2). \tag{4.7}$$

Simplifying the matrix vector product yields

$$X = \frac{[(k_a - m_a\omega^2) + j\omega c_d]\, F_0}{det(K - \omega^2 M + \omega j C)} \tag{4.8}$$

and

$$X_a = \frac{k_a F_0}{det(K - \omega^2 M + \omega j C)}. \tag{4.9}$$

Note that these values are now complex numbers. The maximum deflection of the primary mass is given by equation (4.8) with the determinant in the denominator which is given in equation (4.7). This is the ratio of two complex numbers and hence is a complex number representing the phase and the amplitude of the response of the primary mass. Using complex arithmetic the amplitude of the motion of the primary mass can be written as the real number

$$\left|\frac{Xk}{F_0}\right| = k\sqrt{\frac{(k_a - m_a\omega^2)^2 + c_d^2\omega^2}{[(k - m\omega^2)(k_a - m_a\omega^2) - m_a k_a\omega^2]^2 + (k + k_a - m\omega^2)^2 c_d^2\omega^2}} \tag{4.10}$$

where $|Xk/F_0|$ is the normalized magnitude of the primary system. Figure 4.4 is plotted from equation (4.10) which illustrate how the damping value, as reflected as $\zeta_d = \frac{c_d}{2\sqrt{k_a m_a}}$, affects

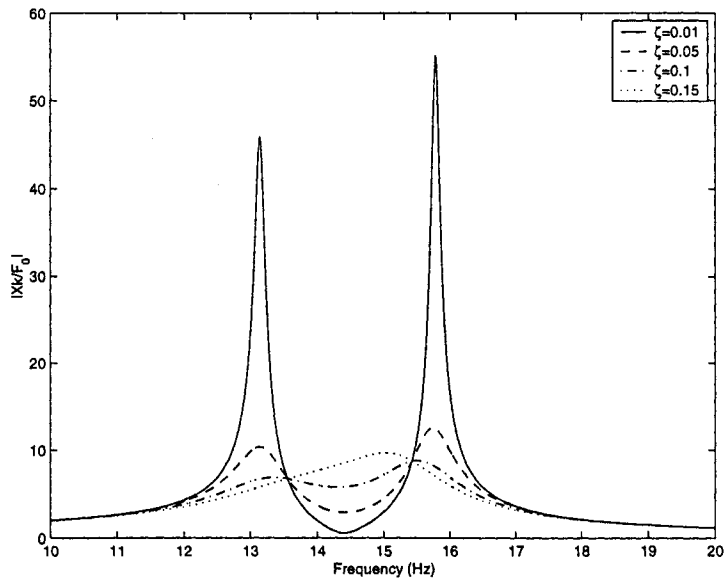

Figure 4.4: Normalized magnitude of vibration of the primary mass as a function of the frequency for several values of the damping in the absorber system

the response. From this figure, when the damping ratio varies, the normalized magnitude varies, there are two crossing points which can be observed from the figure. Between the two points, the smaller the damping ratio, the smaller the normalized magnitude. On the contrary, outside the two points, the bigger the damping ratio, the smaller the normalized

magnitude. It also can be seen that even when the exciting frequency excites at the resonance of the system, if the damping ratio is big enough, the vibration of the primary system can be reduced significantly.

From the observation of Figure 4.4, when c_d or ζ_d varies, there are always two frequencies that make the normalized magnitude $|Xk/F_0|$ same. It is likely for every c_d or ζ, these two crossing points exist. In what follows, it is proved that the two crossing frequencies exist and are independent of the damping values. In equation (4.10), assume

$$D = (k_a - m_a\omega^2)^2, \tag{4.11}$$

$$E = c_d^2\omega^2, \tag{4.12}$$

$$G = \left[(k - m\omega^2)(k_a - m_a\omega^2) - m_a k_a\omega^2\right]^2, \tag{4.13}$$

$$H = (k + k_a - m\omega^2)^2. \tag{4.14}$$

Substituting equations (4.11), (4.12), (4.13) and (4.14) into Equation (4.10) yields

$$\frac{X^2k^2}{F_0^2} = \frac{k^2(D+E)}{G+HE}. \tag{4.15}$$

Because c_d is variable here, when $c_d = c_{d1}$,

$$E_1 = c_{d1}^2\omega^2, \tag{4.16}$$

therefore

$$\frac{X_1^2k^2}{F_0^2} = \frac{k^2(D+E_1)}{G+HE_1} \tag{4.17}$$

where X_1 is the amplitude corresponding to c_{d1}. When $c_d = c_{d2}$,

$$E_2 = c_{d2}^2\omega^2,$$

therefore

$$\frac{X_2^2k^2}{F_0^2} = \frac{k^2(D+E_2)}{G+HE_2} \tag{4.18}$$

where X_2 is the amplitude corresponding to c_{d2}. To find out the frequencies of the crossing points if they exist at the different damping ratio, let $\frac{X_1^2 k^2}{F_0^2} = \frac{X_2^2 k^2}{F_0^2}$. Substituting equations (4.17) and (4.18) into the above equation results in

$$\frac{D + E_1}{G + HE_1} = \frac{D + E_2}{G + HE_2}.$$

Multiplying $(G + HE_1)(G + HE_2)$ to the above equation on both sides yields

$$(D + E_1)(G + HE_2) = (D + E_2)(G + HE_1).$$

Simplifying the above equation yields

$$(E_1 - E_2)(G - DH) = 0.$$

As $c_{d1} \neq c_{d2}$, and $\omega \neq 0$, thus $(E_1 - E_2) \neq 0$, therefore $(G - DH) = 0$, this results in

$$G = DH.$$

Substituting equations (4.13), (4.11), and (4.14) into the above equation yields

$$[(k - m\omega^2)(k_a - m_a\omega^2) - m_a k_a \omega^2]^2 = (k_a - m_a\omega^2)^2(k + k_a - m\omega^2)^2. \tag{4.19}$$

Equation (4.19) can be separated into two equations respectively which can be solved as forms of

$$[(k - m\omega^2)(k_a - m_a\omega^2) - m_a k_a \omega^2] = (k_a - m_a\omega^2)(k + k_a - m\omega^2) \tag{4.20}$$

and

$$[(k - m\omega^2)(k_a - m_d\omega^2) - m_a k_a \omega^2] = -(k_a - m_a\omega^2)(k + k_a - m\omega^2). \tag{4.21}$$

Equation (4.20) does not give reasonable solutions for the frequency ω. Rearranging equation (4.21) yields

$$2mm_a\omega^4 - 2(k_a m_a + k_d m + k m_a)\omega^2 + 2kk_a + k_a^2 = 0. \tag{4.22}$$

To solve equation (4.22) in a convenient way, this equation can be rewritten as

$$2r^4 - 2(\mu\beta^2 + \beta^2 + 1)r^2 + 2\beta^2 + \mu\beta^4 = 0 \tag{4.23}$$

where

$$r = \frac{\omega}{\omega_p}$$

is the ratio of the driving frequency to the natural frequency $\omega_p = \sqrt{\frac{k}{m}}$ of the primary system,

$$\mu = \frac{m_a}{m}$$

is the ratio of the absorber mass to the primary mass,

$$\beta = \frac{\omega_a}{\omega_p}$$

is the ratio of the frequencies, and $\omega_a = \sqrt{k_a/m_a}$ is the natural frequency of the absorber system. For the purpose to suppress the resonance of the primary system, the natural frequency of the absorber ω_a is set to be equal to ω_p, therefore

$$\beta = 1.$$

Use the data given in Table (4.1), the mass of the primary system is given by

$$m = m_b + m_f = 0.9687\ kg,$$

therefore

$$\mu = \frac{m_a}{m} = 0.0337.$$

Substitution of the values of μ and β into Equation (4.23) yields

$$2r^4 - 4.0674r^2 + 2.0337 = 0$$

which has solutions

$$r^2 = \frac{4.0674 \pm \sqrt{4.0674^2 - 4 \times 2 \times 2.0337}}{2 \times 2} = 0.8860,\ 1.1477.$$

Because $r = \omega/\omega_p$ are positive, thus

$$r = 0.9413,\ 1.0713$$

and

$$\omega_p = \sqrt{\frac{k}{m}} = 90.48\ rad/s$$

or

$$f_p = 14.40\ Hz,$$

therefore the two crossing frequencies

$$\omega_c = \omega_p \times r = 85.17,\ 96.93\ rad/s$$

or

$$f_c = 13.56,\ 15.43\ Hz.$$

4.2 Design of Auto-Tuning and Simulation

In this section, an auto-tuning algorithm is developed and computer simulation is carried out to test the algorithm. A Simulink program is used to implement the simulation.

4.2.1 Auto-Tuning Algorithm

Based on Section 4.1, control of the damper can be a simple on/off action. If the exciting frequency is between the crossing frequencies, the damper should be turned off to minimize the damping effect. If the exciting frequency is outside the crossing frequencies, the damper should be turned on fully to maximize the damping effect. The proposed tuning method contains the following steps:

1. Sample the response x of the primary system over a specified time period at a sampling interval Δt. The time period of each group of the data is chosen to be $T = 2^n \Delta t$ where n is an integer such as 10 or 11.

2. Obtain the spectrum of the response by applying the FFT to the sampled responses and find the frequency corresponding to the maximum magnitude of the spectrum. Let this frequency be the measured exciting frequency f^{new}.

frequency. The initial damping ratio ζ_d is set to 0.004 which was measured from the real experimental system when the electromagnet is turned off. The maximum damping ratio ζ_d is assumed to be 0.1 which was measured from the experimental system when the current of the electromagnet was about 2 A.

4.2.3 Tracking a Multi-Step Change in the Exciting Frequency

For this test, the absorber natural frequency is set to be 14.4 Hz which equals the natural frequency of the primary system without the absorber system. The exciting frequency starts from 12.8 Hz, changes to 14.4 Hz at the time $t = 8$ second and changes to 16 Hz at the time $t = 16$ second. The motivation of this test is to verify the tuning of the damper based on the measured exciting frequency.

Figure 4.6 shows the response of the primary beam if the damping ratio remains unchanged, i.e., auto-tuning is not activated. It can be seen the amplitude of the response is

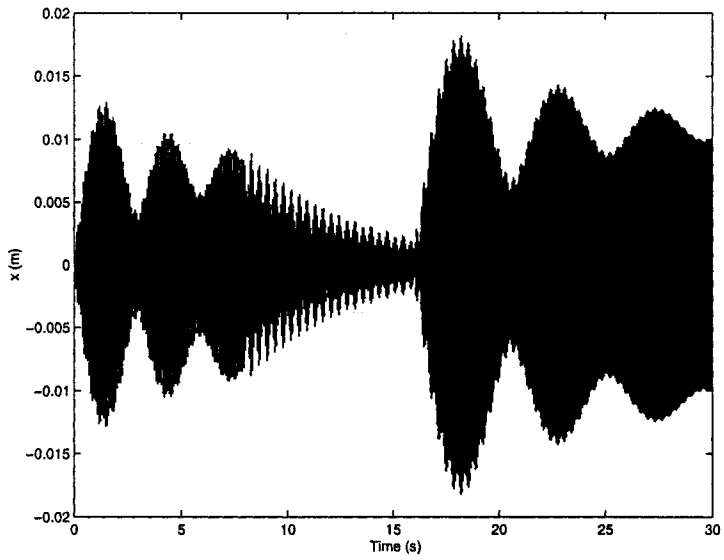

Figure 4.6: Time response of the primary mass without the control of the damper when the exciting frequency experiences a multi-step change

significantly large during the periods of the first 8 seconds and the last 8 seconds when the exciting frequency is close to the natural frequencies of the entire system. During the period

from 8 second to 16 second, the amplitude of the response is decreased because the exciting frequency is equal to the absorber frequency.

Figure 4.7 shows the frequency tracking when the frequency tolerance is chosen to be tol=1.47 Hz. It can be seen that the updated exciting frequency does not converge to

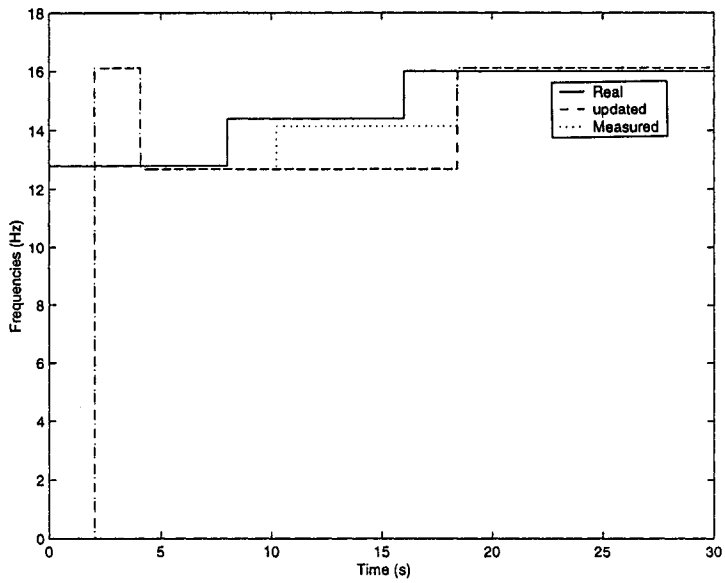

Figure 4.7: Frequency tracking when the exciting frequency experiences a multi-step change: tol=1.47 Hz

the measured exciting frequency when the exciting frequency changes from 12.8 Hz to 14.4 Hz. The change of the measured exciting frequency at $t = 10.24$ second is about 1.46 Hz, therefore the frequency tolerance is too large. Figure 4.8 shows the frequency tracking when the frequency tolerance is chosen to be tol=0.9 Hz. It can be seen that the measured exciting frequency is not stable after the exciting frequency is changed to 14.4 Hz and the updated exciting frequency follows the measured exciting frequency during the period from 8 second to 16 second. The reason is that the frequency tolerance tol is chosen to be relatively small. The transient response is induced and is dominant when the updated exciting frequency is adjusted to be equal to the measured exciting frequency during this period. Figure 4.9 shows the frequency tracking when the frequency tolerance is chosen to be tol=1 Hz. Now with this frequency tolerance it can be seen that the updated exciting frequency follows the real

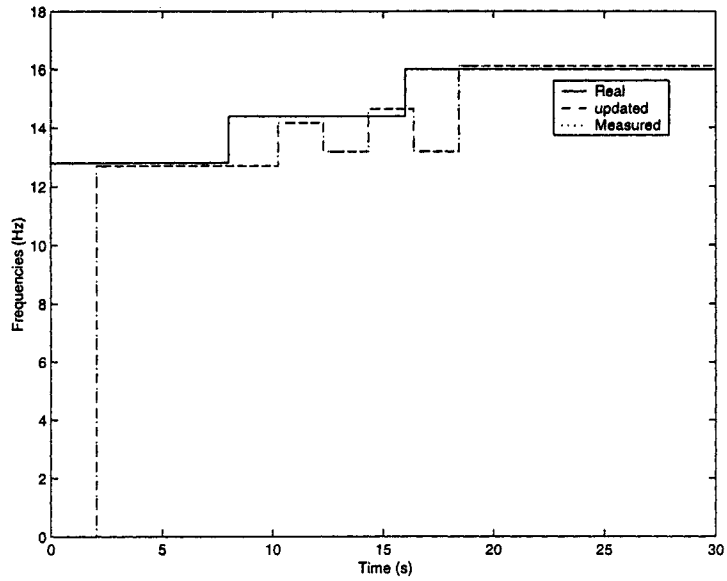

Figure 4.8: Frequency tracking when the exciting frequency experiences a multi-step change: tol=0.9 Hz

exciting frequency. When the transient response is induced at approximately $t = 13$ second, the measured exciting frequency changes slightly. However, the updated exciting frequency keeps unchanged, because $|f^{new} - f^{old}| < 1$ Hz. Therefore 1 Hz is chosen to be a proper frequency tolerance for this simulation.

Figures 4.10 and 4.11 show the responses of the primary mass and absorber mass when the auto-tuning control is enforced. Figure 4.12 shows the values of the damping ratio ζ_d when the exciting frequency varies.

The reduction in the vibration amplitude accomplished by the tunable damping vibration absorber is illustrated. The exciting frequency starts from 12.8 Hz (solid line in Figure 4.9) which is outside the two crossing frequencies, and the initial damping ratio is 0.004, this period lasts for 8 seconds. During this period, for the first 2.048 seconds, the vibration of the primary mass is significantly large and keeps increasing, because 12.8 Hz is close to the first resonance frequency. After 2.048 seconds, which is the execution time of the FFT computation, the exciting frequency is determined and the damping ratio is tuned to be maximum or 0.1, the vibration of the primary mass is suppressed significantly. At the

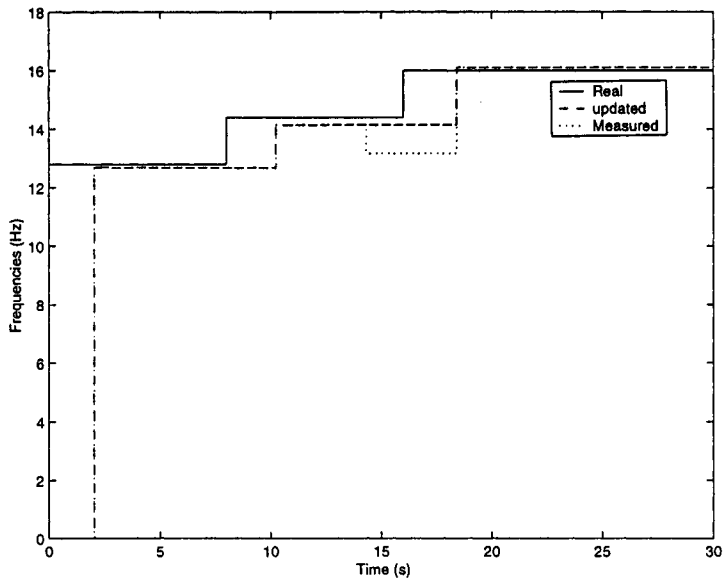

Figure 4.9: Frequency tracking when the exciting frequency experiences a multi-step change: tol=1 Hz

time of 8 second, the exciting frequency is changed to 14.4 Hz which is the anti-resonance frequency of the entire system and is between the two crossing frequencies. Because of the damping, the vibration of the primary mass remains almost unchanged for around 2 seconds. After the new exciting frequency is determined, the damping ratio is tuned to be minimum or 0.004, the vibration of the primary mass starts decreasing while the vibration of the absorber mass increases. During this period, the absorber mass provides the protection to the primary mass and absorbs the exciting force. At the time of 16 second, the exciting frequency is changed to 16 Hz which is very close to the second resonance frequency and is outside the crossing frequencies, the vibration of the primary mass increases significantly again. This lasts for about 2 seconds. After the new exciting frequency is determined, the vibration of the primary mass is reduced to a smaller value after the damping ratio is tuned to be 0.1 again.

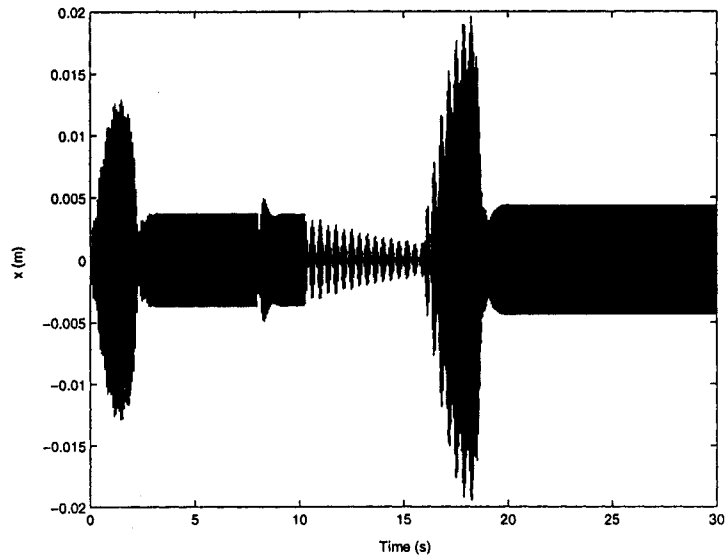

Figure 4.10: Time response of the primary mass when the exciting frequency experiences a multi-step change

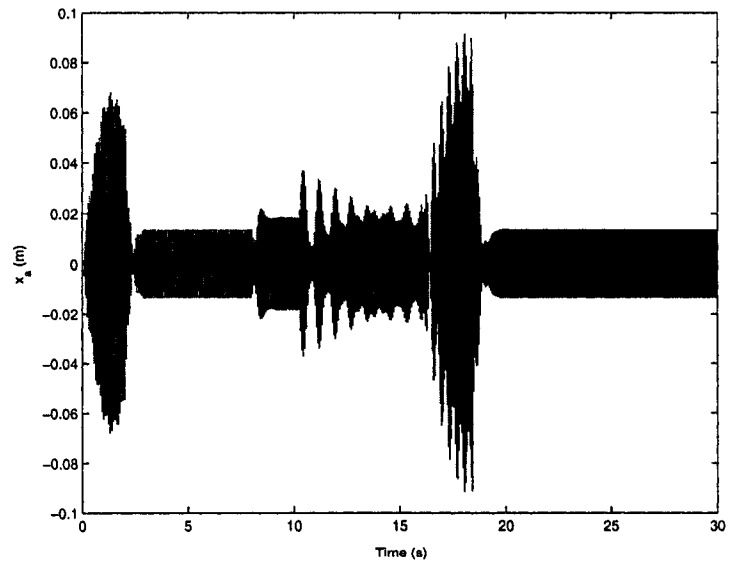

Figure 4.11: Time response of the absorber mass when the exciting frequency experiences a multi-step change

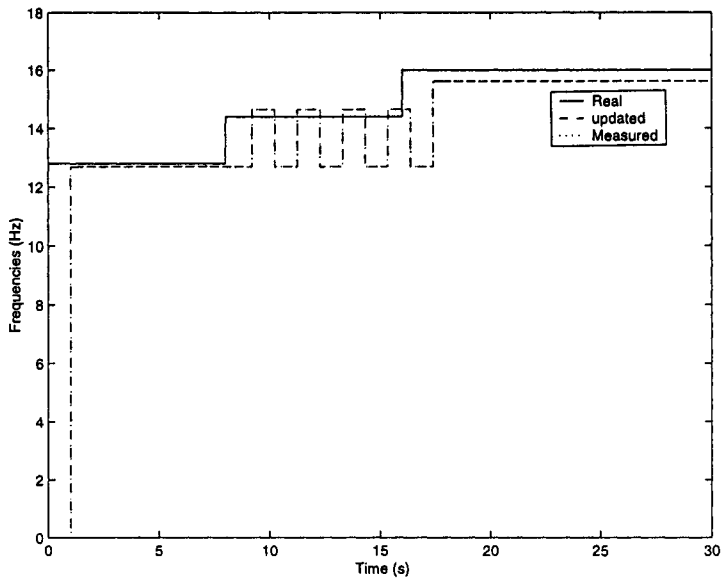

Figure 4.13: Frequency tracking when the exciting frequency experiences a multi-step change: tol=1 Hz

exciting frequency during the period from 8 second to 16 second.

Figures 4.15 and 4.16 show the response of the primary mass and the response of the absorber mass when the frequency tolerance is chosen to be tol=1 Hz. Figure 4.17 shows the values of the damping ratio ζ_d when the exciting frequency varies. With the shorter FFT execution time, the damping ratio can be obtained in a shorter time, the vibration can be suppressed quickly comparing with the situation when the FFT execution time is 2.048 seconds. However during the period from 8 second to 16 second, the frequency tracking is not working properly, a proper damping ratio is not obtained. Therefore the vibration of the primary mass is not suppressed effectively during this period.

Comparing Figures 4.6 and 4.15, with the control of the tunable damping vibration absorber, the vibration attenuation achieved is 7 dB during the entire period.

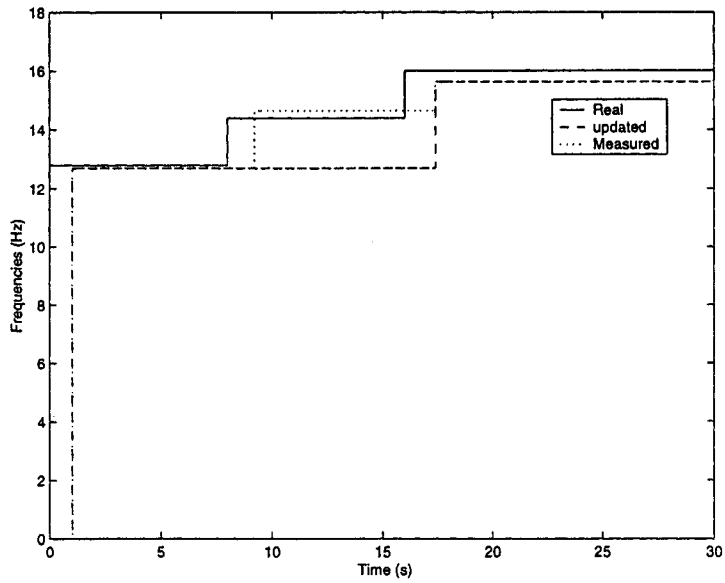

Figure 4.14: Frequency tracking when the exciting frequency experiences a multi-step change: tol=2 Hz

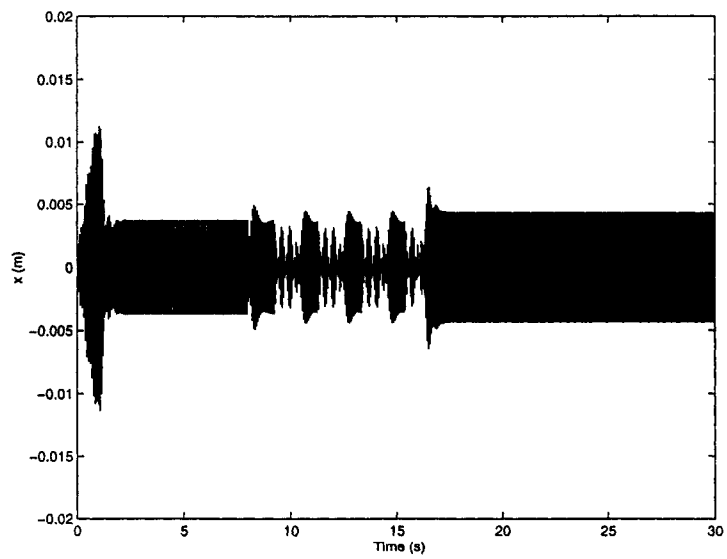

Figure 4.15: Time response of the primary mass when the exciting frequency experiences a multi-step change

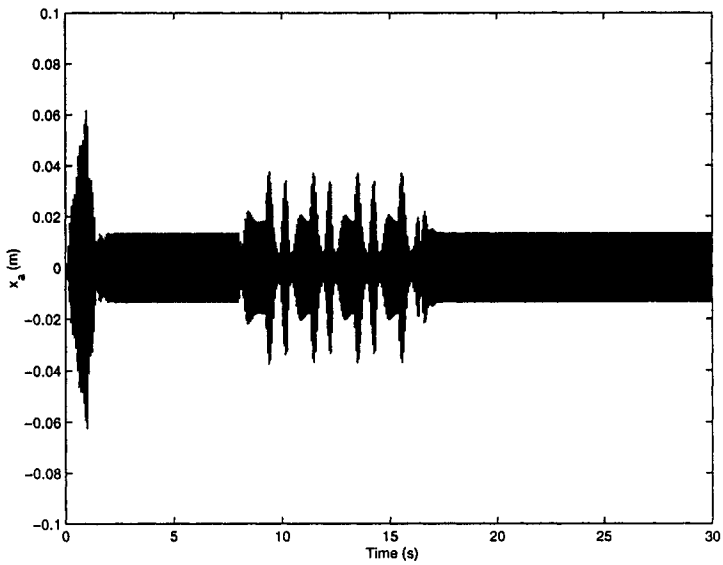

Figure 4.16: Time response of the absorber mass when the exciting frequency experiences a multi-step change

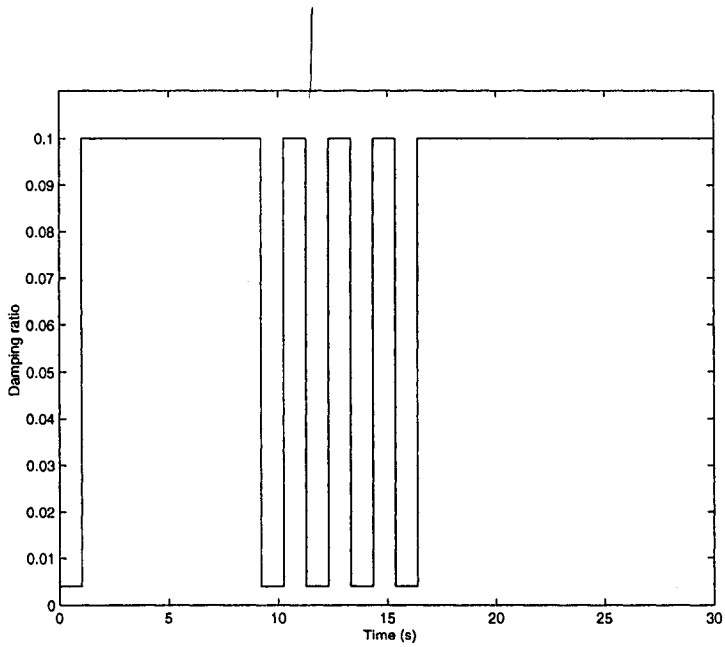

Figure 4.17: Damping ratio change when the exciting frequency experiences a multi-step change

Chapter 5

Experimental Study of a Variable Damping Vibration Absorber

The experimental system consists of 3 subsystem: a clamped-clamped beam, a computer control system and an absorber-damper system as shown in Figure 5.1.

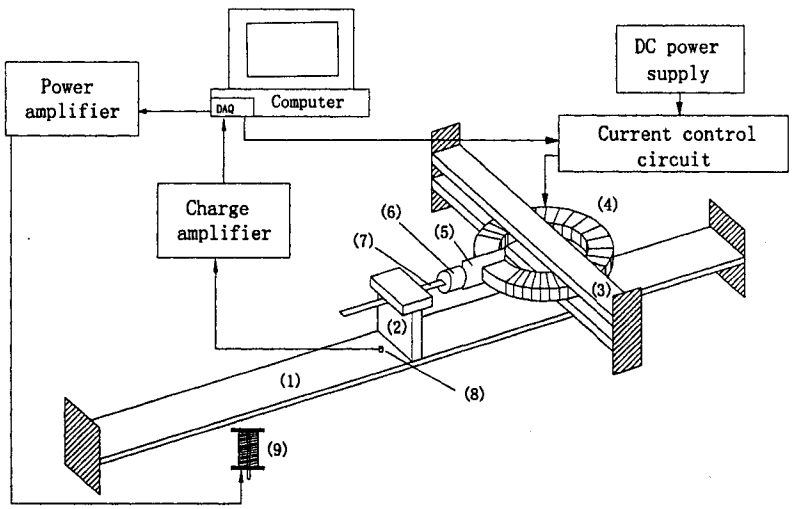

Figure 5.1: Schematic of the experimental system

(1) Primary beam
(2) Absorber beam clamp
(3) Clamp support
(4) Electromagnet
(5) Copper plate
(6) Absorber mass
(7) Absorber Beam
(8) Accelerometer
(9) Electromagnetic shaker

5.1 Current Control Circuit of the Electromagnetic Damper

The electromagnetic damper is driven by a current control circuitry. A control voltage signal is generated by the computer and outputs to channel DAC2 (see Figure 5.5). Figure 5.2 shows the current control circuit built in house. The main component of the circuit is

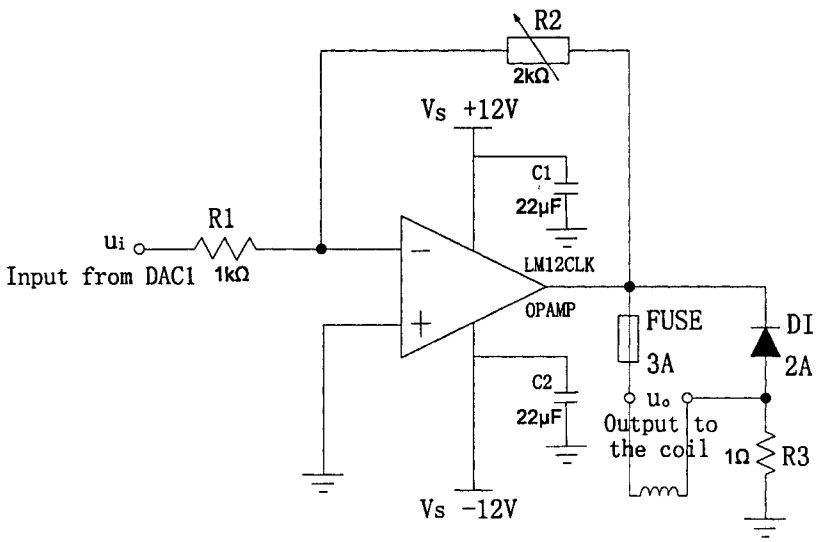

Figure 5.2: Current control circuit of the electromagnetic damper

LM12CLK that is a power op amp capable of driving ±25V at ±10A. In this experiment, the power supply to LM12CLK is ±12V. The supply leads are bypassed by the capacitors c_1 and c_2 to avoid spurious oscillation problems. The diode is used to discharge the stored energy in the load inductance when the circuit is tuned off. The voltage of the 1Ω resistor R_3 is equal to the current of the coil and can be used as a current feedback signal if needed. The output voltage of the current control circuit is given by

$$u_o = -\frac{R_2}{R_1} u_i$$

where u_i is the input control voltage from DAC2 of DAQ board and the range is from 0 to 8 V. R_2 is an adjustable resistor to tune the output voltage u_o. The magnitude of the output voltage is adjusted to be equal to the magnitude of the input voltage.

section with 11 mm (height) × 23.5 mm (width). The air gap length between pole faces of the C shape core is 3.5 mm. Gauge 18 wire is used to wind the coil of about 1800 turns. The resistance of the coil is 3 ohm. The absorber mass has an attached copper plate that locates between the two poles of the electromagnetic damper as shown in Figure 5.1. The damping is introduced by the eddy currents thus providing true viscous damping that can be regulated by changing the current of the electromagnet. The viscous damping generated by the eddy current system is continuously variable.

From the Ohm's Law, the current density inside the copper plate can be determined by

$$\vec{J} = \sigma\vec{E} = \sigma\vec{v} \times \vec{B}$$

where

J=current density inside the copper plate

E=Electric flux density

σ=conductivity of the plate

v=velocity of the plate relative to field

B=magnetic flux density

This induced current in the copper plate, being placed in a magnetic field, will produce an electromagnetic force. The volume density of this force in N/m^3 can be determined by

$$\frac{\triangle\vec{F}}{\triangle V} = \vec{J} \times \vec{B} = \sigma(\vec{v} \times \vec{B}) \times \vec{B}$$

where $\triangle F$ is the electromagnetic force exerted on the portion of the copper plate through which the magnetic field passes and $\triangle V$ is the volume of the copper plate through which the magnetic field passes. As the above vectors are at right angles, the total electromagnetic force on the copper plate generated by the eddy current is given by

$$F = \sigma B^2 V v = cv$$

where $c = \sigma B^2 V$. From the above equation the electromagnetic force is proportional to the velocity but at the direction opposite to that of the velocity, therefore c is equivalent to the damping coefficient of this electromagnetic damper. Assuming the permeability of iron to be infinite, the flux density in the air gap can be calculated approximately by

$$B = \frac{\mu_0 N I}{I_g}$$

where

μ_0=permeability of air=$4\pi \times 10^{-7}$ H/m

N=number of turns in the coil

I=current through the coil

I_g=air gap length between the pole faces

Substituting B into c results in

$$c = \frac{\sigma \mu_0^2 N^2 I^2 V}{I_g^2} = kI^2$$

where

$$k = \frac{\sigma \mu_0^2 N^2 V}{I_g^2}$$

is a constant value. As indicated by the above equation, the damping coefficient c can be varied by changing the current through the coils.

5.3 Relation between the Damping Ratio and the Damper Current

As mentioned in the last section, the damping coefficient c can be varied by changing the damper current. The damping coefficient c is proportional to the damping ratio ζ from the relation

$$\zeta = \frac{c}{2\sqrt{km}}.$$

Therefore the damping ratio ζ can be varied by changing the damper current. An experiment was carried out to determine the relation between the damping ratio and the damper current. The absorber was securely clamped to a fixed support. An accelerometer was placed on the absorber mass. With a known damper current, impact was applied to the absorber mass and the response was measured. The damping ratio was determined from the equation [8]

$$\zeta = \frac{\delta}{\sqrt{4\pi^2 + \delta^2}}$$

where

$$\delta = \frac{1}{n} \ln \left(\frac{\ddot{x}(t)}{\ddot{x}(t + nT)} \right)$$

where n is an integer number of successive peaks, T is the period of oscillation. The experiment was repeated for a new damper current. Figure 5.4 shows the found relation. Circles

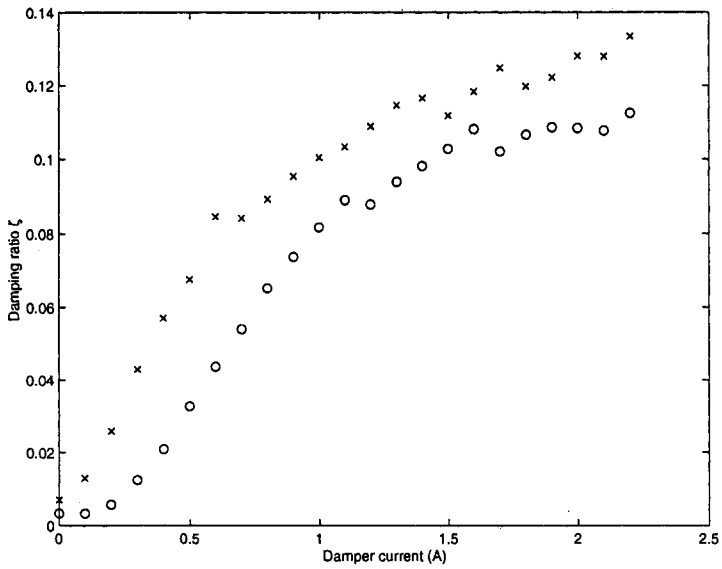

Figure 5.4: Relation between damping ratio and damper current

represent the measured damping ratios at different damper current when the current was increased from 0 A to 2.2 A, crosses respresent the measured damping ratios at different damper currents when the current was decreased from 2.2 A to 0 A. The relation of the damping ratio and the damper current is different when the damper current is increased from that when the damper current is decreased, this behavior is called *hysteresis*. It is also noted that the quadratic relation between the damping ratio and the current is observed for the small to the medium current magnitude. When the current magnitude is large, the varying trend of damping ratio seems to be flattened out. This phenomenon is due to the magnetic saturation. For the experimental study, the on action or maximum damper current is chosen to be 2 A and the off action or the minimum damper current is chosen to be 0 A.

5.4 Experimental Results

In order to validate the control method developed in Chapter 4, experimental tests have been carried out. The tuning algorithm which was used in the simulation is applied. Exper-

imental results include: impact response of the primary system without the absorber mass, impact response of the primary beam with the absorber without damping, forced responses of the primary beam with the absorber and different damping, forced response when exciting frequency experiences step changes.

5.4.1 Simulink Model

The same computer and DAQ board which were used in the previous experiment were used in this experiment. The acceleration signals are measured by the accelerometer. After amplified by the charge amplifier, the acceleration signals are input to channels ADC1 and ADC2 of the DAQ board. The exciting signal is generated and output through channel DAC1 to the power amplifier to drive the shaker. Figure 5.5 is the Simulink Model of the control system which was built up based upon the simulation model used in Chapter 4. The FFT subsystem

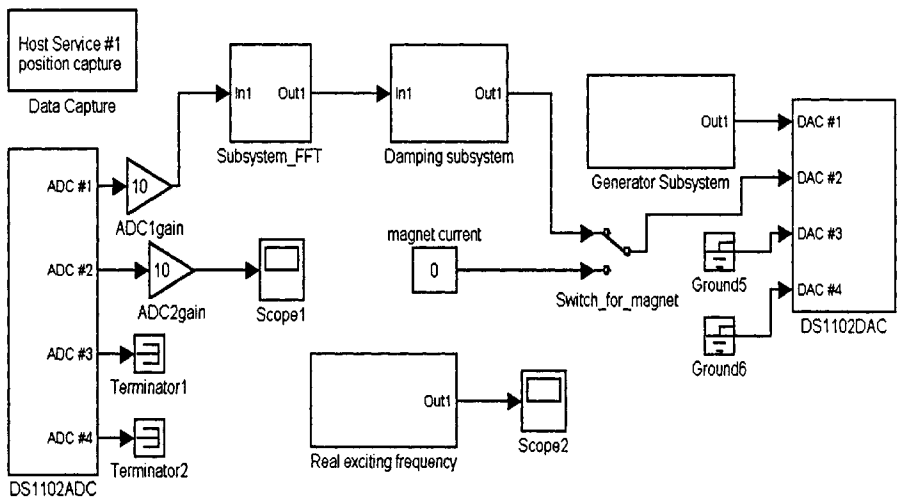

Figure 5.5: Simulink model of the control system

block is the same block used in Chapter 3. Damping subsystem block is the same block used in Chapter 4. The base sampling time of the entire system is 0.001 second, 2048 samples are used in the FFT computation, thus the execution time of Subsystem_FFT is 2.048 seconds.

5.4.2 Experimental Results without and with the Absorber-Damper System

Figure 5.6 depicts the spectrum of the impact response of the primary system without the absorber mass. The system behaves like a 1-DOF system as only one peak at 14.4 Hz is

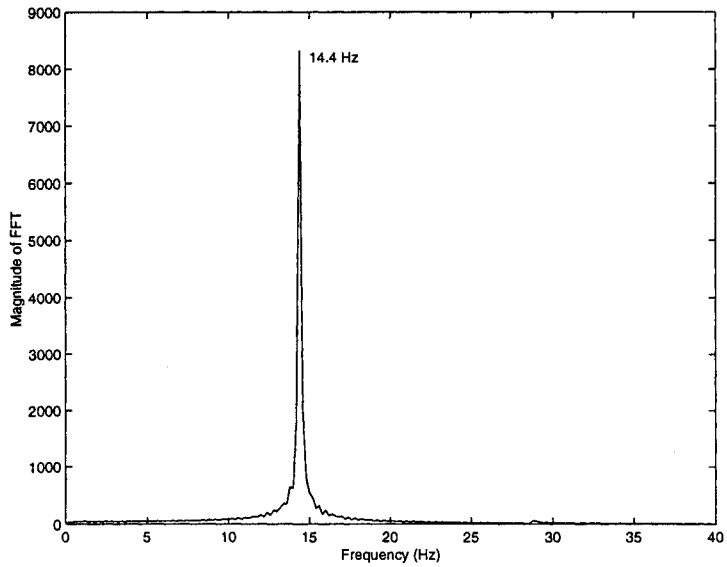

Figure 5.6: Spectrum of an impact response of the primary system

visible in the figure. Figure 5.7 depicts the spectrum of the impact response of the primary system with the absorber mass. The absorber frequency f_a was tuned to be 14.4 Hz which equals to the natural frequency of the primary system. The new natural frequencies of the entire system are 12.4 Hz and 16.8 Hz. These two new frequencies are close which makes the performance of the absorber system sensitive to the variation of the exciting frequency. Figure 5.7 also shows that the anti-resonance frequency is around 14.4 Hz as predicted by the absorber natural frequency. From the absorber theory, when the exciting force is excited at this frequency, the vibration of the primary beam will be suppressed to a minimum value.

To experimentally determine the crossing frequencies, a forced response test was conducted. With a different current supplied to the damper, the beam was excited at a constant frequency until the steady state was established. The FFT magnitude of the steady state

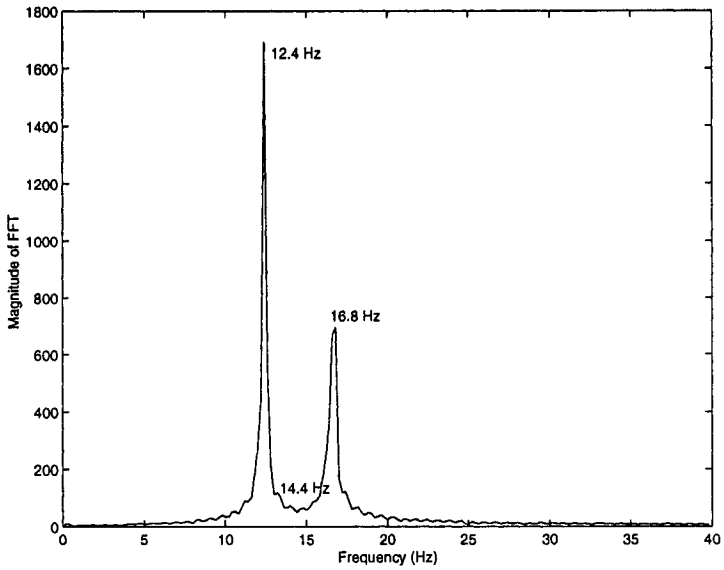

Figure 5.7: Spectrum of an impact response of the primary system with the absorber

response was determined. Then the exciting frequency was increased by a small amount. The experiment was repeated. This way, the frequency was swept from 11 Hz to 18 Hz in a step size of 0.2 Hz. Three different damper currents were employed. The results are shown in Figure 5.8. From the figure the crossing frequencies were found to be 12.75 Hz and 15.70 Hz, respectively.

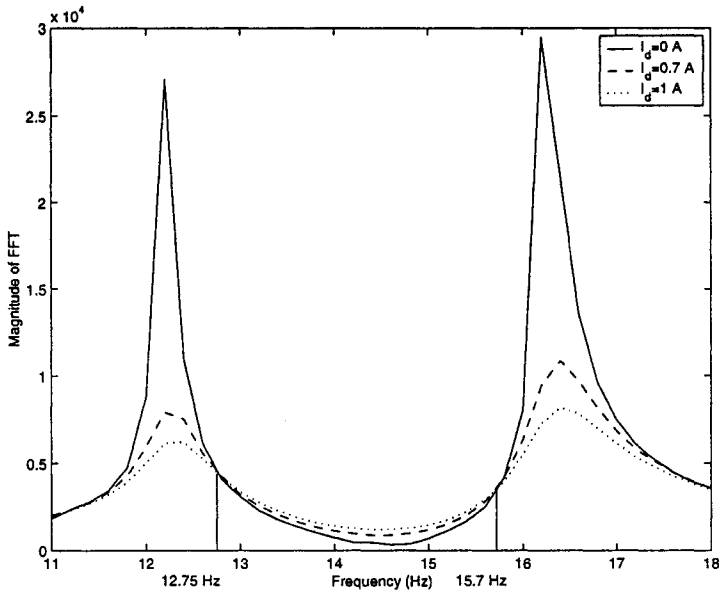

Figure 5.8: Crossing frequencies

5.4.3 Tracking a Multi-Step Change in the Exciting Frequency

For this test, the absorber natural frequency was fixed at 14.4 Hz which equals the natural frequency of the primary system without the absorber system. The exciting frequency started from 12.4 Hz, after 6 seconds was changed to 14.4 Hz and after 12 seconds was changed to 16.8 Hz.

Figure 5.9 shows the response of the primary beam when the damper was off, i.e., auto-tuning was not activated. It can be seen that the amplitude of the response was significantly large during the periods of the first 6 seconds and the last 6 seconds when the exciting frequency was equal to the natural frequencies of the entire system. During the period from 6 second to 12 second, the amplitude of the response was decreased because the exciting frequency was equal to the absorber frequency.

Figure 5.10 shows the frequency tracking when the tolerance was chosen to be tol=0.4 Hz. The updated exciting frequency was equal to the measured exciting frequency during the entire period. At the time $t = 4.096$ second, the measured changed slightly. The change was about 0.5 Hz which was greater than the frequency tolerance, the updated exciting frequency

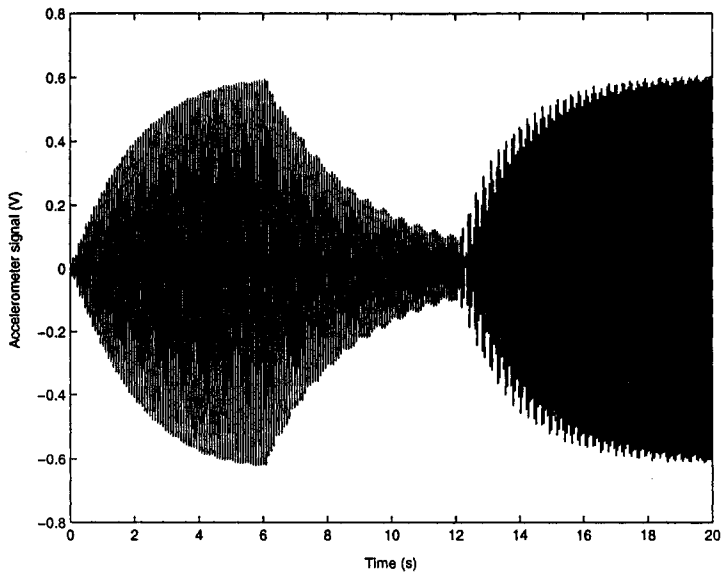

Figure 5.9: Response of the primary beam without the control of the damper when the exciting frequency experiences a multi-step change

followed the measured exciting frequency. When the exciting frequency varied, the transient response was induced and was dominant in the response, therefore the measured exciting frequency was not the real exciting frequency, but one of the natural frequencies of the entire system.

In the following test a larger frequency tolerance was used. Figure 5.11 shows the frequency tracking when the frequency tolerance was chosen to be tol=0.5 Hz. It can be seen that the updated exciting frequency followed the real exciting frequency. At the time $t = 4.096$ second, the measured exciting changed slightly but within the frequency tolerance, the updated exciting frequency was not updated and kept unchanged. Therefore 0.5 Hz was chosen to be a proper frequency tolerance for this experimental test.

Figures 5.12 and 5.13 show the responses of the primary beam and absorber mass when the auto-tuning control was enforced. Figure 5.14 shows the values of the damper current when the exciting frequency varied. The reduction in the vibration amplitude accomplished by the tunable damping vibration absorber is illustrated. During the first 2.048 seconds, as the damper was off and the exciting frequency was equal to the first natural frequency,

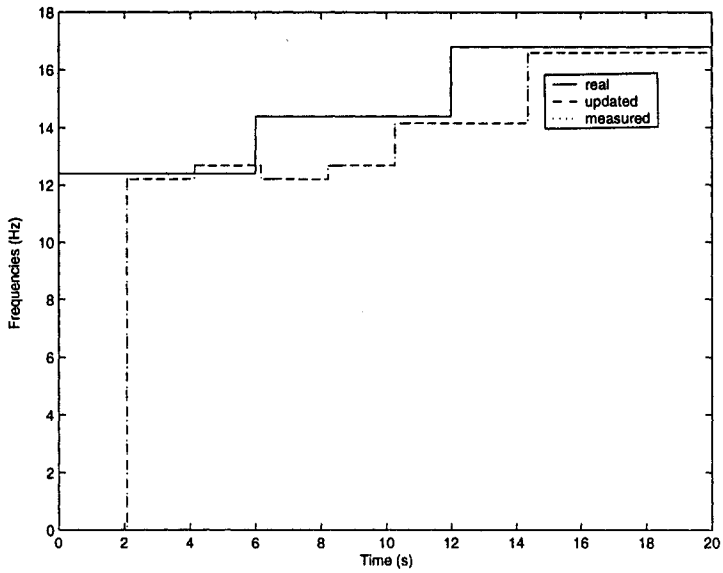

Figure 5.10: Frequency tracking when the exciting frequency experiences a multi-step change: tol=0.4 Hz

the response of the primary beam appeared diverging. At the time of 2.048 second, the exciting frequency was determined. As it was outside the crossing frequencies, the damper was turned on, the amplitude of the response was quickly reduced. At the time of 6 second, the exciting frequency was changed to 14.4 Hz, or the anti-resonance frequency, the response was further reduced. However as the damping ratio was still at the maximum value, the response was not minimized. After approximately 2 seconds, the exciting frequency was identified. As it was within the crossing frequencies, the damper was shut off. Now the response was minimized as the situation was close to an ideal vibration absorber without damping. At the time of 12 second, the exciting frequency became 16.8 Hz which was equal to the second natural frequency of the entire system. As the damper was still off, the response amplitude of the primary beam was increased significantly. After approximately 2 seconds, the damper was turned on again as the exciting frequency was found to be outside the crossing frequencies, the amplitude of the response was quickly reduced to the minimum. The vibration attenuation achieved by controlling the damper was 9.2 dB.

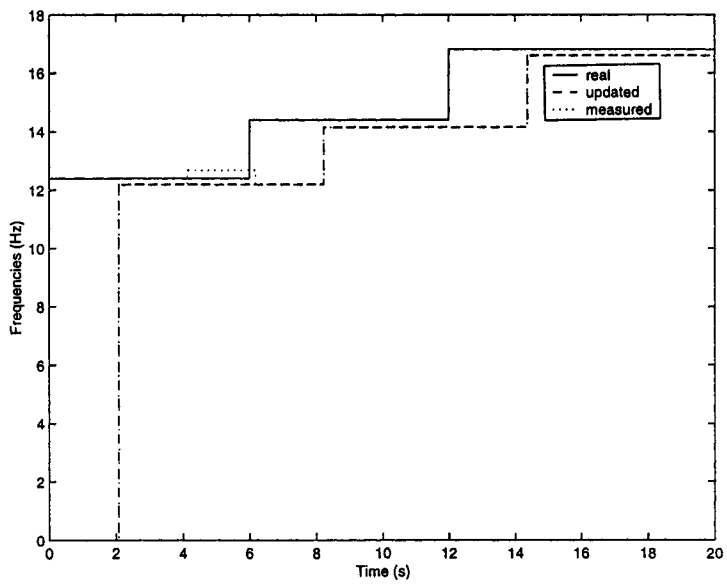

Figure 5.11: Frequency tracking when the exciting frequency experiences a multi-step change: tol=0.5 Hz

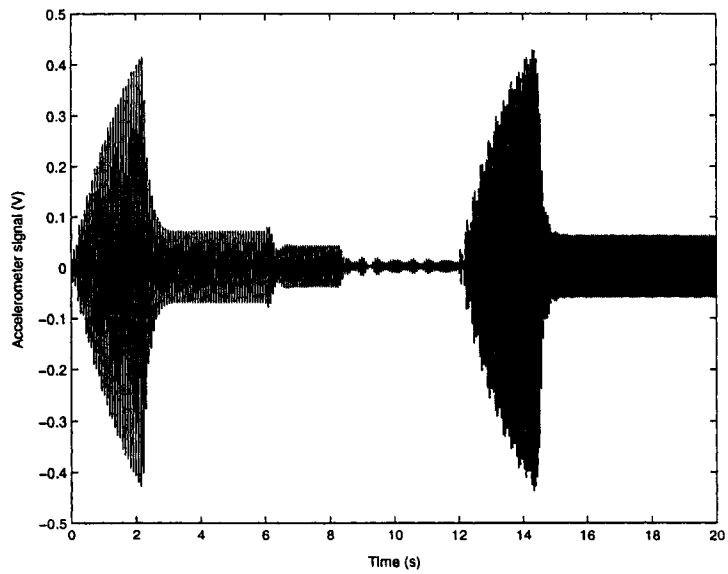

Figure 5.12: Response of the primary beam with the control of the damper when the exciting frequency experiences a multi-step change

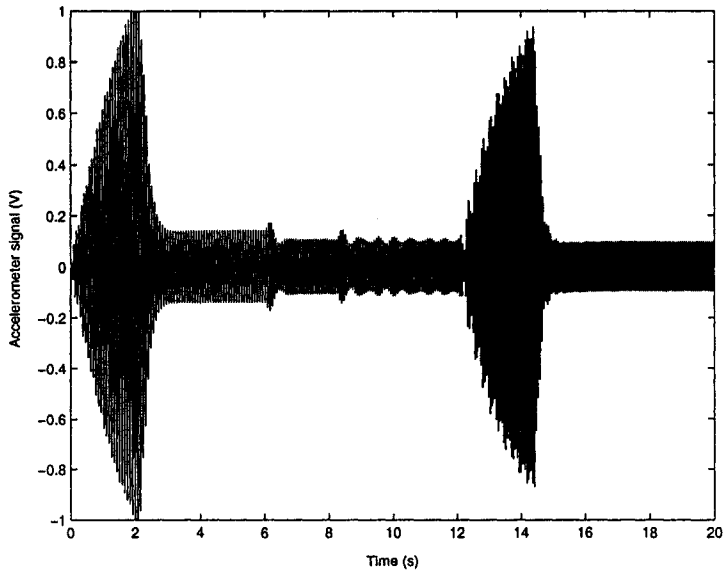

Figure 5.13: Response of the absorber mass with the control of the damper when the exciting frequency experiences a multi-step change

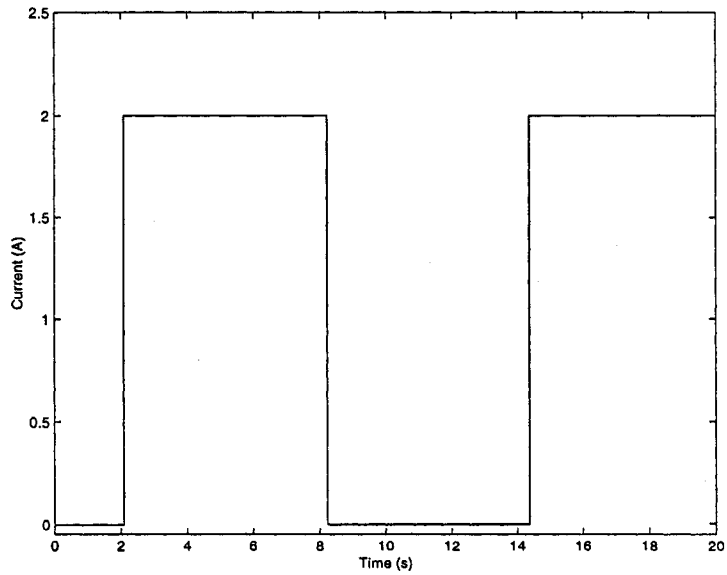

Figure 5.14: The current of the electromagnetic damper when the exciting frequency experiences a multi-step change

Next, some experimental tests have also been carried out when 1024 samples were used for FFT computation or the execution time of the FFT subsystem was 1.024 seconds. Figure 5.15 shows the frequency tracking when the tolerance was chosen to be tol=0.5 Hz. It can

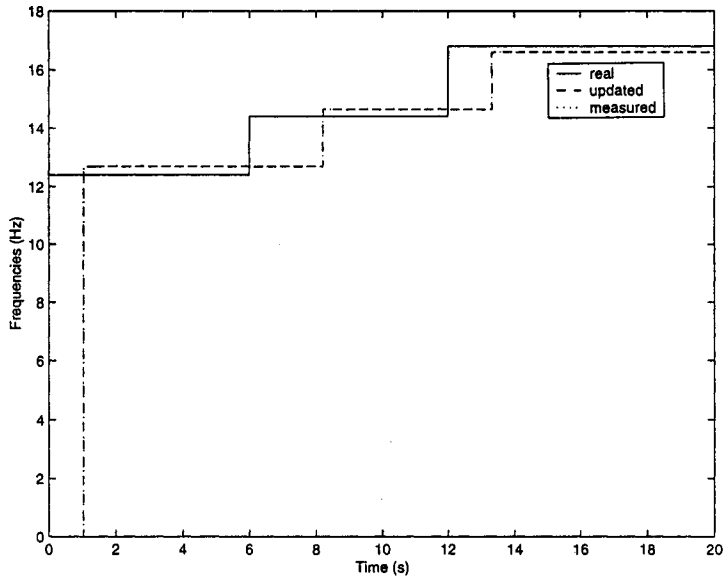

Figure 5.15: Frequency tracking when the exciting frequency experiences a multi-step change: tol=0.5 Hz

be seen that the updated exciting frequency was equal to the exciting frequency completely during the entire period, and the measured exciting frequency followed the real exciting frequency during the entire period too. Therefore in this case, the frequency tolerance can be chosen as 0 Hz.

Figures 5.16 and 5.17 show the responses of the primary beam and the response of the absorber mass. Figure 5.18 shows the values of the damper current when the exciting frequency varied.

The vibration attenuation achieved by controlling the damper during the entire test time was 13.63 dB. It can be seen that the vibration reduction is more effective when the FFT computation time is chosen to be 1.024 seconds. The on/off control action for the damper can be carried out in a shorter time, therefore the vibration amplitude of the primary beam can be reduced much faster.

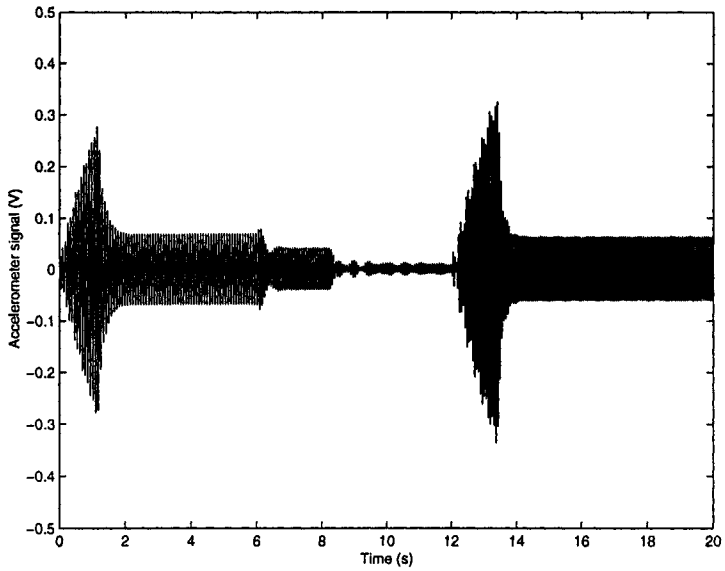

Figure 5.16: Response of the primary beam when the exciting frequency experiences a multi-step change

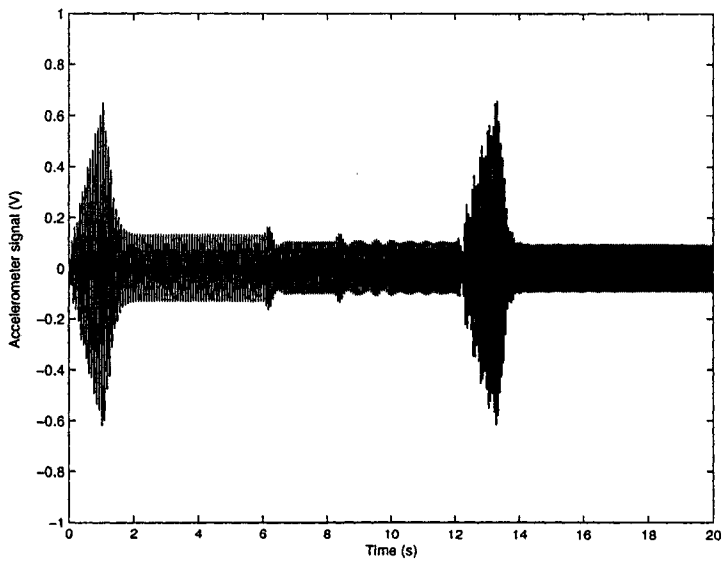

Figure 5.17: Response of the absorber when the exciting frequency experiences a multi-step change

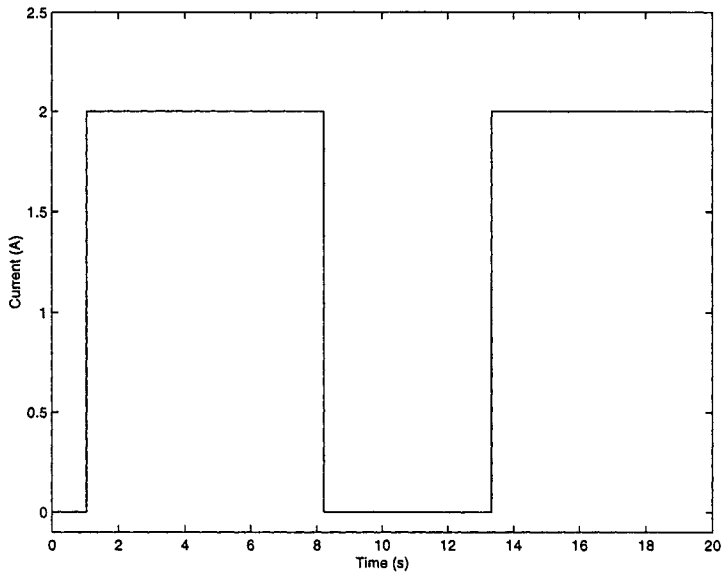

Figure 5.18: The current of the electromagnetic damper when the exciting frequency experiences a multi-step change

Chapter 6

Summary and Future Work

The summary of the thesis study is described as follows:

1. Two analytical modelling procedures have been conducted to model the variable stiffness vibration absorber and the variable damping vibration absorber. A feedback auto-tuning algorithm has been developed. Several Simulink S functions have been built up for the simulation. The simulation results confirm that the vibration absorbers provide protection to the primary system and reduce the vibration when the exciting frequency varies. The transient response is induced when the system parameters or the exciting frequency vary. The effectiveness of the control method is influenced when the transient response is dominant. The FFT computation result is sensitive to the FFT execution time.

2. A developed feedback auto-tuning algorithm has been applied to the experimental system. The study has addressed several important issues, such as the methods of generating the exciting force, the relation between the absorber beam lengths and the absorber natural frequencies, the frequency tolerance, the electromagnetic damper system, the relation between the damping ratio and the damper current. The variable stiffness vibration absorber can reduce the vibration effectively but the tuning speed is slow. The tuning speed is restricted by the mechanical system that adjusts the variable stiffness. The variable damping vibration absorber provides a faster tuning speed, but the vibration attenuation is not as effective as the variable stiffness vibration absorber.

[10] Nejat Olgac, Hankan Elmali, Mark Renzulli, and Martin Hosek 1995 *Active 95 : International Symposium on Active Control of Sound and Vibration.* High frequency implementation of delayed resonator concept using pizoelectric actuators.

[11] N. Pattern William, L. Sack Ronald and Q. He 1996 *Journal of Structural Engineering* 122 187-192. Controlled semiactive hydraulic vibration absorber for bridges.

[12] L. A. Minanzo 1992 M. Sc. Thesis, *Pennsylvania State University*, An adaptable vibration to minimize steady state and start-up transient vibrations–an analytical and experimental study.

[13] D. L. Margolis and D. Baker 1992 *Journal of Dynamic Systems, Measurement, and control* 114, 148-154. The variable fulcrum isolator: a low power, nonlinear, vibration control component.

[14] E. H. Waterman 1998 *Vibration absorber with controllable resonance frequency* United States Patent Number 4724923.

[15] William T. Thomson 1988 *Theory of Vibration with Applications*: Third Edition. Prentice-Hall, New Jersey.

[16] Hugh D. Young 1992 *Univeristy Physics*: Eighth Edition. Addison Wesley.